

UNIVERSITY OF LIÈGE
FACULTY OF APPLIED SCIENCES
DEPARTMENT OF ELECTRICAL ENGINEERING AND COMPUTER SCIENCE



Cellular regulation mechanisms : case study of up and down states in the Purkinje cell

Final year project realized with the aim of obtaining the degree of Master in Electrical Engineering
by **Marie Wehenkel**

Supervised by Prof. Rodolphe Sepulchre

Academic year 2013-2014

Cellular regulation mechanisms : case study of up and down states in the Purkinje cell

Wehenkel Marie

2nd year of the degree of Master in Electrical Engineering

Academic year 2013-2014

Abstract

In 1963, Hodgkin and Huxley obtained the Nobel Prize to have shown that the electrical activity of a neuron could be modelled by an electrical RC circuit containing non-linear conductances. This discovery made it possible to reproduce the electrical behaviour of neurons with a level of detail that has steadily increased over the last fifty years as new quantitative knowledge became available about the specific ionic currents that regulate the activity of a given neuron. But models with too many details are often non-robust and too complex for analysis. As control engineers need simplified models for control design, experimental neurophysiologists are in need of models that are amenable to sensitivity and robustness analysis, beyond the mere simulation of a given neuronal behaviour recorded experimentally.

The Purkinje cell has been studied for over hundred years because its large dendritic tree enables to recognize it easily with a microscope. This neuron exhibits a bistability between a stable hyperpolarized down-state and a stable depolarized spiking state. It is one of the first discovered neurons, however its electrical behaviour is not well understood so far. The principal question of the thesis is to model the electrophysiology of the Purkinje cell to advance the understanding of its regulation mechanisms. More particularly, the objective of the thesis is to explore recent work about the role of the calcium current in neuronal excitability as a possible mechanism underlying the bistability observed in the Purkinje cell.

The electrical activity of the Purkinje cell is reproduced in this thesis thanks to a reduced physiological model which can be seen as an intermediate between a detailed model with dendritic compartments [De Schutter and Bower, 1994a] and an abstract model of bistability [Franci et al., 2012]. This novel model is the main contribution of the thesis. Its main ingredients are on the one hand a fast sodium current and a slow potassium restorative current whose particular kinetics account for the up-state excitability, and on the other hand a slow regenerative calcium current and an ultraslow calcium-dependent potassium current for bistability.

The proposed model suggests several implications. First, a complex compartmental model seems unnecessary to reproduce the electrophysiology of the cell, although the profuse dendrites are an important characteristic of the Purkinje neuron. Secondly, the Purkinje neuron appears to be regulated by the same mechanisms as other bistable neurons such as the thalamocortical (TC) or subthalamic nucleus (STN) neurons. Its behaviour depends on the same feedback mechanisms (a fast regenerative sodium current, a slow restorative potassium current and a slow regenerative calcium current), even though the temporal signature is markedly different because of the specific channel kinetics primarily of the slow potassium current. Finally this novel model makes the Purkinje cell modelling amenable to robustness and modulation studies, as recently shown for similar neurons [Drion et al., 2013].

Cellular regulation mechanisms : case study of up and down states in the Purkinje cell

Wehenkel Marie

2^e année du grade de Master en ingénieur civil électricien, à finalité approfondie

Année académique 2013-2014

Résumé

En 1963, Hodgkin et Huxley obtinrent le Prix Nobel pour avoir montré que l'activité électrique neuronale pouvait être modélisée par un circuit RC à conductances non-linéaires. Cette découverte permit de reproduire le comportement électrique des neurones avec un niveau de détail qui n'a cessé d'augmenter au cours des cinquante dernières années au fur et à mesure que de nouvelles connaissances quantitatives sur les courants ioniques régulant l'activité d'un neurone donnés devenaient disponibles. Néanmoins des modèles trop détaillés sont souvent non-robustes et trop complexes pour être analysés. Tout comme les ingénieurs "contrôle" ont besoin de modèles simplifiés pour la conception de contrôleurs, les neurophysiologistes expérimentaux ont besoin de modèles permettant des analyses de sensibilité et de robustesse, au delà de la simple reproduction d'enregistrements expérimentaux.

La cellule de Purkinje est étudiée depuis une centaine d'années grâce à ses dendrites très étendues la rendant facilement repérable au microscope. Ce neurone présente une bistabilité entre un état de repos hyperpolarisé et un état excitable dépolarisé. Bien qu'il soit l'un des premiers neurones découverts, son activité électrique n'est pas encore bien comprise. La principale question de ce mémoire est donc de modéliser l'activité électrique de ce neurone afin d'améliorer la compréhension des ses mécanismes de régulation. Plus particulièrement, l'objectif de ce travail est de considérer des récents travaux à propos du rôle du courant calcique dans l'excitabilité neuronale comme un possible mécanisme responsable de la bistabilité observée dans les cellules de Purkinje.

L'activité électrique des cellules de Purkinje est reproduite dans cette thèse par un modèle physiologique réduit à mi-chemin entre un modèle détaillé à compartiments [De Schutter and Bower, 1994a] et un modèle abstrait de la bistabilité [Franci et al., 2012]. Ce nouveau modèle est la principale contribution de ce mémoire. Ses principaux composants sont, d'une part, un courant sodique régénérateur rapide et un courant potassique restorateur lent dont les cinétiques particulières expliquent l'excitabilité dans l'état haut et, d'un autre côté, un courant calcique régénérateur lent et un courant potassique calcium-dépendant ultra-lent pour la bistabilité.

Le modèle proposé suggère plusieurs implications. Premièrement, bien que l'abondance de dendrites soit une caractéristique importante des cellules de Purkinje, il n'est pas nécessaire d'utiliser un modèle complexe à compartiments pour en reproduire son électrophysiologie. Deuxièmement, le neurone de Purkinje présente les mêmes mécanismes de régulation que d'autres neurones bistables tels que les neurones thalamo-corticaux ou sous-thalamiques. Son comportement dépend des mêmes mécanismes de régulation (un courant sodique régénérateur rapide, un courant potassique restorateur lent et un courant calcique régénérateur lent), bien que la signature temporelle soit significativement différente principalement à cause des cinétiques particulières des canaux du courant potassique lent. Enfin ce nouveau modèle de la cellule de Purkinje permet des études de sensibilité et de robustesse, comme cela a récemment été réalisé pour d'autres neurones [Drion et al., 2013].

Acknowledgements

First I would like to thank my supervisor Professor Rodolphe Sepulchre thanks to whom I could work on this fascinating subject. I am infinitely grateful to him for having proposed to me this subject and for having supervised me during this year with his many wise advices. I also want to thank him for giving me the opportunity to realize a training at the University of Cambridge (UK).

I also wish to emphasize my gratefulness to Guillaume Drion and Alessio Franci. Many thanks for their availability and the precious help that they provided me during the year, as much as for discussions about papers or modelling questions.

I express a special thought to my dear parents. I would not be there without them. A big thank-you to my mother for her unwavering patience and her precious kind thoughts. Many thanks to my father for having always helped me in my choices and for his support.

I also express my thanks to my family and friends, who supported me during this year.

Finally, I thank all those who have contributed to the achievement of this work, in one way or another, and who are not mentioned here.

Contents

1	Introduction	1
2	Electrophysiology and modelling of single cell neuronal activity	3
2.1	Electrophysiology of a neuron	3
2.2	State of the art in computational neuroscience	6
2.2.1	Hodgkin-Huxley model	6
2.2.2	A novel phase portrait for neuronal excitability	9
2.2.3	Regenerativity vs restorativity	12
3	Physiology of Purkinje cells	15
3.1	The cerebellum	15
3.1.1	Anatomy	15
3.1.2	Scientific and clinical motivations to study Purkinje cells	18
3.2	Electrophysiology of Purkinje cells	20
3.2.1	State of the art in electrophysiology	20
3.2.2	State of the art in modelling	25
4	Qualitative and quantitative modelling	30
4.1	A qualitative model	30
4.1.1	Modelling	31
4.1.2	Results	32
4.2	A quantitative model	33
4.2.1	Modelling	34
4.2.2	Results	40
4.2.2.1	Comparison of experimental and model simulations	40
4.2.2.2	Regulation mechanisms	43
5	A reduced physiological model of Purkinje cell	46
5.1	Modelling of the restorative currents	46
5.2	Modelling the source of bistability	47
5.3	Results	48
5.3.1	Regulation mechanisms	49
5.3.2	Comparison with the qualitative model	60
5.4	Advantages of the proposed model	60
5.5	Limitations of the proposed model	61
5.5.1	Physiological reduction	61
5.5.1.1	Motivation	61

5.5.1.2	Attempt at a formal reduction	61
5.5.2	P-type calcium current	64
6	Conclusions and perspectives	68
6.1	Perspectives	69
6.1.1	Physiological modelling	69
6.1.2	Spatial phenomena	70
	Bibliography	71

List of Figures

1.1	Purkinje cell [Wikipedia, 2014b].	1
2.1	Anatomy of a neuron [Wikipedia, 2014a].	3
2.2	Communication between neurons.	4
2.3	A voltage-gated sodium channel [Izhikevich, 2007].	5
2.4	A conductance-based model.	6
2.5	Steady-state activation variables and time constants [Izhikevich, 2007].	8
2.6	Nullclines of the reduced Hodgkin-Huxley model in the phase plane (V, n).	9
2.7	A distinct phase portrait by addition of calcium current [Drion et al., 2012].	10
2.8	Types of excitability [Franci et al., 2012].	11
2.9	Classification of regenerative and restorative channels between three types of time scales [Drion et al., 2013].	12
2.10	Robustness property [Drion et al., 2013].	13
2.11	Modulation property [Drion et al., 2013].	13
3.1	The brain [Bear et al., 2007].	16
3.2	Motor loop through the cerebellum [Mot, 2002].	16
3.3	The cerebellum anatomy [Bear et al., 2007].	17
3.4	The cerebellar cortex [Bear et al., 2007].	17
3.5	Microcircuitry of the cerebellum. (+): excitatory; (-): inhibitory; MF: Mossy fiber; DCN: Deep cerebellar nuclei; IO: Inferior olive; CF: Climbing fiber; GC: Granule cell; PF: Parallel fiber; PC: Purkinje cell; GgC: Golgi cell; SC: Stellate cell; BC: Basket cell [Wikipedia, 2014b].	18
3.6	Morphology of a rat Purkinje cells [Shelton, 1985].	19
3.7	Somatic and dendritic action potentials of a guinea pig Purkinje cell following DC depolarization [Llinas and Sugimori, 1980b].	20
3.8	Somatic firing resulting of a DC depolarization for a guinea pig Purkinje cell : In A-D short current pulse is injected, whereas long-duration current experiments are shown in E-G [Llinas and Sugimori, 1980a].	21
3.9	Spontaneous repetitive activation of guinea pig Purkinje cells [Llinas and Sugimori, 1980a].	22
3.10	Intracellular recording of a guinea pig Purkinje cell [Rapp et al., 1994].	22
3.11	Whole-cell recording of a rat Purkinje cell [Loewenstein et al., 2005].	23
3.12	Whole-cell recording in vivo [Loewenstein et al., 2005].	23
3.13	Whole-cell recording from a guinea pig Purkinje cell in vitro [Loewenstein et al., 2005].	24
3.14	Extracellular recording from a guinea pig Purkinje cell in vivo [Loewenstein et al., 2005].	24

3.15	Morphology of the modelled Purkinje cell [De Schutter and Bower, 1994a]. . .	26
3.16	Model simulation by somatic current injection [De Schutter and Bower, 1994a].	28
3.17	Model simulation by climbing fibre activation [De Schutter and Bower, 1994b].	29
4.1	Mirrored FitzHugh-Nagumo phase portrait of the Type V.	32
4.2	Type V with $I_{app} = \frac{2}{3} + 0.9$ and initial conditions of $(-4, 0)$	32
4.3	Simulation of model (4.1). Successive application of a current $I_{app} = \frac{2}{3} + 0.9$ and a current $I_{app} = \frac{2}{3} - \frac{2}{3}$	33
4.4	First model with the somatic currents.	35
4.5	Steady-state (in)activation functions and time constants for the fast sodium current.	36
4.6	Steady-state (in)activation functions and time constants for the potassium de- layed rectifier.	36
4.7	Steady-state (in)activation functions and time constants for the T-type calcium current.	37
4.8	Steady-state (in)activation functions for the h-potassium current.	38
4.9	Steady-state (in)activation functions and time constants for the persistent sodium current.	38
4.10	Steady-state (in)activation functions and time constants for the persistent potas- sium current and the A-type potassium current.	39
4.11	Model (4.4) with all maximal conductances set to zero except for I_{NaF} and I_{Kdr} ; $\bar{g}_{Na,F} = 7500$ mS/cm ² and $\bar{g}_{Kdr} = 600$ mS/cm ² . Long-step current with an amplitude of 0.8 nA and a duration of 7 s.	40
4.12	Intracellular recording of a guinea pig Purkinje cell [Rapp et al., 1994].	41
4.13	Somatic firing resulting of a DC depolarization for a guinea pig Purkinje cell [Llinas and Sugimori, 1980a].	42
4.14	Details of the temporal traces for another similar simulation than that of Figure 4.11. Model (4.4) with all maximal conductances set to zero except for I_{NaF} and I_{Kdr} ; $\bar{g}_{Na,F} = 7500$ mS/cm ² and $\bar{g}_{Kdr} = 600$ mS/cm ² . Long-step current with an amplitude of 0.8 nA and a duration of 7 s. Simulation time of 42 s.	42
4.15	Complex spike obtained with model (4.4). (a) Cellular response for a triangu- lar current; $\bar{g}_{Na,F} = 60 \cdot 10^{-3}$ mS and $\bar{g}_{Kdr} = 20 \cdot 10^{-3}$ mS. (b) Climbing fibre activation : complex spike recorded in the soma [Llinas and Sugimori, 1980a].	43
4.16	Response of the model (4.4) for a 0.5 nA current.	44
4.17	Simulation of model (4.4). Modulation of the up-state activity by a variation of \bar{g}_{NaF}	44
4.18	Simulation of model (4.4). Modulation of the up-state activity by a variation of \bar{g}_{Kdr}	45
5.1	Steady-state (in)activation functions and time constants for the calcium cur- rent.	47
5.2	Steady-state (in)activation functions and time constants for the calcium P-type current.	48

5.3	Simulation of model (5.5) for different pulses of applied current; a short high pulse, a long small pulse and a short hyperpolarizing pulse. The maximum conductance values are fixed such as $\bar{g}_{NaF} = 750 \mu\text{S}$, $\bar{g}_{Kdr} = 60 \mu\text{S}$ and $\bar{g}_{K,Ca} = 0 \mu\text{S}$ whereas $\bar{g}_{Ca} = 0 \mu\text{S}$ and $\bar{g}_{Ca} = 0.02 \mu\text{S}$ for the first and the second plot respectively.	49
5.4	Simulation of model (5.5) for a short pulse of applied current. The consequences of the calcium current. The maximum conductance values are fixed such as $\bar{g}_{NaF} = 750 \mu\text{S}$, $\bar{g}_{Kdr} = 60 \mu\text{S}$, $\bar{g}_{K,Ca} = 0 \mu\text{S}$ and $\bar{g}_{Ca} = 0.02 \mu\text{S}$	50
5.5	Simulation of model (5.5) for different pulses of hyperpolarizing applied current. The maximum conductance values are fixed such as $\bar{g}_{NaF} = 750 \mu\text{S}$, $\bar{g}_{Kdr} = 60 \mu\text{S}$, $\bar{g}_{K,Ca} = 0 \mu\text{S}$ and $\bar{g}_{Ca} = 0.02 \mu\text{S}$	51
5.6	Simulation of model (5.5) for different pulses of applied current; a short small pulse, a long high pulse and a short hyperpolarizing pulse. The maximum conductance values are fixed such as $\bar{g}_{NaF} = 750 \mu\text{S}$, $\bar{g}_{Kdr} = 60 \mu\text{S}$ and $\bar{g}_{K,Ca} = 0 \mu\text{S}$ whereas $\bar{g}_{Ca} = 0 \mu\text{S}$ and $\bar{g}_{Ca} = 0.02 \mu\text{S}$ for the first and the second plot respectively.	52
5.7	Simulation of model (5.5). Addition of a SK channel such as $\bar{g}_{SK,Ca} = 0.0144 \mu\text{S}$, $k_1 = 0.1375 \cdot 10^{-3}$, $k_c = 0$, $k_2 = 0.018 \cdot 10^{-4}$ and $K_D = 0.4 \cdot 10^{-3} \text{ nM}$. Same simultaneous tests than Figure 5.3 with $\bar{g}_{NaF} = 750 \mu\text{S}$, $\bar{g}_{Kdr} = 60 \mu\text{S}$ and $\bar{g}_{Ca} = 0.02 \mu\text{S}$	53
5.8	Simulation of model (5.5). Addition of a SK channel. The effect of a long duration current.	54
5.9	Simulation of model (5.5). Addition of a SK channel such as $\bar{g}_{SK,Ca} = 0.0144 \mu\text{S}$, $k_1 = 0.1375 \cdot 10^{-3}$, $k_c = 0$, $k_2 = 0.018 \cdot 10^{-4}$ and $K_D = 0.4 \cdot 10^{-3} \text{ nM}$. Same simultaneous tests than Figure 5.6 with $\bar{g}_{NaF} = 750 \mu\text{S}$, $\bar{g}_{Kdr} = 60 \mu\text{S}$ and $\bar{g}_{Ca} = 0.02 \mu\text{S}$	54
5.10	Simulation of model (5.5). Addition of a SK channel. Spontaneous cellular activity after a short strong pulse.	55
5.11	Somatic firing resulting of a DC depolarization for a guinea pig Purkinje cell : In B-D a short current pulse is injected [Llinas and Sugimori, 1980a].	56
5.12	Simulation of model (5.5). Results for $\bar{g}_{SK,Ca} = 6 \times 0.002 \mu\text{S}$	56
5.13	Simulation of model (5.5); the modulation principle. Results for $I_{app} = 14 \text{ nA}$ from $t = 130 \text{ ms}$ to $t = 200 \text{ ms}$	57
5.14	Simulation of model (5.5); the robustness principle. Results for $I_{app} = 14 \text{ nA}$ from $t = 130 \text{ ms}$ to $t = 200 \text{ ms}$ and $\bar{g}_{Na} = 750 \mu\text{S}$	58
5.15	Simulation of model (5.5); analysis of $g_{SK,Ca}$. Results for $I_{app} = 14 \text{ nA}$ from $t = 130 \text{ ms}$ to $t = 200 \text{ ms}$ and $\bar{g}_{Na} = 750 \mu\text{S}$	59
5.16	Simulation of model (5.5); $K_D = 0.4 \text{ nM}$. $I_{app} = 14 \text{ nA}$ from $t = 130 \text{ ms}$ to $t = 200 \text{ ms}$, $\bar{g}_{Na} = 750 \mu\text{S}$, $\bar{g}_{Kdr} = 60 \mu\text{S}$, $\bar{g}_{Ca} = 0.02 \mu\text{S}$ and $\bar{g}_{SK,Ca} = 0.0144 \mu\text{S}$	59
5.17	Result with the qualitative model and the model (5.5).	60
5.18	Time constants of the model (5.5).	63
5.19	Comparison of the reduced model with the non-reduced model. $I_{app} = 5 \text{ nA}$ from $t = 300 \text{ ms}$. Reduction such as we chose the sodium activation for the fast scale, the potassium activation for the slow scale and the potassium inactivation for the ultraslow scale.	63
5.20	Substitution of the T-type calcium current by a P-type calcium current.	65

5.21	Example of modulation for \bar{g}_{Ca} for P-type current.	65
5.22	Simulation of model (5.5). Modification of the half-activation potential for the calcium current.	66

Chapter 1

Introduction

In a series of papers published in the early fifties, Hodgkin and Huxley laid the foundations of modern neuroscience by showing that the electrical activity of neurons can be modelled as the dynamic behaviour of non-linear circuits obeying precise biophysical principles. Nowadays, electrophysiologists routinely accumulate detailed experimental knowledge of a particular neuron in a mathematical model that can accurately reproduce a given experimental behaviour of the neuron.

But increased biological information goes with an increase in the model complexity, making the simulation of those models fragile and their analysis often intractable. For this reason, novel methodologies are needed to assist neurophysiologists in addressing important questions such as sensitivity, robustness, and modulation. Those questions are frequently addressed in engineering with linear modelling but the non-linear nature of electrophysiological mathematical models makes it an important current research challenge.

The objective of the present work is to apply recent reduced modelling work to a particular neuron, the Purkinje cell illustrated in Figure 1.1.

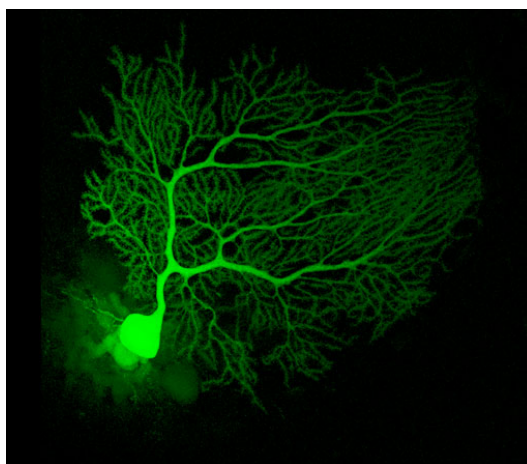


Figure 1.1: Purkinje cell [Wikipedia, 2014b].

The particular anatomy of this neuron embedded in the cerebellar cortex and its important role in motor control and learning makes it one of neurons that has been studied for the

longest time. Its electrical behaviour is characterized by a distinct bistability between a stable silent hyperpolarized “down-state” and a stable but strongly excitable depolarized “up-state”.

Because it was recently found that specific calcium currents are crucial to account for such a bistability in other neurons [Drion et al., 2012], the objective of the thesis is to explore the role of calcium in the bistability of Purkinje cell and to extract the minimal model that could account both for its bistability and for its particular excitability properties. The value of such a model would not be so much in reproducing numerical simulations of the recorded behaviours but rather to shed light on the robustness and modulation mechanisms that regulate the electrical activity of the Purkinje cell.

The thesis is organized as follows. It contains four main chapters presenting an important stage of the thesis and a final chapter for concluding about this work.

Chapter 2 introduces the electrophysiology of a neuron and the modelling of single cell neuronal activity. Indeed, this dissertation therefore begins by discussing the electrical activity of a neuron and recalling some interesting knowledge about non-linear system theory applied to Neuroscience. Furthermore, this chapter presents the state of the art in computational neuroscience necessary to know to deal with the subject of the thesis. A part of the work of Hodgkin and Huxley and the recent discoveries about the role of calcium current in bistability will be presented.

Then the next chapter introduces the physiological context. The thesis deals with the modelling of a particular neuron in the cerebellum: the Purkinje cell. So, this brain area and these cells will be presented in Chapter 3 and the reasons why these neurons are interesting to study will be clarified. The Purkinje cell electrical activity will be explained in details.

Chapter 4 describes two models; a qualitative model and a quantitative model. The qualitative model aims at reproducing the main phenomena without any quantitative information. This type of model misses some information but the principal characteristics of the electrical activity are clearly shown by such a model. On the other hand, a quantitative model will give the whole temporal activity of a neuron, which means that all details of the electrophysiology will be illustrated. Furthermore, in this chapter, the link between a simple empirical model and a complex conductance-based model will be highlighted.

Chapter 5 proposes a novel model situated between the qualitative model and the very detailed quantitative model which were introduced in the previous chapter. It is the main contribution of the thesis.

Finally, some conclusions about this work will be stated and directions for future work will be discussed.

Chapter 2

Electrophysiology and modelling of single cell neuronal activity

This chapter summarizes the basic biophysical principle of conductance-based models, that is, mathematical models of neurons associated to their circuit representation introduced in the seminal work of Hodgkin and Huxley [Hodgkin and Huxley, 1952].

We highlight some recent developments that aimed at capturing the role of calcium in neuronal firing. On the one hand, we explain how the classical phase portrait of neurodynamics is affected just by adding a different ionic current and what this induces. On the other hand, we focus on the role of mathematical modelling to capture the robustness and modulation properties of a neuron, beyond the numerical simulations of a given firing pattern.

2.1 Electrophysiology of a neuron

The nervous system is controlled by the electrical activity of neurons. The anatomy of a neuron is shown in Figure 2.1.

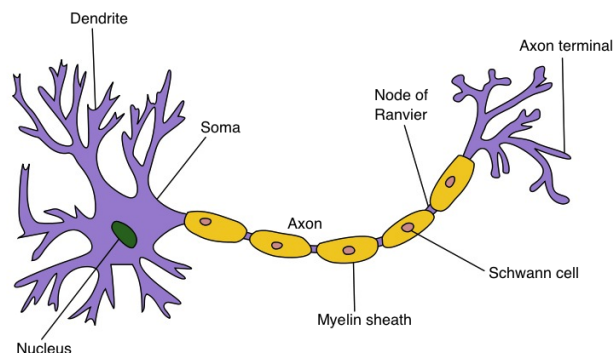
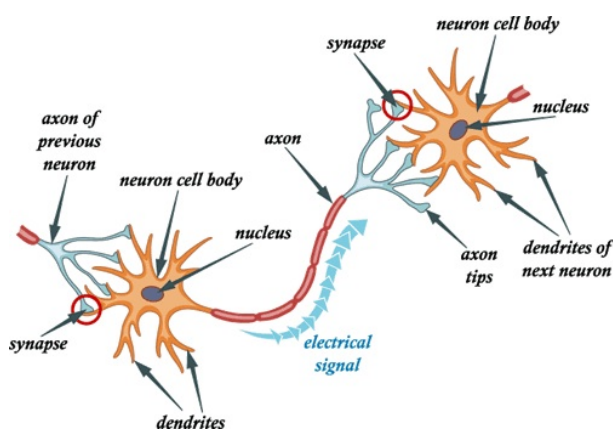


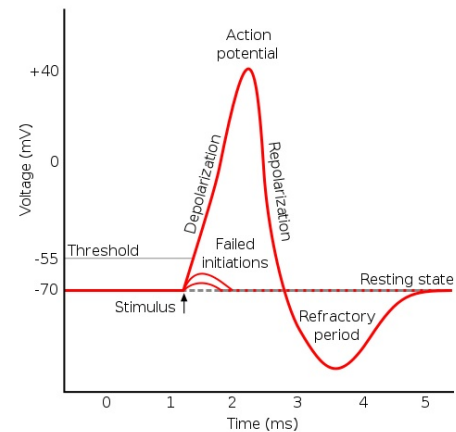
Figure 2.1: Anatomy of a neuron [Wikipedia, 2014a].

The neurons interact with each other by generating electrical impulses which travel through their axon and arrive at another neuron. More precisely, a neuron receives many inputs from

other neurons thanks to the synaptic contacts which are made by the axon terminals of the transmitting neurons with the dendrites of the receptor. This communication mechanism is shown in Figure 2.2(a). The electrical impulse that is generated in a neuron by a stimulation of other neurons is called an action potential. In Figure 2.2(b), V represents the difference of potential between the intracellular medium and the extracellular medium; the potential is positive for a positively charged cell. An action potential is composed of a fast depolarization followed by a slower hyperpolarization. The stimuli have to be strong enough in order to actually induce an action potential in the membrane of the receiving neuron.



(a) Connection between two neurons [Hum, 2011].



(b) The action potential [Wikipedia, 2014a].

Figure 2.2: Communication between neurons.

The action potential is induced and propagated by ionic exchanges in the membrane of the neuron. The three important ions that are involved in the ionic transmembrane currents are Na^+ , K^+ and Ca^{2+} , and these ions move across the membrane through ionic channels. There are two forces responsible for the membrane voltage: the diffusion force and the electrical potential gradient. On the one hand, the diffusion forces induce the ions to flow from the high concentration medium to the medium where there is a lower concentration in these ions. On the other hand, the electrical potential gradient created by the accumulation of positive and negative charges in the extracellular and intracellular media opposes the diffusion of ions across the membrane. When the diffusion force of a certain ionic species is canceled by electrical force, the membrane voltage is called the Nernst equilibrium potential for this ionic species.

An action potential in a neuron is elicited because the kinetics of the different ionic channels are very different in their time scale.

An ionic channel is controlled by gates, and depending on the states of these gates the channel can itself be either open or closed. The state of a channel can depend on the membrane potential (in the case of a voltage-gated channel), or on intracellular agents, like Ca^{2+} -dependent K^+ channels, or on extracellular agents.

Figure 2.3 illustrates the example of a voltage-gated sodium channel. The channel has

two gates: an activation gate and an inactivation gate. For the channel to be open, both the activation gate and the inactivation gate must be in the open state; in this case the ions can flow down their electrochemical gradient. On the other hand, if the activation gate is in the closed state, the channel will be closed too, while if the activation gate is open but the inactivation gate is closed, the channel is also closed.

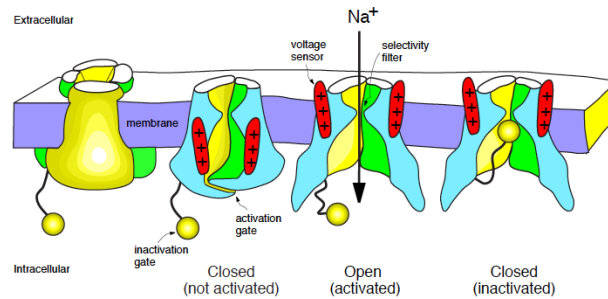


Figure 2.3: A voltage-gated sodium channel [Izhikevich, 2007].

Activation of ion channels is at the root of the mechanism of the action potential generation in a neuron (see in Figure 2.2(b) again). In general, a neuron has a voltage-gated sodium channel which presents a fast activation and a slow inactivation gate and a voltage-gated potassium channel with a slow activation kinetic.

A stimulation strong enough will induce an increase in the membrane voltage slightly higher than the activation threshold of the sodium channel. The sodium channel will then activate and the sodium ions will be able to cross the membrane from the extracellular medium to the intracellular medium. Thus the membrane potential continues to increase until the potassium activation gate is open. Moreover, the sodium inactivation gate tends to the closed state. The potassium ionic concentration is increasing in the extracellular medium and the membrane voltage is decreasing: this is the repolarization stage. After that, the potential is near the rest potential but the potassium current continues to decrease the potential because the sodium inactivation gate and the potassium activation gate have slower kinetics. Furthermore, as the voltage V is reducing, the sodium inactivation gate begins to open and the potassium activation gate begins to close after a time. Finally, the neuron returns to rest.

Generally a neuron does not fire just once but there exists a particular pattern in its activity. Different neurons lead to different types of firing patterns.

The signalling information of a neuron is actually stored in the pattern of its firing activity. Information can be encoded in the frequency of the action potentials, the type of spiking activity (Is it a periodical train of simple spikes? Is there a quiescent period between the simple spiking?) and the switching between different types of firing patterns. Neuronal degeneration will often affect the firing patterns. As a consequence, a change in firing pattern can sometimes lead to the molecular mechanism responsible for the neurodegeneration.

2.2 State of the art in computational neuroscience

2.2.1 Hodgkin-Huxley model

In the fifties, Hodgkin and Huxley [1952] obtained the Nobel Prize for their brilliant discovery. They studied the squid giant axon and found that its electrical activity could be modelled by an electrical circuit. This circuit represents the ionic exchanges in the active membrane of the axon. This discovery is general and founded modern neuroscience. It applies to any type of neuron. Indeed, every neuron can be modelled by an electrical circuit which contains the ionic currents that play an important role in the cell activity. A model of a neuron including the most important ionic currents is called a conductance-based model. Figure 2.4 illustrates the circuit representation of a neuron with the three ionic currents of Hodgkin-Huxley model : a sodium current, a potassium current and a leak current accounting for all remaining ion channels.

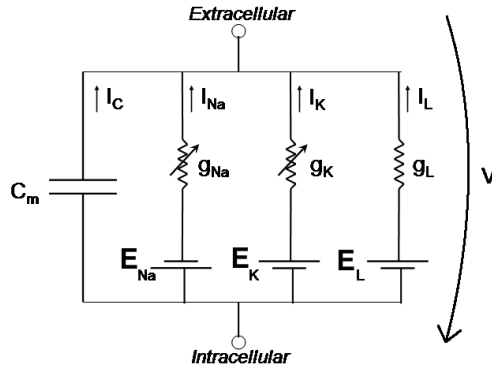


Figure 2.4: A conductance-based model.

The circuit can be converted into a mathematical model whose solutions reproduce the action potential generation in a neuron. The evolution of the membrane potential obeys the law of an RC circuit :

$$C_m \dot{V} = - \sum_i I_i(V, t) + I_{app} \quad (2.1)$$

where

- V is the membrane potential,
- $I_i(V, t)$ is an ionic current of type i ,
- I_{app} is the total outward current.

By convention, an inward current is negative whereas an outward current is positive. Generally, the potassium current is outward and the sodium and calcium currents are inward.

Most of time, the currents are voltage and time-dependent. Thus the current densities are modelled by the product of a variable conductance and a difference of potentials :

$$I_i = g_i(V, t) (V - E_i) \quad (2.2)$$

where E_i [mV] is the Nernst equilibrium potential of the channel i , which means the potential where diffusion and electrical forces are counter-balanced, V [mV] is the membrane potential and $g_i(V, t)$ [mS/cm²] is the variable conductance of the channel i .

The conductance is a function of the membrane potential and time because its expression depends on the activation and inactivation variable that reproduce the kinetic of the activation and inactivation gates of a channel. The variable conductance of a channel is typically expressed by an equation such as

$$g_i(V, t) = \bar{g} m_i^a h_i^b. \quad (2.3)$$

In this expression, \bar{g} represents the maximal conductance of the channel whereas m is the activation variable and h is the inactivation variable. They model the probability that an activation gate or an inactivation gate respectively is in the open state. The exponent represents the number of activation gates or inactivation gates in the channel. Moreover, these variables depend on time and their dynamics can be described by a first-order differential equation:

$$\dot{m}_i = \frac{m_{\infty,i}(V) - m_i}{\tau_{m_i}(V)} \quad \text{et} \quad \dot{h}_i = \frac{h_{\infty,i}(V) - h_i}{\tau_{h_i}(V)}. \quad (2.4)$$

Those models capture the steady-state voltage dependence of the conductance, with monotone curves $m_{\infty,i}(V)$.

Hodgkin and Huxley model includes only three types of currents: a sodium current, a potassium current and a leak current. This last current represents the passive ionic exchanges like for the Cl^- ions. The Hodgkin-Huxley model is given by

$$\begin{cases} C_m \dot{V} &= I_{app} - \bar{g}_K n^4 (V - E_K) - \bar{g}_{Na} m^3 h (V - E_{Na}) - g_{Leak} (V - E_{Leak}), \\ \tau_n(V) \dot{n} &= n_{\infty}(V) - n, \\ \tau_m(V) \dot{m} &= m_{\infty}(V) - m, \\ \tau_h(V) \dot{h} &= h_{\infty}(V) - h, \end{cases} \quad (2.5)$$

where n is the potassium channel activation variable, m is the sodium channel activation variable and h is the sodium channel inactivation variable. $n_{\infty}(V)$, $m_{\infty}(V)$ and $h_{\infty}(V)$ are sigmoid functions of the membrane potential, while the time constants $\tau_n(V)$, $\tau_m(V)$ and $\tau_h(V)$ are unimodal functions of the membrane potential. The steady-state activation functions and the time constants of the Hodgkin-Huxley model are illustrated in Figure 2.5.

We can immediately observe that the sodium activation gate has a fast dynamic, by contrast to the potassium activation and the sodium inactivation. A standard approximation is to consider that the sodium activation is instantaneous and to put it at steady-state such that $m(V) \simeq m_{\infty}(V)$. Moreover, a good empirical assumption is $h \simeq 1 - n$. Indeed, for reducing a model we remove one variable by expressing it in function of another. We can do this easily if we have two variables for which the time constants are approximately equal. Since if $\tau_n \simeq \tau_h \simeq \tau$, then we look for a function $F(n(V)) = h(V)$ such that

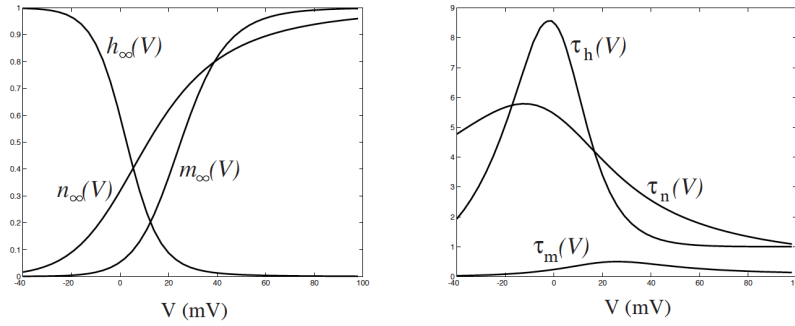


Figure 2.5: Steady-state activation variables and time constants [Izhikevich, 2007].

$$\tau \dot{h} = h_\infty(V) - h \quad (2.6)$$

is still satisfied. It is the case if the function F satisfies the relation

$$F(n_\infty(V)) = h_\infty(V) \quad (2.7)$$

$$\Leftrightarrow (F \circ n_\infty)(V) = h_\infty(V) \quad (2.8)$$

$$\Leftrightarrow F(x) = (h_\infty \circ n_\infty^{-1})(x). \quad (2.9)$$

In our example, we have approximately $h_\infty(V) \simeq 1 - n_\infty(V)$ with $\tau_h \simeq \tau_n$ (same order of magnitude), as one can observe in Figure 2.5.

These simplifications provides a two-dimensional reduction of the model, leading to the phase portrait shown in Figure 2.6. A phase portrait is a graph of a two-dimensional system in which an arrow is attached to each point of the state space and the integral curves of the vector field are sketched. An integral curve of the vector field is a trajectory. Moreover, drawing a phase portrait means plotting the nullclines of the system because the intersections of these curves give the equilibria of the system. Mathematically, the differential equations

$$\begin{aligned} \dot{x}_1 &= f_1(x_1, x_2) \\ \dot{x}_2 &= f_2(x_1, x_2) \end{aligned} \quad \Leftrightarrow \quad \dot{\underline{x}} = f(\underline{x}) \quad (2.10)$$

describe a two-dimensional system whose the state is the vector $\underline{x} = (x_1, x_2) \in \mathbf{R}^2$. $f : \mathbf{R}^2 \rightarrow \mathbf{R}^2$ is the vector field. It assigns an arrow (\dot{x}_1, \dot{x}_2) to each point (x_1, x_2) in the plane. Furthermore, the nullclines of the system are the loci of zero slope, which means that the two nullclines of the system are the curves $\dot{x}_1 = 0$, on the one hand, and $\dot{x}_2 = 0$, on the other hand. Hence the fixed points of the system (the equilibria) are the points satisfying $\dot{\underline{x}} = 0$.

Figure 2.6 illustrates the nullclines of the system for the two-order reduction of Hodgkin-Huxley model. The reduced model is

$$\begin{cases} C_m \dot{V} &= I_{app} - \bar{g}_K n^4 (V - E_K) - \bar{g}_{Na} m_\infty(V)^3 (1 - n) (V - E_{Na}) - g_{Leak} (V - E_{Leak}), \\ \tau_n(V) \dot{n} &= n_\infty(V) - n, \end{cases} \quad (2.11)$$

and the nullclines are

$$\begin{cases} 0 &= I_{app} - \bar{g}_K n_\infty(V)^4 (V - E_K) - \bar{g}_{Na} m_\infty(V)^3 (1 - n_\infty(V)) (V - E_{Na}) - g_{Leak} (V - E_{Leak}), \\ n &= n_\infty(V). \end{cases} \quad (2.12)$$

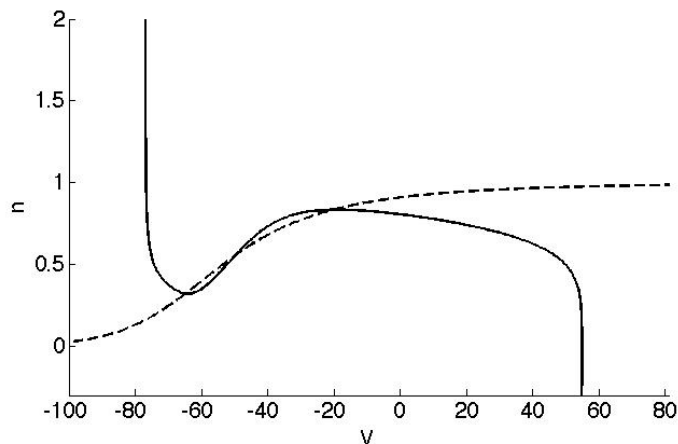


Figure 2.6: Nullclines of the reduced Hodgkin-Huxley model in the phase plane (V, n) .

2.2.2 A novel phase portrait for neuronal excitability

The significant role of the calcium in the firing activity of a neuron is well accepted by the scientific community. However, the classical conductance-based models, like Hodgkin-Huxley or FitzHugh-Nagumo model, do not include any calcium current.

Drion et al. [2012] showed that including a calcium current in the Hodgkin-Huxley model results in a different phase portrait. The difference between the Hodgkin-Huxley phase portrait and the novel phase portrait is shown in Figure 2.7(a). These phase portraits were obtained by reducing the complex conductance-based models. Without reduction, the analysis of a conductance-based model can be very complex for a neuron which can switch between different types of excitability in function of environmental parameters. The transcritical bifurcation appears now in the physiological part and plays an important role in neuronal excitability.

By considering the calcium current, we obtain a more realistic model of the firing activity observed for many important neurons like thalamocortical neurons. As illustrated in Figure 2.7(b), a step of applied current generates a spike train in both models but, for the new phase portrait, the temporal trace reproduces some patterns typical of thalamocortical neurons where the presence of calcium channels is well-known. These distinct features, illustrated in Figure 2.7(b), are :

- the latency observed just before the spiking activity,
- the plateau potential thanks to which the rest state is lower than the lowest level of an action potential,

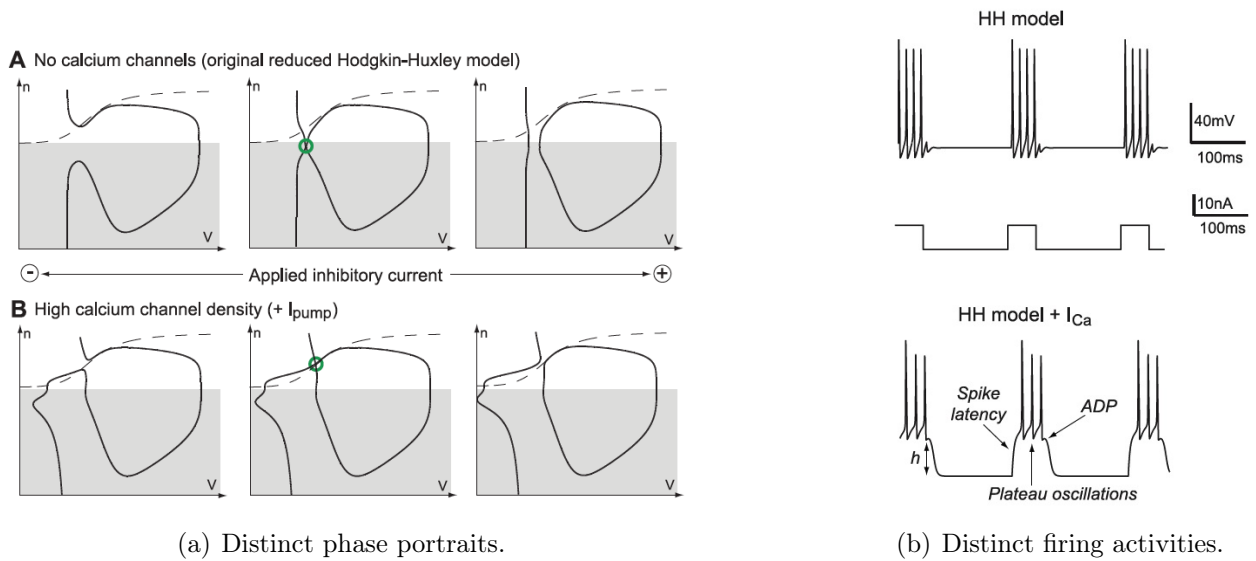


Figure 2.7: A distinct phase portrait by addition of calcium current [Drion et al., 2012].

- the after depolarizing potential which is a small potential increase observed at the end of the spiking activity.

An important observation can be made about Figure 2.7(b). If we added an adaptation variable to this new model to represent the variation of calcium concentration or the slower inactivation of calcium channel, the phenomenon of burst is observed with a constant applied current. A bursting behaviour is made up of periodical simple spike trains separated by quiescent period. The Thalamocortical neurons contain calcium channels and exhibit two types of firing pattern; either a continuous regular spiking or a plateau burst spiking. The novel phase portrait permits to reproduce this second type of behaviour. Thus it is a good model for bursting behaviour.

In conclusion, the discussion above illustrates that important signalling patterns can be understood by including the calcium currents in Hodgkin-Huxley model. Moreover some channels depend on the calcium concentration, like calcium-dependent potassium channels, so this type of current is important to consider when we establish a model of a neuron. Their influence is significant in the results we can obtain by modelling.

Besides, these results allow one to show the existence of two other types of excitability, in addition to the three already stated by Hodgkin (Type I, II and III). The resulting five types of excitability are shown in Figure 2.8: the temporal traces and the corresponding phase portraits are drawn for an applied current sufficiently large to cross the transcritical bifurcation in the parameter space.

We now detail the five types of excitability represented in Figure 2.8. The first type is a low frequency firing because there is a saddle-node on invariant circle bifurcation elicited by the applied current. It makes a limit cycle to appear whereas the saddle merges with the node and, then, disappears. The limit cycle has a large amplitude which does not change with the current amplitude. The second type exhibits higher frequency and small ripple oscillations at

the end. The reason for these oscillations is explained by the phase portrait. Indeed, there is only one stable node at the beginning. When the applied current is increasing, the stable node loses its stability and a limit cycle is created. The amplitude of the limit cycle increases with the applied current: it is a Hopf bifurcation. The third type of excitability is just a simple spike because the node keeps its stability, the effect of the current step is just to increase the potential of the resting state.

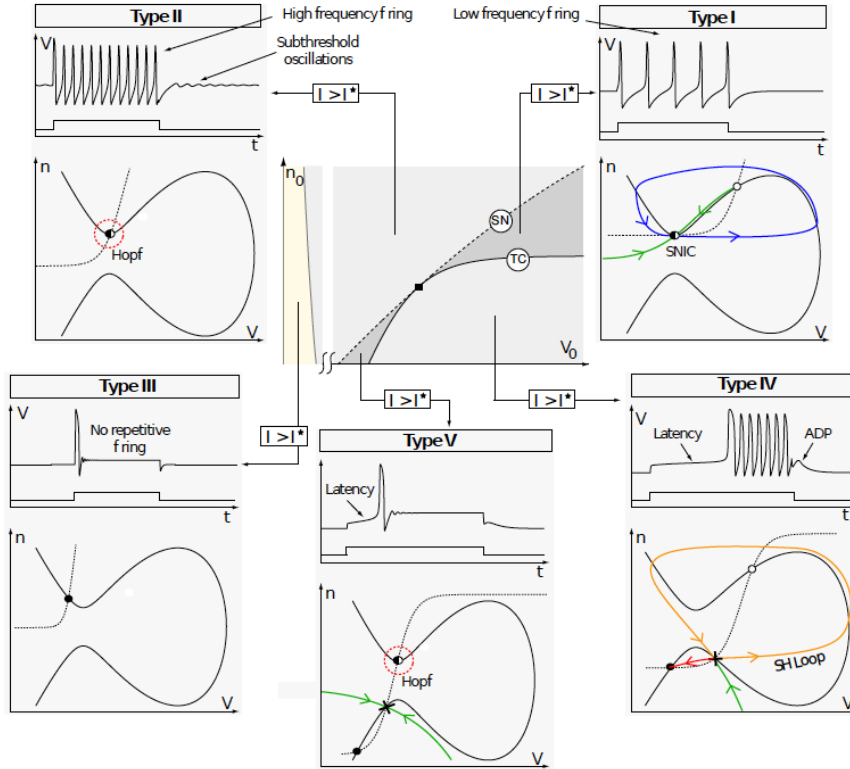


Figure 2.8: Types of excitability [Franci et al., 2012].

About the two other types of excitability, we see in Figure 2.8 that the mirrored part of the classical FitzHugh-Nagumo phase portrait plays a role. Indeed, the fourth type exhibits three fixed points : a stable node, a saddle node and an unstable focus. When a current is applied, a limit cycle appears because of a saddle homoclinic bifurcation. If the current is increasing, there will be a saddle-node bifurcation. The saddle-node disappears and now there is only an unstable focus with a limit cycle. However, the disappeared saddle-node has still an effect on the excitability : it induces a latency before the spiking. This is referred to as a “ghost” phenomenon. A plateau potential exists because the potential of the resting state is lower than the lowest potential in the limit cycle. The after depolarization potential is induced after the current pulse because the potential follows the left branch of the V-nullcline to come back to the resting state, so there is a small increase in amplitude before the repolarization. The fifth type shows a bistability too, which can be either between a down stable state and an up stable state or a limit cycle.

2.2.3 Regenerativity vs restorativity

The important physiological difference between the two phase portraits discussed in the previous section can be understood from the distinct feedback nature of distinct ionic currents. The transcritical bifurcation in Figure 2.7(a) occurs at the balance between restorative and regenerative variables [Drion et al., 2013]. A restorative channel provides a negative feedback whereas it is a positive feedback for a regenerative channel.

A conductance-based model is composed of ionic currents that have distinct time scales and can be either regenerative or restorative. It is possible to obtain an abstract model with the same temporal features by aggregating the variables in three different time scales: a fast and regenerative scale \bar{g}_f for the depolarization, a slow scale \bar{g}_s which contains restorative and regenerative currents and an ultraslow scale \bar{g}_{us} . Generally, the slow restorative channels are useful for the repolarizing stage whereas the slow regenerative channels play a role near the resting potential and are responsible of bistability. Moreover, the bursting behaviour can be shown up because of adaptation in the ultraslow scale, which regulates the intraburst frequency.

For instance, the classification procedure for a STG (stomatogastric ganglion) neuron is represented in Figure 2.9.

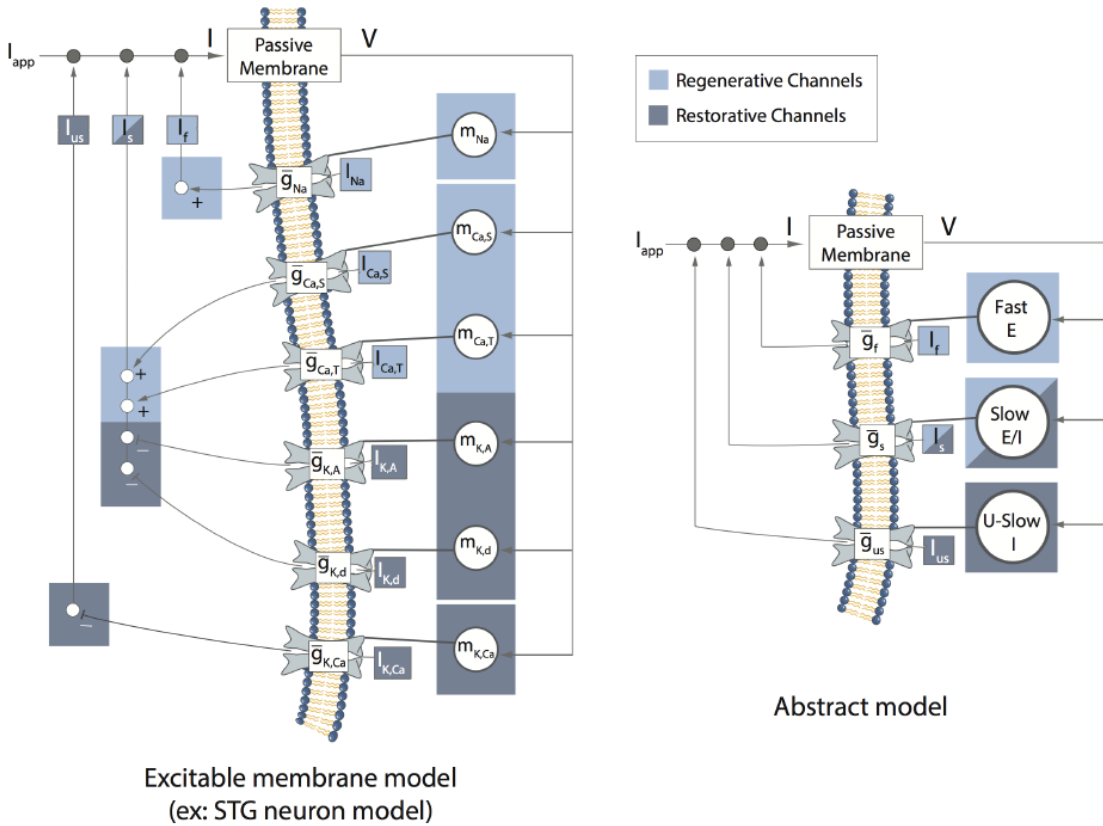


Figure 2.9: Classification of regenerative and restorative channels between three types of time scales [Drion et al., 2013].

Drion et al. [2013] showed some interesting conclusions for the STG neuron which can be applied more generally.

If we change the maximal conductance of a slow regenerative current, a slow restorative current and the ultraslow scale simultaneously, we can conserve the same behaviour and keep the same \bar{g}_s in the abstract model because the net slow feedback gain has kept the same contribution than before the modification. It illustrates the robustness property of the model which is a characteristic that exhibits the neuronal spiking. We observe in Figure 2.10 the influence of changing simultaneously a potassium current, a calcium current and a calcium-dependent potassium current. The time scale of these currents are slow and restorative, slow and regenerative and ultraslow restorative respectively. It is clearly shown that the spiking behaviour does not change despite the imposed conductance variations.

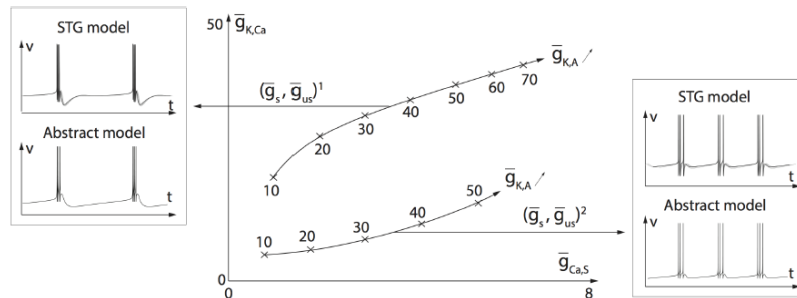


Figure 2.10: Robustness property [Drion et al., 2013].

Another feature of neuronal firing is the modulation property, illustrated in Figure 2.11. It means that changing one parameter (a maximal conductance) could completely modify the type of spiking like to switch from a simple spike train to a burster¹. Moreover, the modulation characteristic permits to keep the sort of spiking but to change in the same time its patterns like the frequency or the amplitude of the spikes.

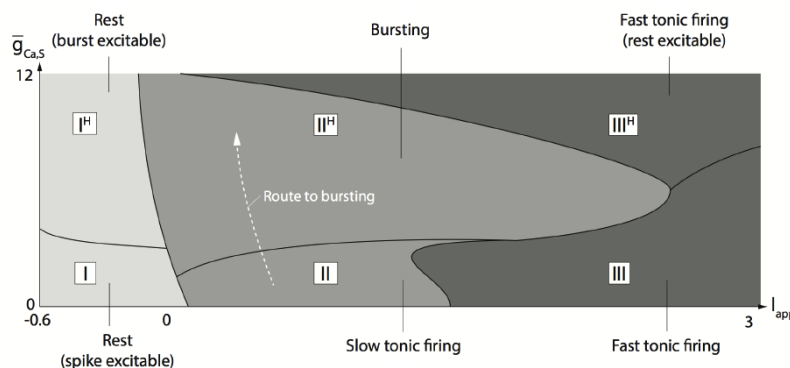


Figure 2.11: Modulation property [Drion et al., 2013].

¹A burster is a neuron that exhibits a bursting behaviour. It means that the electrical behaviour is a periodical spiking activity interrupted by quiescent period.

In conclusion, a model which exhibits robustness and modulation properties is a very good result to obtain. Indeed, on one hand, we keep the same spiking behaviour in a certain range of the maximal conductances ; the neuronal model is not too sensitive. On the other hand, the model can switch smoothly between a spiking behaviour to another by conductance variation large enough. The spiking behaviour of a neuron is obtained by a certain balance between slow restorative channels, slow regenerative channels and ultraslow scale.

Chapter 3

Physiology of Purkinje cells

This chapter aims at introducing the targeted neuron; the Purkinje cell.

First of all, we talk about the cerebellum in which this type of neurons are localized. It is also stated which roles the cerebellum plays in the brain functioning.

Then, there are a lot of reasons to continue researches about this brain area and some of them are explained below.

After that, we will precisely focus on the Purkinje cell, because it is its neuron electrophysiology we want to model. The state of the art has to be presented: two points of view are necessary; a physiological view and a computational view. Indeed, there are a lot of experimental results about the ionic currents, the bistability and the synaptic solicitations that have been obtained to date for the Purkinje cell. On the other side, many researches about Purkinje cell models have been carried out. It is important to talk about both subjects before beginning our modelling.

3.1 The cerebellum

3.1.1 Anatomy

The cerebellum is a brain area (see in Figure 3.1) involved in the motor control and in some cognitive tasks like language, memory, attention, ...

Its main function is about the tactic of the movement: the cerebellum, associated with the motor cortex, monitors the accurate sequence of actions, in time and space, required to achieve the movement smoothly and accurately. There are two other important parts of the brain involved in motor control. On the one hand, the association areas of neocortex and basal ganglia are involved in motor planning: what is the goal of the movement and what is the best way to accomplish it? On the other hand, the final task, which means the movement execution, is executed by the brain stem and the spinal cord. They interact directly with the cerebellum through a number of control loops.

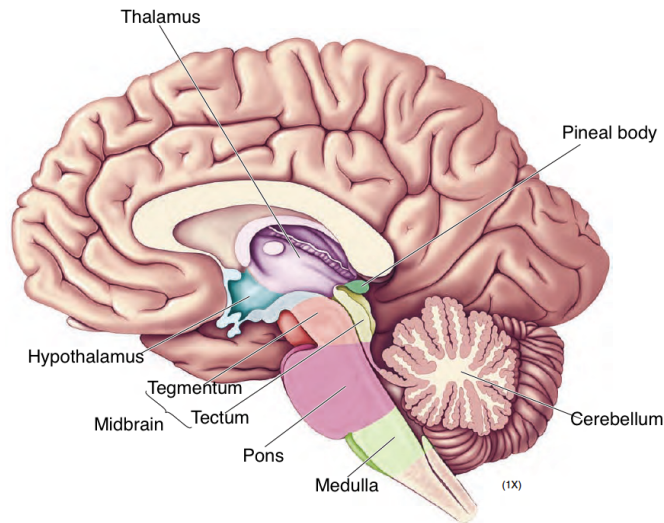


Figure 3.1: The brain [Bear et al., 2007].

In particular, there is one motor control loop involving the three hierarchical levels discussed above (strategy, tactic and execution), and there are some correction stages in the interaction between the spinal cord and the cerebellum.

Figure 3.2 is useful to explain the main feedback principle involving the cerebellum. We observe that the cortex interacts directly with the cerebellum and with the basal ganglia. They communicate with the cerebellum via the thalamus. There are two distinct feedback loops: one between the cortex and the cerebellum via the thalamus and one between the cerebellum and the spinal cord via the brain stem or the thalamus. The main function of this symmetrical structure between the midbrain/cerebral cortex is to relay motor/sensory information for the cerebral cortex.

The anatomy of the cerebellum (Figure 3.3) is mainly composed of the pontine nuclei, the deep cerebellar nuclei and the cerebellar cortex. Most of the inputs to the cerebellar cortex come from the pontine nuclei cells whereas the main output is localized in the deep cerebellar nuclei. The brain area that is particularly interesting in the context of this thesis is the cerebellar cortex (Figure 3.4) because it contains the Purkinje cells.

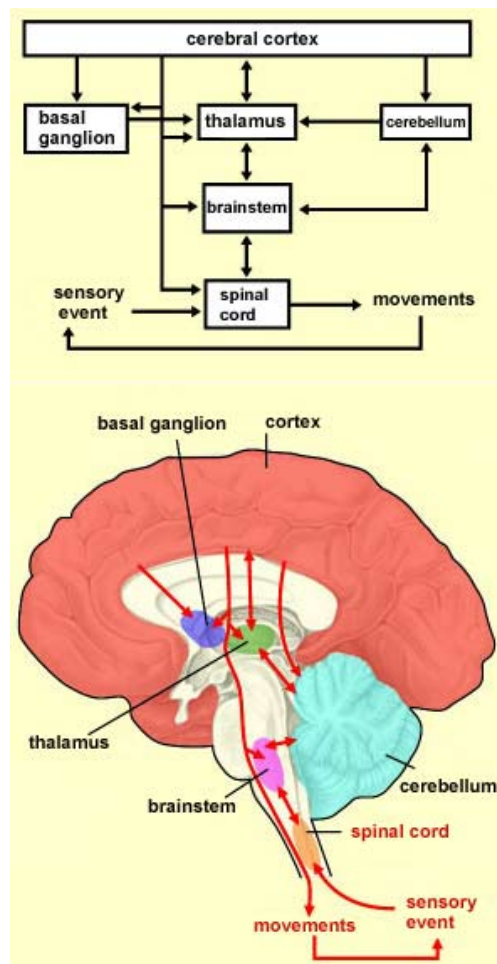


Figure 3.2: Motor loop through the cerebellum [Mot, 2002].

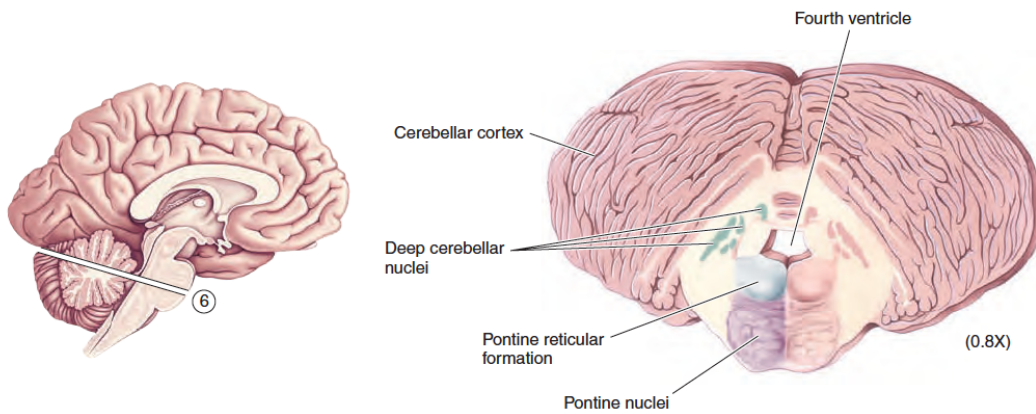


Figure 3.3: The cerebellum anatomy [Bear et al., 2007].

The Purkinje cells and the granule cells play a very important role in the cerebellum. The Purkinje cells send inhibitory inputs, via GABA neurotransmitters, to the deep cerebellar nuclei whose emerging fibres represent the main outputs of the cerebellum. Thus, these neurons and their activity are critical in the motor circuit.

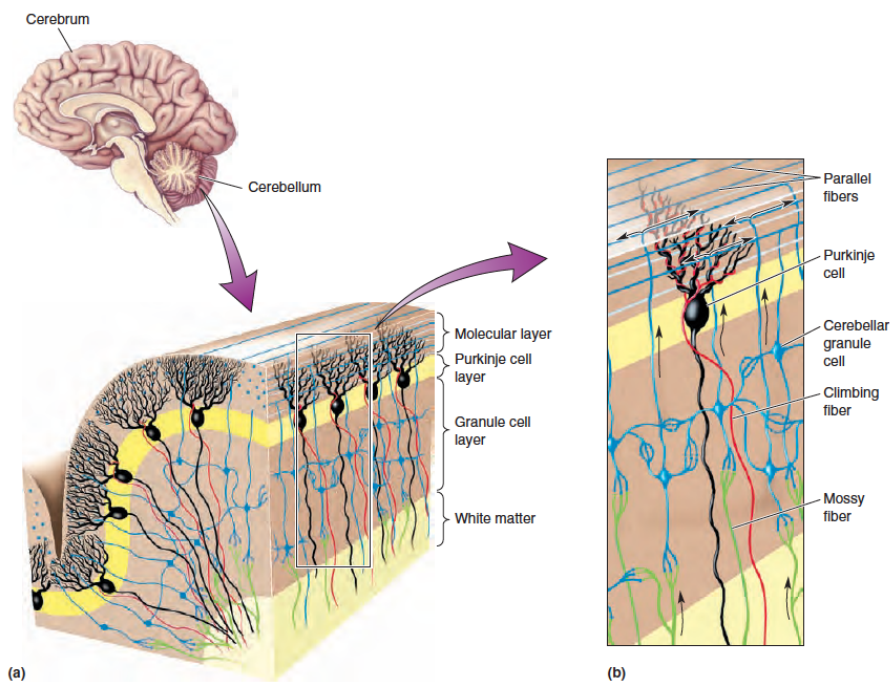


Figure 3.4: The cerebellar cortex [Bear et al., 2007].

The cerebellar cortex is composed of three layers: the granule cell layer, the Purkinje cell layer and the molecular layer in which the dendrites of the Purkinje cells extend. As for the white matter, it contains the deep cerebellar nuclei and so the output of the cerebellum.

We discussed, above, the functional motor control loop. Figure 3.5 illustrates a cellular view of the feedback in the cerebellar activity.

The two inputs of the Purkinje neurons are one climbing fibre and many parallel fibres.

More precisely, we have the mossy fibres that excite the granule cells. The granular axon, called parallel fibre, synapses at right angles with the dendritic spines covering the Purkinje cell dendrites. Moreover, these mossy fibres excite directly the deep cerebellar nuclei cells.

On the other hand, the climbing fibres are fibres coming from the inferior olivary nucleus ; this nucleus in the olivary body (part of a brain stem portion: the medulla oblongata) receives inputs from the cerebrum, the cerebellum and the spinal cord and sends signals to the cerebellum only via the axons of olivocerebellar fibres which make allusion to the climbing fibres when they penetrate into the cerebellum. A Purkinje cell is solicited by only one climbing fibre but this climbing fibre creates a lot of excitatory synapses with the dendritic tree of the neuron. The climbing fibre activation elicits what is called a complex spike. Furthermore, the climbing fibres can reach directly the deep cerebellar nuclei.

Each Purkinje cell receives more than 100,000 inputs from parallel fibres but only one input from one climbing fibre. However the climbing fibre wraps around the dendritic tree of the Purkinje neuron and makes a total of up to 300 synaptic contacts [Wikipedia, 2014b]: it implies that the net input provided by the climbing fibre is enough strong to generate an action potential.

The interneurons in the cerebellar circuit include the basket cells and stellate cells in the molecular layer and the Golgi cells. An interneuron is a relay neuron that inhibits or excites in a local way. For instance, the stellate cells inhibit directly the smooth dendrites whereas the basket cells have an inhibitory role on the soma [Eccles et al., 1966, Barmack and Yakhnitsa, 2008].

3.1.2 Scientific and clinical motivations to study Purkinje cells

Firstly, it is interesting to establish models about cerebellar cells to obtain a better understanding of cerebellar dysfunction and diseases. Most of the time, a dysfunction in the cerebellum will involve a loss of accuracy and timing in the execution of the movement; the movement generation is preserved but the motor control is affected. Depending on the cerebellar area that is damaged, the symptoms are different; for instance, a dysfunction of the cerebellar

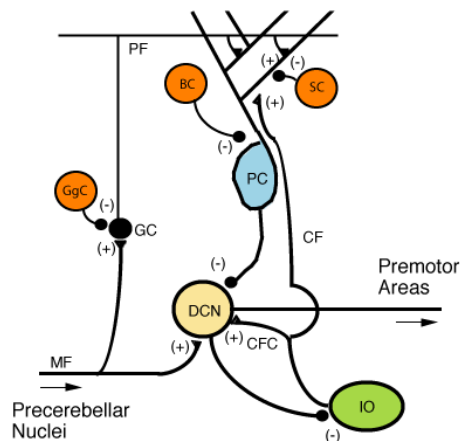


Figure 3.5: Microcircuitry of the cerebellum. (+): excitatory; (-): inhibitory; MF: Mossy fiber; DCN: Deep cerebellar nuclei; IO: Inferior olive; CF: Climbing fiber; GC: Granule cell; PF: Parallel fiber; PC: Purkinje cell; GgC: Golgi cell; SC: Stellate cell; BC: Basket cell [Wikipedia, 2014b].

lateral hemispheres causes an inability to judge distances and to perform rapid alternating movements. A well-known disease is the Ataxia which is responsible for various symptoms in the loss of coordination and can imply other parts of the brain than the cerebellum, like the thalamus or parietal lobes. A lot of research is devoted to the disorders of the cerebellum (e.g. [Schmahmann, 2004, Zhuchenko et al., 1997]). Moreover, some abnormal changes in Purkinje cell activity could explain cerebellar dysfunctions, which motivate the study of these cells which have a dominant role in the cerebellum [Walter et al., 2006, Sausbier et al., 2004].

Secondly, the Purkinje cell is one of the first neurons discovered and studied in the brain in 1837 by Jan Purkinje. It is easily recognizable because of its dendritic tree that is very extended and flattened, as illustrated in Figure 3.6. However, the electrophysiological behaviour of the Purkinje cell is still not completely understood to date. In particular, the bistability observed in these neurons is difficult to explain for the biologists and the physiologists. The climbing fibre input resulting in a “ complex spike ” and the different way to switch between the two states lead to many research questions. With the help of mathematical modelling and non-linear system theory, we can hope to contribute to a better understanding of the functional role of the Purkinje cells and the cerebellum and thus to know which type of communication is underlined by the firing properties of a Purkinje cell.

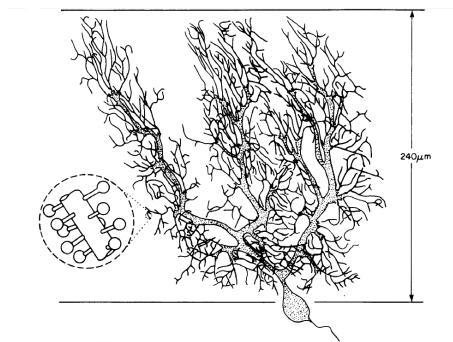


Figure 3.6: Morphology of a rat Purkinje cells [Shelton, 1985].

The cerebellum is also involved in learning tasks because there is a correction stage when the movement is imperfectly achieved. Purkinje neurons seem responsible for the cerebellar learning and motivate a lot of current research in this area [Gilbert and Thach, 1977, Feil et al., 2003, Wetmore et al., 2014]. Indeed, a memory or a learning process can result from synaptic plasticity and a Purkinje cell exhibits this mechanism, which means that a Purkinje cell synapse could strengthen or weaken as a function of their activity. The plasticity is exhibited in these neurons when the climbing fibres and parallel fibres are stimulated simultaneously. More precisely, the post-synaptic response to the activation of parallel fibres alone is smaller after this pairing stimulation than before it. This phenomenon is referred to as long-term depression: “ long-term ” because it lasts from minutes until hours and “ depression ” because of the reduction in synaptic response (loss of excitability). Furthermore, the Purkinje neuron exhibits an increase in the calcium concentration when it exhibits long-term depression.

3.2 Electrophysiology of Purkinje cells

In 1837, Johannes Evangelist Purkinje discovered the Purkinje cell. More than a century of research has significantly advanced the understanding of its role in the brain but many questions remain, notably about its particular electrophysiology.

3.2.1 State of the art in electrophysiology

Bistability is the coexistence of a stable up-state and a stable down-state. The cell can remain in either of the two states and stay at this state until a strong enough external stimulus switches the neuron to the other state.

Purkinje cells exhibit an intrinsic bistability, both in vitro [Llinas and Sugimori, 1980a, Williams et al., 2002] and in vivo [Loewenstein et al., 2005]. However, this bistable mechanism is not well understood to date. There are a lot of experiments that have been realized to improve the understanding of this behaviour. Many ionic currents that play a role (important or not) in the electrical activity of a Purkinje cell have been identified but to understand the mechanism of bistability we have to identify which currents are really important to create the switch between the two states and the stability of both states. Mathematical modelling may help to address this challenge.

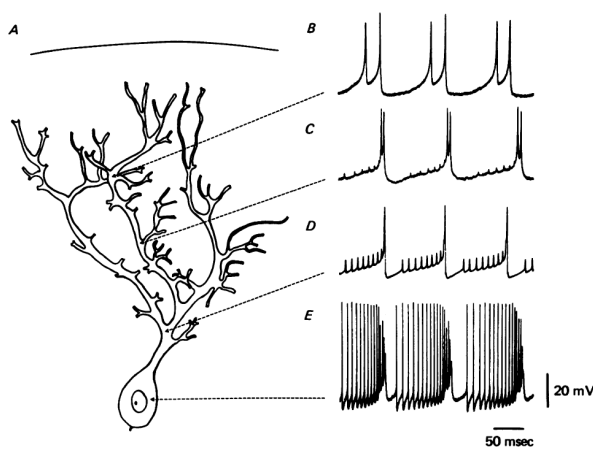


Figure 3.7: Somatic and dendritic action potentials of a guinea pig Purkinje cell following DC depolarization [Llinas and Sugimori, 1980b].

In 1980, Llinas and Sugimori [1980a,b] showed that Purkinje cells in vitro fire in response to a depolarizing current (Figure 3.7) and spontaneously. The result of a depolarizing current depends on its duration and its strength. Indeed, as we can observe in Figure 3.8, a short pulse of current produces a repetitive firing of fast spikes with spike latency and after-depolarization potential. As the pulse amplitude is increased, the firing frequency increases and, after having reached a current threshold, the after-depolarization period exhibits repetitive firing too. Moreover, with a long pulse of small amplitude, the behaviour is similar than that observed for a short pulse. An increase in the amplitude involves a burst (“dendritic spike burst”) : it is preceded by a decrease in the amplitude of fast spikes (“somatic spikes”) and followed

by repetitive firing whose spike amplitude is decreasing, and so on until the end of the pulse. The higher is the current amplitude, the larger is the number of bursts.

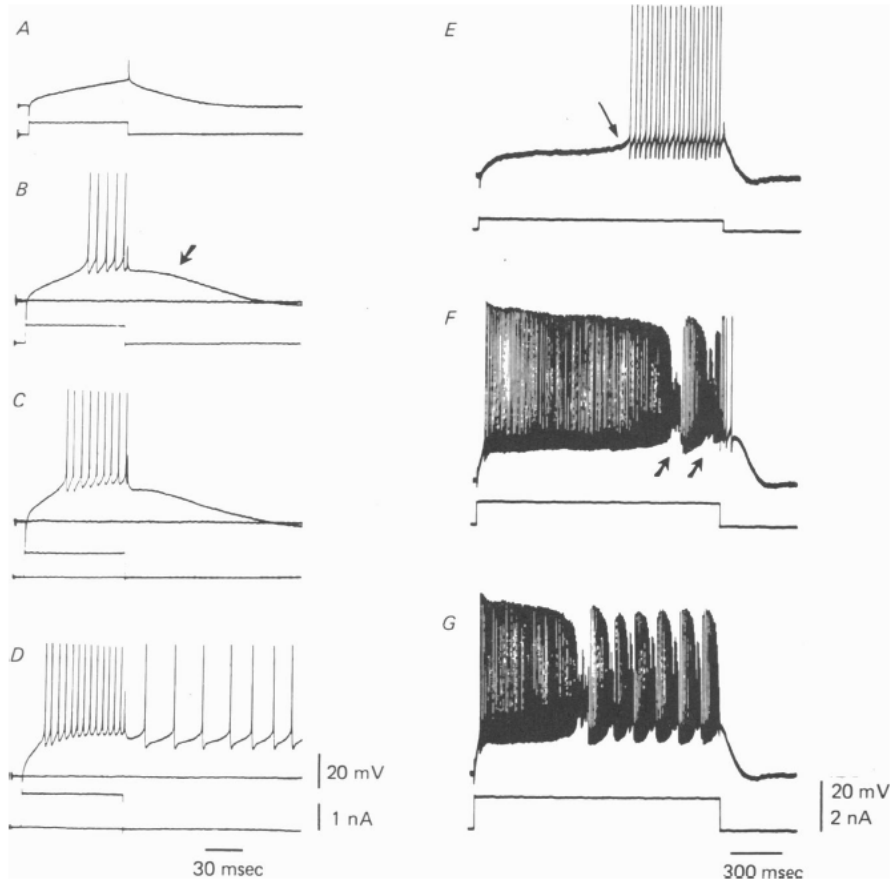


Figure 3.8: Somatic firing resulting of a DC depolarization for a guinea pig Purkinje cell : In A-D short current pulse is injected, whereas long-duration current experiments are shown in E-G [Llinas and Sugimori, 1980a].

Additionally, Llinas and Sugimori [1980a] showed the existence of spontaneous firing activity. Indeed, in the absence of stimulation, similar behaviours can be observed.

Spontaneously the cell switches between a quiescent state and a firing state, at which there are repetitive fast spikes and bursts, as it is shown by the experimental traces in Figure 3.9. The quiescent state is the down-state and the firing level represents the up-state. The Figure 3.9(a) shows the firing state whose duration is about five seconds (it can be longer; until 15 seconds) whereas the down level is maintained for the same duration. More precisely, the up state is made up of a bursting and fast spiking alternating, as it is illustrated in Figure 3.9(b). The firing level looks like the bursting behaviour observed in Figure 3.8 with an applied depolarizing current in the soma.

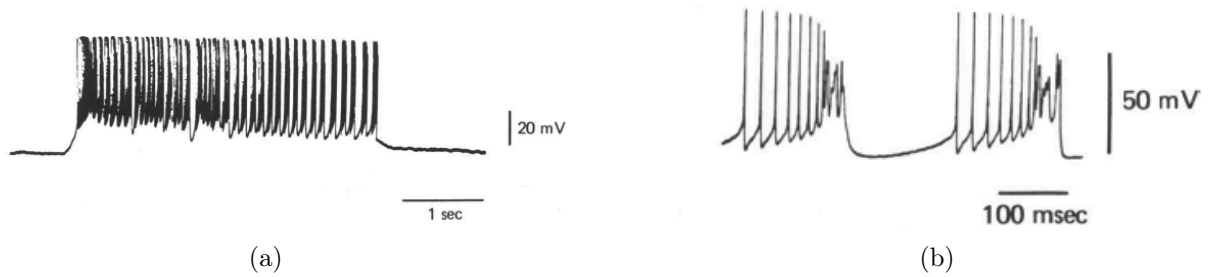


Figure 3.9: Spontaneous repetitive activation of guinea pig Purkinje cells [Llinas and Sugimori, 1980a].

About the currents responsible for the firing pattern, the presence of a fast sodium current and a slow potassium current in the Purkinje neuron explains the ability of the cell to fire. Moreover, as the electrical responsiveness is kept for a blockage of Na channels, it means that there exist voltage-activated calcium conductances. They produce the dendritic spike bursts because in absence of Na conductances, the bursts are maintained whereas the somatic spikes are removed. It is likely that it is the interaction of a calcium current and a calcium-dependent potassium current which makes the dendritic spike burst (d.s.b.) response. Furthermore, when calcium channels are blocked, a plateau potential is reached and this pattern indicates the presence of an inactivating sodium current.

Obviously there are a lot of other examples of in vitro recordings. For instance, Rapp et al. [1994] studied the Purkinje cell physiology in vitro too. The intracellular recordings obtained for this paper are very similar to those of Llinas and Sugimori [1980a] as we can see in Figure 3.10.

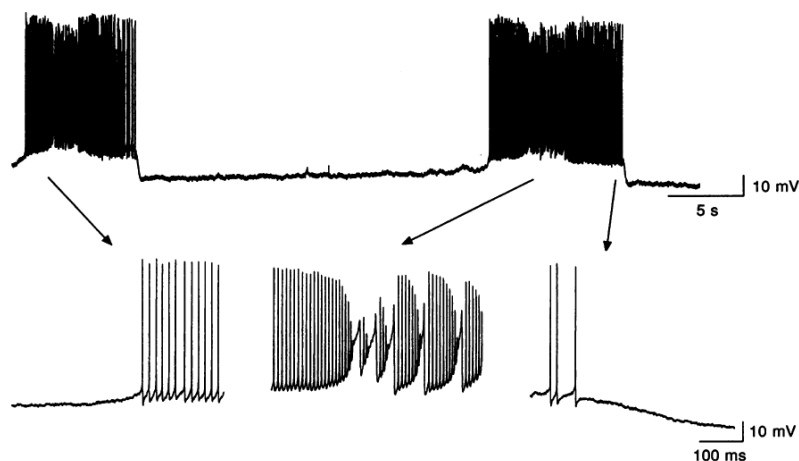


Figure 3.10: Intracellular recording of a guinea pig Purkinje cell [Rapp et al., 1994].

Currently it is well known that Purkinje cells exhibit intrinsic bistability both in vitro and in vivo. Indeed, Loewenstein et al. [2005] demonstrated this property in 2005: Purkinje cells in vivo show fluctuations between two distinct states: a quiescent and hyperpolarized state and a depolarized and spiking state. Researchers tend to find which currents are really the

basis of this intrinsic feature of Purkinje neuron. The spontaneous transitions between the two levels are illustrated in Figure 3.11.

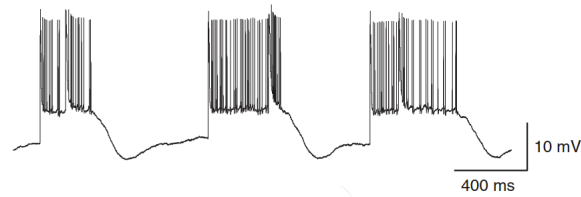
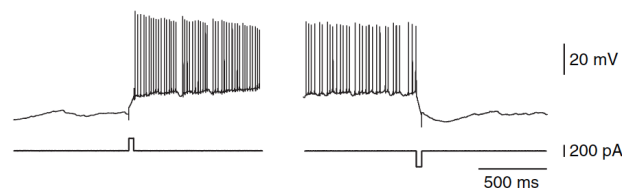


Figure 3.11: Whole-cell recording of a rat Purkinje cell [Loewenstein et al., 2005].

Although the traces depicted in Figure 3.11 are not very precise, we can easily imagine that there are dendritic spike bursts appearing in the up-states of these temporal traces. Indeed, we see some jumps in the lowest voltage level of simple spikes.

By climbing fibre activation, the cell can switch in both states depending on their state before the stimulation. The same behaviour is observed by the injection of a current pulse in the soma.

Indeed, if the rat Purkinje cell is in the down-state, it will switch in the up-state and fire when a short pulse of depolarizing current is applied. Similarly, the cell will switch from the up-state to the down-state if a short hyperpolarizing current is injected. See these transitions in Figure 3.12(a). Moreover, as we can observe in Figure 3.12(b), the injection of a short hyperpolarizing current pulse can switch the cell in the other state in function of the state in which it is.



(a) A rat Purkinje cell recording.



(b) A guinea pig Purkinje cell recording.

Figure 3.12: Whole-cell recording in vivo [Loewenstein et al., 2005].

In fact, the climbing fibre activation induces the same behaviour than the hyperpolarizing current. Thus the same synaptic input can involve transitions between the two states. As an

example in vitro, the beginning of the recording in Figure 3.13(a) matches a quiescent period: so, the climbing fibre activation switches the neuron to the up-state, whereas the synaptic activation during the depolarized level induces a transition to the down-state. Moreover, the expanded traces in Figure 3.13(b) illustrate a particular pattern that is referred to as the complex spike. In fact, these traces match the somatic spike and the dendritic spike burst shown above.

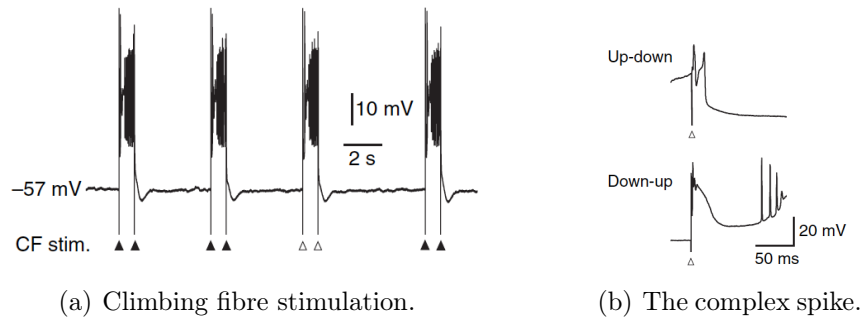


Figure 3.13: Whole-cell recording from a guinea pig Purkinje cell in vitro [Loewenstein et al., 2005].

In vivo, the complex spike is still present and is generated by climbing fibre activation: it has the same effect on the membrane potential. If the climbing fibre is activated, we observe a transition from the down-state to the up-state or the inverse and at the time of the activation there is a complex spike that appears in the membrane potential traces. It is well illustrated by the extracellular recording in Figure 3.14. This is an example for a guinea pig but the complex spike and the transitions induced by the climbing fibre activation is observed for a rat too and the traces are quite similar.

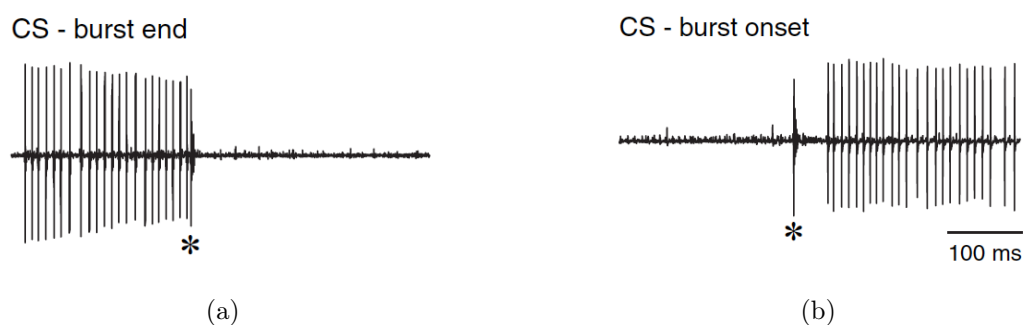


Figure 3.14: Extracellular recording from a guinea pig Purkinje cell in vivo [Loewenstein et al., 2005].

However, sometimes quite a long delay is observed between the complex spike and the state transition; this means that the climbing fibre activation does not always generate a transition. It could be a spontaneous transition. In general, when the delay is less than 100 ms, we can consider that the switching is induced by the synaptic activation.

We close this section with a list of identified ionic currents in Purkinje cells. Like most neurons, the Purkinje cell has a voltage-gated potassium and sodium channel: the sodium channel is fast activating and the potassium channel is persistent and exhibits a slower kinetics [Llinas and Sugimori, 1980a, Swensen and Bean, 2003]. Moreover, the existence of a persistent sodium current was proven experimentally [De Schutter and Bower, 1994a, Edgerton and Reinhart, 2003]. The neuron exhibits more than one type of potassium current: in addition to the usual potassium current of the Hodgkin and Huxley model, an A-type current, which is rapidly inactivating, and a delayed rectifier current, slowly inactivating, have been reported [Hirano and Hagiwara, 1989, Swensen and Bean, 2003]. It is also clear that there exists a hyperpolarization-activated potassium current, as it was identified by Edgerton and Reinhart [2003] and Engbers et al. [2013]. Furthermore, it seems that two types of calcium currents are present in the neuron and that they act on calcium-dependent potassium currents. The two types of calcium channels are T-type and P-type [Engbers et al., 2013, Swensen and Bean, 2003, Edgerton and Reinhart, 2003]. By modifying the calcium concentration, they change the value of the small conductance (SK) and large conductance (BK) Ca^{2+} - activated K^+ currents, which are well known to play a role in the Purkinje cell neuronal activity [De Schutter and Bower, 1994a, Engbers et al., 2013].

3.2.2 State of the art in modelling

The Purkinje cell is special because of its very extended dendritic tree. Its dendrites are active which means that the conductances of ionic channels are not constant in the dendrites. It requires a model including currents with voltage-dependent conductances; they play an important role in the response to synaptic inputs, like climbing fibres and parallel fibres. Moreover it was shown experimentally that the maximal conductances are not homogeneous over the whole cell but that they depend on the localization in the cell. For instance, at certain places there are calcium currents and at other places their maximal conductance is very low. The channel distribution is not homogeneous.

These reasons justify the fact that a lot of compartmental models were built for the Purkinje cell. A compartmental model for the dendrites helps to account for the spatial properties of the neuron. Briefly, a compartmental model for a neuron is a system describing a neuronal mechanism with the help of several compartments. Every compartment is a small sub-system whose the dynamics can be described by a Hodgkin-Huxley formalism and it is homogeneous with regard to the ionic channels. Each compartment is paired with its neighbours. Hence, a compartmental model takes into account the variation of ionic densities existing in a neuron. Indeed, the types of ionic channels can be very different in two distinct areas of the dendrites for instance.

Several Purkinje cell models have been proposed in the literature since the seventies. However, at the beginning of these researches, not all the types of currents that exist in the cell were known. For this reason, some older models are incomplete, like the model built by Pelionisz and Llinás [1977]. Furthermore, there exist some models that do not include active conductances in the dendrites and, thus, are much less realistic. In this case, we can cite the model of Shelton [1985] and the one of Rapp et al. [1994].

The challenge is to build a model which is not too complex and still reproduces well the reality. For instance, it is not always necessary to include all existing currents in a model because sometimes their impact is minor. A model with too much information could become very sensitive to small parameter variations. Robustness considerations suggest to focus on few relevant parameters in a model. However increased detailed knowledge and realism suggests to include in the model the currents that have been demonstrated to exist in the neuron and sometimes there are many of them.

The model built by De Schutter and Bower [1994a] is probably the most complete modelling effort of Purkinje cells. This model includes ten different voltage-dependent ionic currents whose existence in this cell has been established. It contains 1,600 compartments, is based on real Purkinje cell morphology and considers active dendrites. The chosen morphology is illustrated in Figure 3.15.

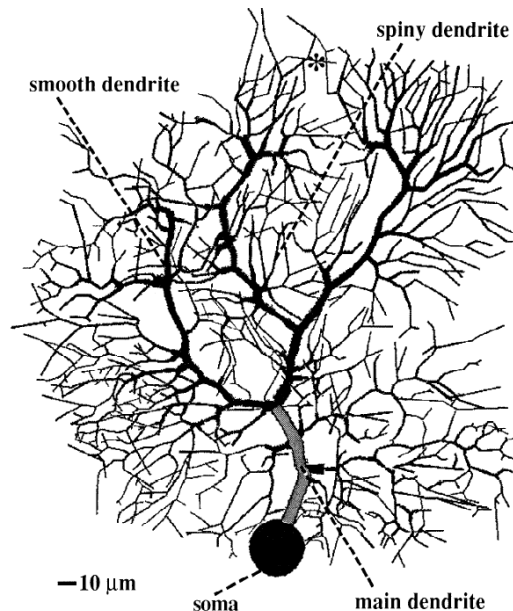


Figure 3.15: Morphology of the modelled Purkinje cell [De Schutter and Bower, 1994a].

The ten currents are

- a fast and a persistent Na^+ current;
- a T-type and a P-type Ca^{2+} current;
- an anomalous rectifier (a K^+ current), a delayed rectifier, a persistent K^+ current and a A-type K^+ current;
- a BK and a K2 Ca^{2+} -dependent K^+ current.

Each of these currents was cited in the preceding section. The model is based on experimental studies. More precisely, the current dynamics in the model are obtained from in vitro

recordings, voltage-clamp studies and single-channel studies.

Another advantage of the model is that its publication comes with a detailed description of every ionic current. Every voltage-dependent current is described by the Hodgkin-Huxley formalism. It means that the activation or inactivation variables have a kinetics similar to the one introduced in Chapter 2. It is obvious that, for example for an activation variable m ,

$$\dot{m} = \frac{m_\infty(V) - m}{\tau(V)} \text{ is equivalent to } \dot{m} = \alpha_m(V) (1 - m) - \beta_m(V) m$$

$$\text{with } m_\infty(V) = \frac{\alpha_m}{\alpha_m + \beta_m} \text{ and } \tau(V) = \frac{1}{\alpha_m + \beta_m}.$$

The same expression is valid for an inactivation variable h . Every kinetic equation in the paper is expressed by the second equation form where $\alpha(V)$ and $\beta(V)$ are sigmoid functions such that

$$\alpha(V) = \frac{A}{B + \exp \frac{V+C}{D}} \text{ and } \beta(V) = \frac{E}{F + \exp \frac{V+G}{H}}.$$

A drawback of the paper is the technique used to model the calcium concentration dynamic. It is not made realistically, so maybe it could be better to stimulate the Ca^{2+} variations differently. However it is mandatory to be interested in this parameter because there are calcium-dependent potassium currents in the dendrites and the consequences of their time evolution on the electrical activity in the dendrites (and more generally in the Purkinje cell) are not negligible.

Moreover the paper does not use experimental data for maximum channel conductances because these data are only indicative in general; generally they are not constant in experimental studies.

The maximum conductances were finally chosen to obtain temporal traces that would match with the experimental simulations in vitro presented in the paper of Llinas and Sugimori [1980a]. An example of the results which can be obtained by this complex compartmental model is illustrated in Figure 3.16. These curves can be compared with those of Figure 3.8, which were obtained experimentally.

However it should be possible to obtain the same behaviour with different conductances, if the model was robust. Indeed, in Section 2.2.2 of Chapter 2 it was explained that if two maximum conductances had the same scale but different feedback gain sign, they could be modified simultaneously and there would not be any consequence on the excitability. This is a question which we will deal with further in the next chapter.

In this paper the cell is stimulated only by current injections in the soma. For a short pulse, Figure 3.16(a) shows that the latency decreases as the current amplitude is increased. The direct consequence is that there are more spikes elicited during the pulse. The experimental data exhibit an after-depolarization potential when the current is small; Figure 3.8 proves it.

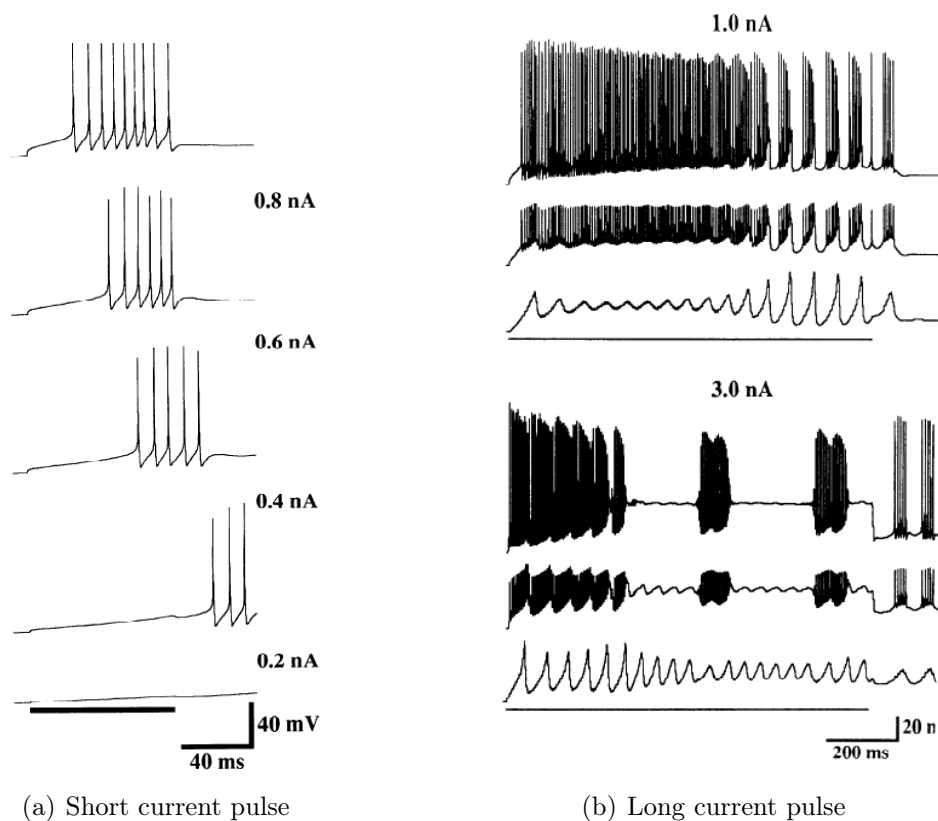


Figure 3.16: Model simulation by somatic current injection [De Schutter and Bower, 1994a].

This feature seems absent in model stimulations. The firing pattern is very different when a long-duration current is applied. From the comparison of the curves of Figure 3.8 G and those of Figure 3.16(b), we observe that the simulation permits apparently to reproduce the dendritic spike bursts and the somatic spikes.

The spontaneous activity of the cell shown experimentally (Figure 3.9) can be obtained with the model too; it is achieved by the addition of a small bias current. As any computer model it has limitations and cannot reproduce the whole reality, nevertheless it was a good progress in the modelling of the Purkinje neuron.

The model was tuned to reproduce well the somatic current injection. But it was important to be sure the model was not good only for some specific stimulations. For this reason, another paper followed the first to confirm that the model is enough general and can be applied to a large set of questions. Notably the effect of the climbing fibre activation was tested. The evolution of the somatic membrane potential is shown in Figure 3.17.

Many recent models are based on the model of De Schutter and Bower [1994a]. Currently the trend is to build a simpler model than the above discussed very detailed model. A model with only one or two compartments can indeed be reduced and we can then analyse more easily the bifurcations underlined by the model. There are much fewer parameters and it is easier to modulate its electrical behaviour. For instance, Coop and Reeke [2000] established four

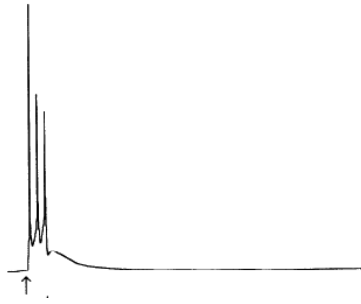


Figure 3.17: Model simulation by climbing fibre activation [De Schutter and Bower, 1994b].

models of the Purkinje cell based especially on the work of De Schutter and Bower [1994a]. These models contain only one or two compartments and give behaviours quite similar to those illustrated above with the model containing 1,600 compartments.

Chapter 4

Qualitative and quantitative modelling

This chapter presents two distinct models used to exhibit and explain the electrical activity of the Purkinje cell; a qualitative model and a quantitative model.

The qualitative model permits to establish a link between this work and the recently proposed phase portrait introduced in Chapter 2.

The quantitative model is a state-of-the-art model of the literature. It aims at introducing the different ionic currents present in the Purkinje neuron. Moreover a parallel will be drawn between this model and the previous one.

4.1 A qualitative model

This model provides a phenomenological reproduction of the Purkinje cell behaviour and is useful to reveal the central role played by the calcium current in the Purkinje cell activity. In particular, the model simulations will illustrate the qualitative behaviours only.

The Purkinje cell exhibits a bistability between a stable quiescent down-state and a stable spiking up-state. Moreover, it has been shown that the neuronal activity has some electrophysiological signatures like a plateau potential and a spike latency.

As it was explained in Chapter 2, bistability requires a slow regenerative current. Hence, the introduction of a calcium current in the classical Hodgkin-Huxley model permits to exhibit the bistability mechanism.

In contrast, the up-state excitability does not involve slow regenerative currents but rather the interaction between sodium and potassium currents. The particular excitability of the Purkinje neuron in its up-state can be explained by a purely restorative mechanism.

4.1.1 Modelling

If we go back to Section 2.2.2 of Chapter 2 and review the five types of excitability, it would seem that the Type V is the closest type to the Purkinje cell electrical activity. Indeed, the Type V exhibits a bistability between a down-state and an up-state, the latter being a limit cycle in a certain parameter range. Moreover, a spike latency and a plateau potential appear in the electrical signature of this type of excitability. Type IV excitability shows similarly a spike latency signature and bistability but the plateau potential is a characteristic that appears only in the Type V and it is a clear characteristic of the Purkinje cell.

For those reasons we consider the mirrored FitzHugh-Nagumo model presented in [Franci et al., 2012]. The model contains two states: the membrane potential V and the sodium activation n . The equations describing the two-dimensional system are

$$\begin{cases} \dot{V} &= V - \frac{V^3}{3} - 4(n + n_0)^2 + I_{app}, \\ \dot{n} &= 0.1(n_\infty(V - V_0) - n), \end{cases} \quad (4.1)$$

where $n_\infty(V - V_0)$ is a sigmoid function such that

$$n_\infty(V - V_0) = \frac{2}{1 + \exp^{-4(V - V_0)}} \quad (4.2)$$

and n_0 , V_0 and I_{app} are parameters. These parameters help to move the nullclines of the system such as to obtain the desired type of excitability.

Note that the transition from the Type IV to the Type V is very sensitive and we could study the boundary that exists between both to understand better the similarities of these two excitability types. A little bit of noise could induce the transition and it is not certain that some patterns in the experimental recordings are not shown because of the noise.

Type V excitability is illustrated by the phase portrait in Figure 4.1; it is obtained with the parameters $I_{app} = \frac{2}{3}$, $V_0 = -1$ and $n_0 = -0.7$. By choosing $I_{app} = \frac{V_0^3}{3} - V_0$, we can obtain the different types of excitability with the variation of V_0 and n_0 which represent the coordinates (V_0, n_0) of the point where the two mirrored parts of the V-nullcline intersect each other.

The phase portrait in Figure 4.1(a) exhibits three fixed points, which are the intersection between the V-nullcline and the n-nullcline. There are two stable nodes (one down-state and one up-state) and one saddle node appearing between the two other fixed points on the n-nullcline. The saddle point and its stable manifold separate the two basins of attraction of the stable nodes. For the chosen value of applied current, there is no limit cycle and we will not observe a periodic spiking behaviour. In Figure 4.1(a), the trajectory converges to the down state. In Figure 4.1(b), the simulated trajectory converges to the up-state because the initial condition is in the other basin of attraction. There will be a spike followed by a return to the stable up-state.

As we increase the current I_{app} , the phase portrait changes and a limit cycle appears. This is illustrated in Figure 4.2. The stable down-state and the saddle point have disappeared in a saddle-node bifurcation while the stable up-state lost its stability in a Hopf-bifurcation, giving rise to a limit cycle. The amplitude of this limit cycle increases as a function of the

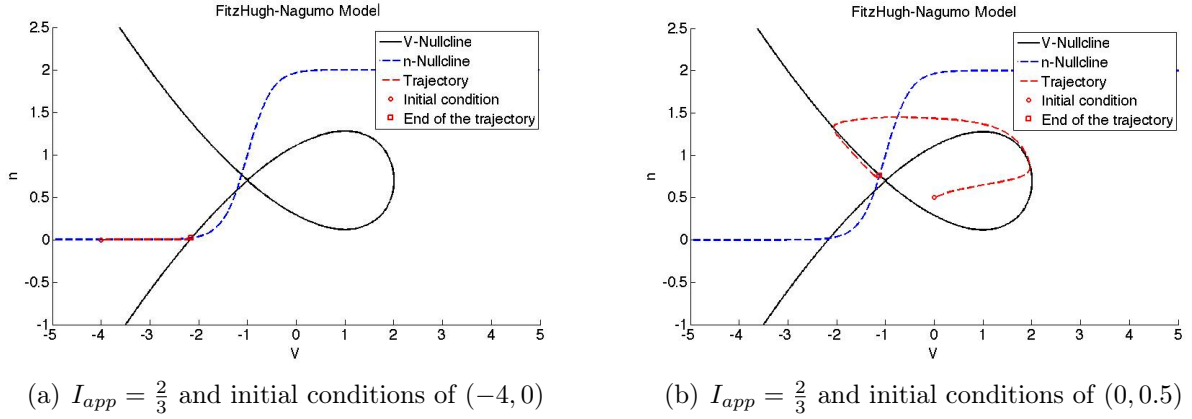


Figure 4.1: Mirrored FitzHugh-Nagumo phase portrait of the Type V.

applied current. There is a thin funnel between the nullclines around the point $(-2, 0)$; the consequence on the electrical behaviour is called the ghost of the saddle-node. Indeed, despite the removal of the saddle-node, the temporal trace will show a pronounced latency because the vector field almost vanishes in this area. Moreover, we see that the limit cycle amplitude is smaller than the amplitude of the first spike. The first spike will have a maximum amplitude about $V = 2.3$ whereas the maximum amplitude in the limit cycle is about $V = 1.8$.

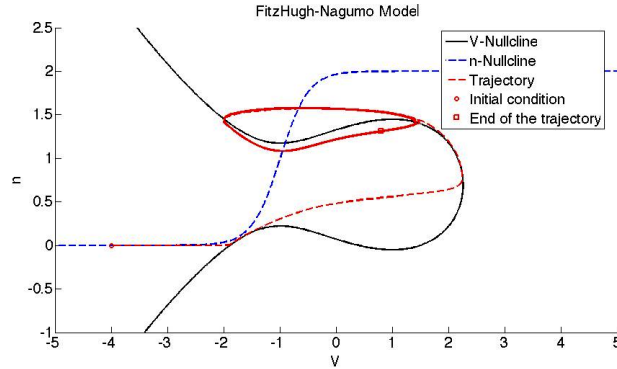


Figure 4.2: Type V with $I_{app} = \frac{2}{3} + 0.9$ and initial conditions of $(-4, 0)$.

4.1.2 Results

In this subsection, we illustrate some qualitative behaviours that can be obtained with the generic model for Type V excitability.

Firstly, we present our procedure by reminding some explanations provided in the previous subsection. A constant current $I_{app} = \frac{2}{3}$ will be applied during the whole simulation to have behaviours which can be predicted with the phase portrait in Figure 4.1 drawn in Subsection 4.1.1. Thus, for $I_{app} = \frac{2}{3}$, our model exhibits two stable fixed points; a stable up-state node and a stable down-state node.

The injection of a supplementary positive current induces an Hopf-bifurcation between the stable up-state node and the saddle node which is present also in the phase portrait. Hence a limit cycle appears and will give rise to an oscillatory pattern. When the current will be relaxed, the limit cycle will disappear and the neuron state will converge to the up-state. A hyperpolarizing current with a sufficient amplitude will induce the return to the down-state. Indeed, this is the electrical activity that we obtain in Figure 4.3.

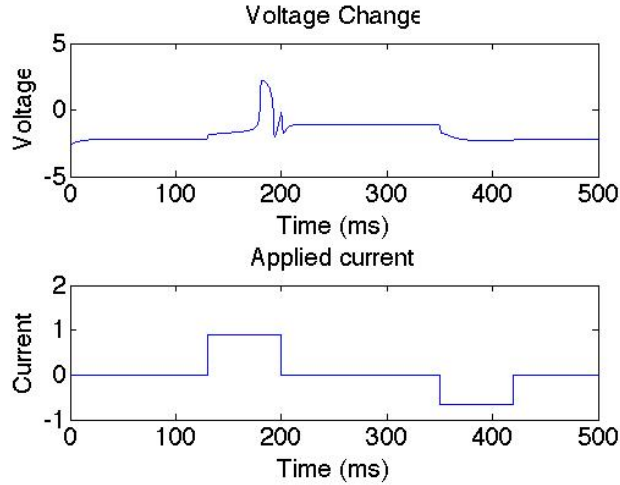


Figure 4.3: Simulation of model (4.1). Successive application of a current $I_{app} = \frac{2}{3} + 0.9$ and a current $I_{app} = \frac{2}{3} - \frac{2}{3}$.

In Figure 4.3, we also notice a small oscillation which is a characteristic of the Hopf-bifurcation.

This is a very simple model and it would not be able to reproduce the whole behaviour of a neuron; it is not the aim of such a model. It captures the most important characteristics of the excitability of a neuron. Indeed, we see the latency, the oscillation, the bistability between a down-state and an up-state which could be a stable node or a limit cycle and a plateau potential.

4.2 A quantitative model

In contrast to the qualitative model of the previous section, the final quantitative model presented in this section is a conductance-based model of the Purkinje neuron built on the basis of a compartmental model. It contains most of the ionic currents whose existence in the cell is well known. The aim is to obtain a very complete model, allowing for a detailed study of the role of each current.

Moreover, we want to establish a link with the previous model which involved only one potassium current, one sodium current and one calcium current expressed with a generic formalism. One current in the qualitative model could correspond to several aggregated currents in the quantitative model. All sodium currents could be aggregated in a unique sodium current, all potassium currents would be aggregated in a unique potassium current and the same

principle for the calcium currents too.

The compartmental model is a quantitative model, modelling the spatial heterogeneity of currents. A related important question will be to assess whether the spatial features of the model play a role in the electrophysiological activity.

4.2.1 Modelling

The model presented in this section is primarily based on the work of De Schutter and Bower [1994a]. The corresponding model is very well documented and contains most of the currents found experimentally in the Purkinje cell. Some channel kinetics, like the SK or BK case, are not plausible from a physiological viewpoint but it is something that we will be able to change in our modelling.

The role of the dendritic compartments in the Purkinje cell models is not very clear. A compartmental model is useful to take into account the difference of ionic channels in the distinct parts of the cell. Spatial effects were a particular focus, in the early nineties and it could be one of the reasons to have chosen a model with several compartments. However, it may not be necessary to represent with so many details the whole behaviour of the cell (i.e. by a thousand of compartments), as it is done in the model of De Schutter and Bower [1994a]. Indeed, a limitation of many compartmental models seen in the literature is that the increased complexity leads to non robust observations. Furthermore, the bistability of the neuron is not exhibited in the paper, which exclusively focuses on the up-state excitability.

There are three groups of compartments in the model: one for the soma, one for the main dendrite and one for the rest of the dendrites. The three distinct cellular parts are illustrated in Figure 3.15 of Chapter 3. The maximum conductance of each ionic current varies depending on the group, as illustrated in Table 4.1.

Name	Soma	Main Dendrite	Rest of Dendrite
NaF	7,500	0.0	0.0
NaP	1.0	0.0	0.0
CaP	0.0	4.5	4.5
CaT	0.5	0.5	0.5
Kh	0.3	0.0	0.0
Kdr	600.0	60.0	0.0
KM	0.040	0.010	0.013
KA	15.0	2.0	0.0
KC	0.0	80.0	80.0
K2	0.0	0.39	0.39

Table 4.1: \bar{g} mS/cm² for the voltage and Ca^{2+} -dependent channels in one version of the Purkinje cell model [De Schutter and Bower, 1994a].

An important feature of the model is the absence of calcium-dependent channels in the soma.

The model considered here is a simplification of the model [De Schutter and Bower, 1994a]. We aggregate all currents in one single compartment and seek to reproduce the behaviours presented in [De Schutter and Bower, 1994a]. The SIMULINK representation of the model is shown in Figure 4.4.

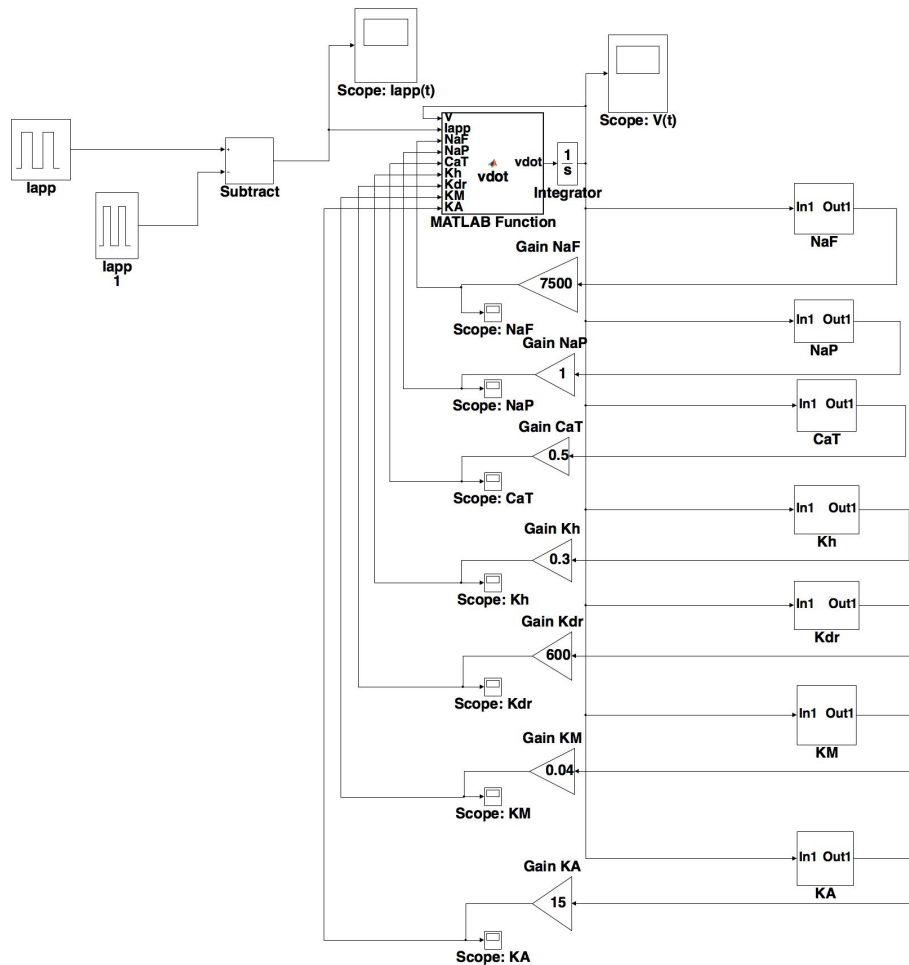


Figure 4.4: First model with the somatic currents.

This first model only includes the somatic currents, that is:

- two types of sodium currents; NaF, characterised by fast activation dynamics and NaP, characterised by the absence of an inactivation variable (persistent sodium current),
- one single calcium channel; the T-type,
- four types of potassium currents; an hyperpolarization-activated current (Kh), a delayed rectifier (Kdr), a persistent potassium current (KM) and an A-type potassium current (KA), characterised by its rapidly inactivation,
- a leak current to adjust the resting potential.

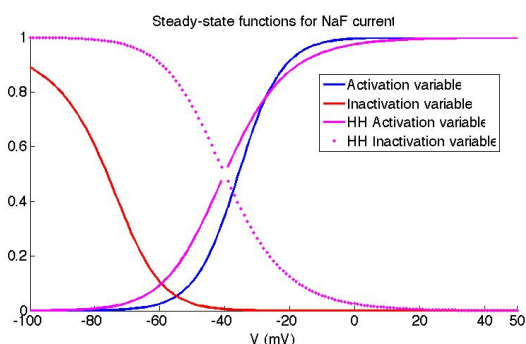
The time evolution of the membrane potential is thus given by the equation

$$C \dot{V} = I_{app} - I_{NaF} - I_{NaP} - I_{CaT} - I_{Kh} - I_{Kdr} - I_{KM} - I_{KA} - I_{leak}, \quad (4.3)$$

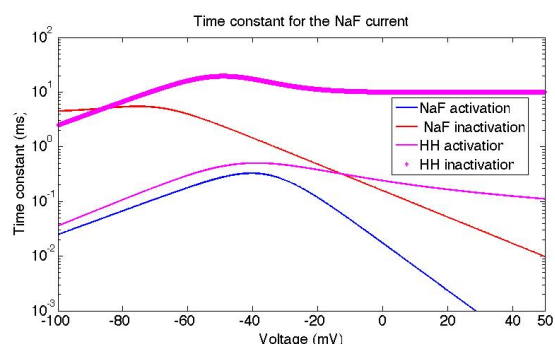
which is coupled with the kinetic equations of the ionic channels. The model uses the Hodgkin-Huxley formalism, which was introduced in Chapter 2, and contains a total of thirteen variables because of the (in)activation variables of each current.

The differential equations associated with the (in)activation variables are taken from the paper of De Schutter and Bower [1994a] with maximum conductance values initially set as in Table 4.1. The kinetics of the ionic currents are mostly based on many experimental recordings and the maximum conductance values were chosen to reproduce some in vitro recordings.

The maximum conductance values are especially high for two types of currents: the fast sodium current and the potassium delayed rectifier current. It is of interest to compare them with the sodium and potassium currents of the Hodgkin-Huxley model studied in Chapter 2. The steady-state functions and the time constants are shown in Figure 4.5 and Figure 4.6.

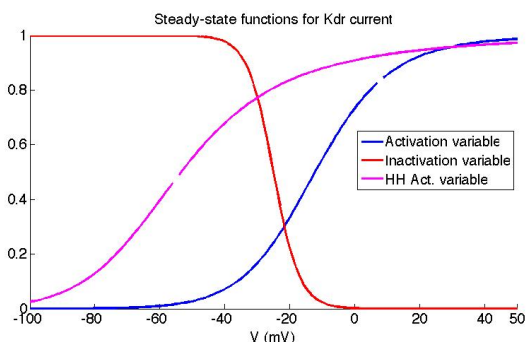


(a) Steady-state (in)activation functions.

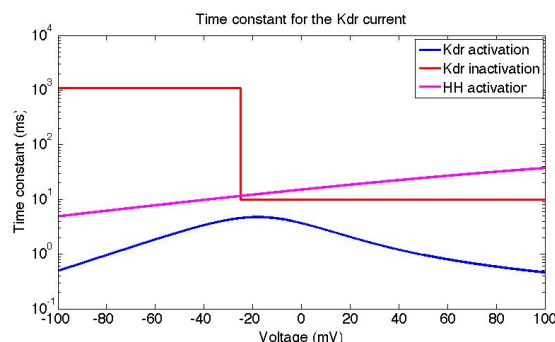


(b) Time constants.

Figure 4.5: Steady-state (in)activation functions and time constants for the fast sodium current.



(a) Steady-state (in)activation functions.



(b) Time constants.

Figure 4.6: Steady-state (in)activation functions and time constants for the potassium delayed rectifier.

In Hodgkin-Huxley model, the window defined by the two sigmoid functions and their intersection are larger than the window observed in Figure 4.5(a). Moreover, at low voltage, the time scales of the activation and the inactivation variable respectively are very distinct but as the voltage increases, the time scales are so different anymore. The time scale becomes equally fast for both variables at around -20 mV.

The potassium current in Figure 4.6 also differs from Hodgkin-Huxley model. Delayed rectifiers represent potassium currents which are either slowly inactivating or non-inactivating. There is no inactivation in the model of Chapter 2; the potassium current is persistent. In contrast, the delayed rectifier in Figure 4.6 has an inactivating gate. In addition, the inactivation is very specific; its time constant is ultraslow at very low potential level and loses two orders of magnitude at -25 mV. This particular feature was found to be critical for most of the simulations of the model.

The only source of slow regenerativity in the model are the T-type calcium current and the potassium Kh current. They are a source of regenerativity because their slow variable induces a positive feedback on membrane potential variations [Franci et al., 2013]. Indeed, the T-type calcium current is an inward current and has a slow activation variable whereas the Kh current is an outward current and has a slow inactivation.

In Figure 4.7, we observe that a T-type calcium channel is activated at low potential and the dynamic is slow. The sodium currents have a Nernst potential at 45 mV while the calcium Nernst potential is at 135 mV. Thus this current is always negative when it is activated. An anomalous rectifier is a potassium current that provides a positive feedback also; the Nernst potential is at -30 mV and the steady-state function, shown in Figure 4.8¹, is non-zero until about -50 mV.

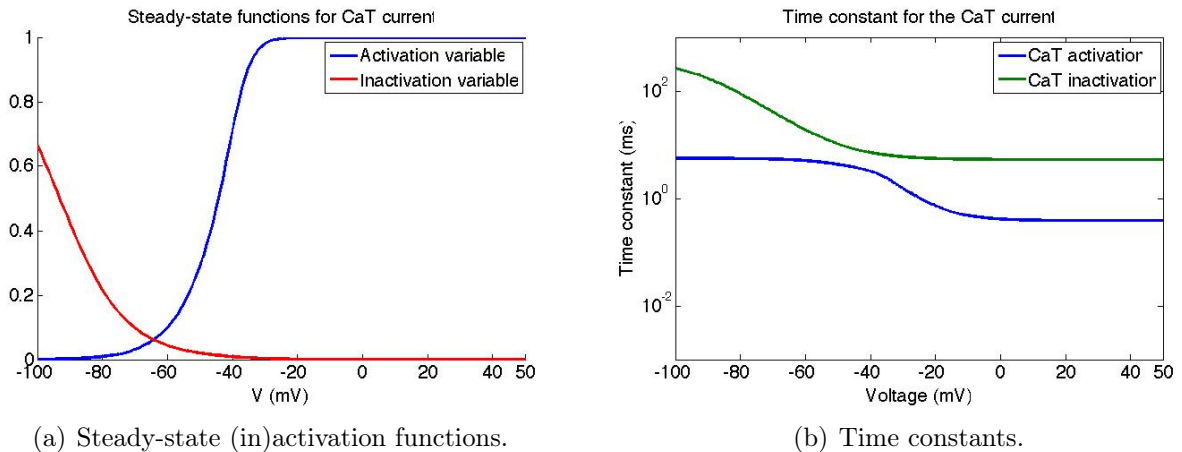
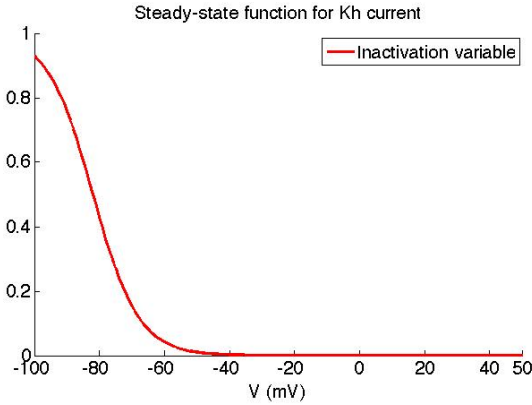


Figure 4.7: Steady-state (in)activation functions and time constants for the T-type calcium current.

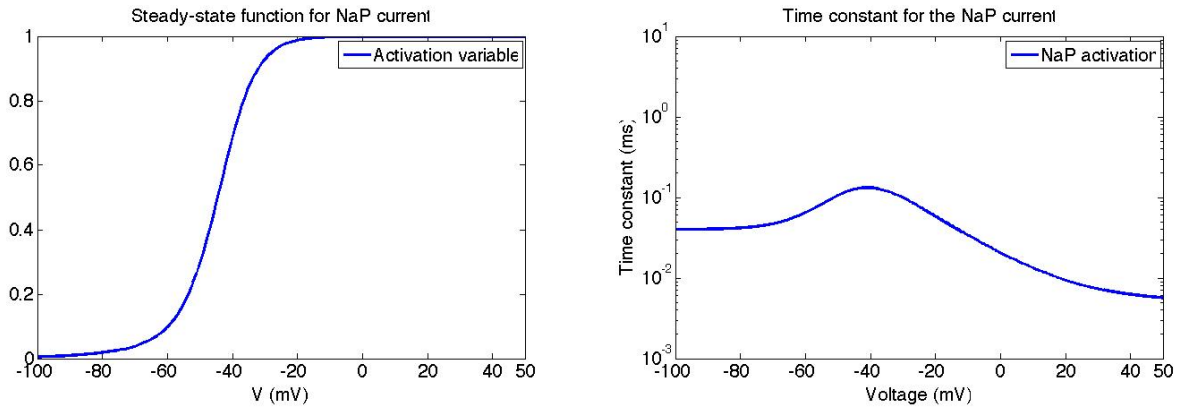
¹The time constant is not shown because it is simply the combination of two constant time constants of 8 ms and 40 ms.



(a) Steady-state (in)activation functions.

Figure 4.8: Steady-state (in)activation functions for the h-potassium current.

Now, let us discuss briefly the other currents. They play a secondary role. The persistent sodium is neutral because it has not a slow variable; the activation is fast. This current does not depend on an inactivation gate and its activation variable has an evolution very similar than that of the fast sodium NaF activation: the characteristics of the persistent sodium channel can be seen in Figure 4.9. The remaining currents are slow restorative: they are outward currents and they have slow activation variables, which provide a negative feedback. The persistent delayed rectifier in Figure 4.10 has no specific characteristic. However, in Figure 4.10, we see that the time constants of the A-type current of the Purkinje cell converge to the same value at high potential. We have not identified a specific role for this feature.



(a) Steady-state (in)activation functions.

(b) Time constants.

Figure 4.9: Steady-state (in)activation functions and time constants for the persistent sodium current.

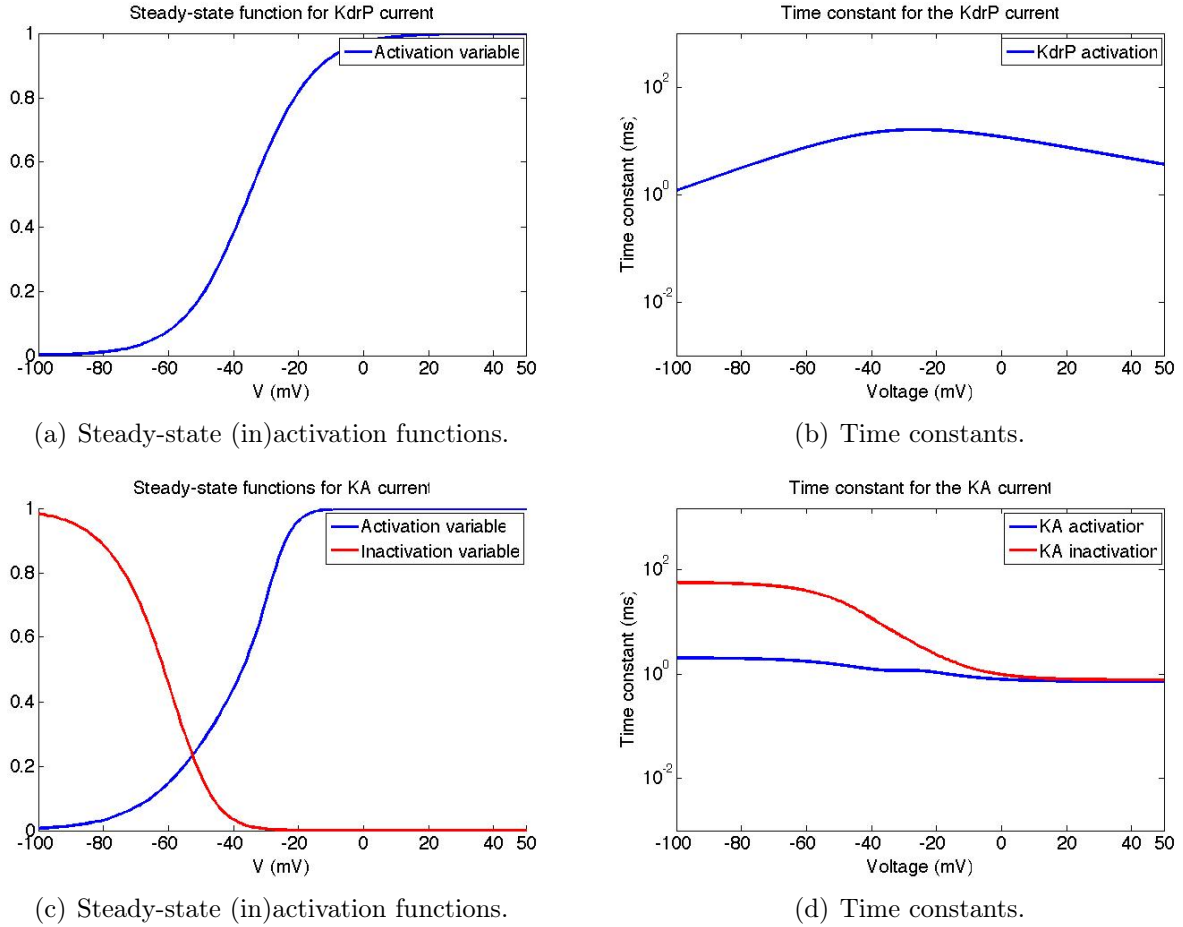


Figure 4.10: Steady-state (in)activation functions and time constants for the persistent potassium current and the A-type potassium current.

The relative importance of these currents and their special dynamics in the electrical behaviour will be dealt with in Subsection 4.2.2 as much as possible. We will show which experimental traces from papers are close to those obtained here. Furthermore, the regulation mechanisms of this model will be presented in details afterwards.

The proposed model suggests that the detailed spatial structure of the model [De Schutter and Bower, 1994a] is not necessary to capture the excitability properties of the Purkinje cell. Most behaviours found in this paper can be reproduced with only one compartment. Moreover, the firing patterns of the cell that can be reproduced with the model are not numerous. The spontaneous cellular activity or the switching to one state or the other by a short stimulation is not shown by such a model, as it will be illustrated in Subsection 4.2.2. This is not surprising in view of the qualitative analysis in Section 4.1. Slow regenerativity seems essential to robust bistability, but calcium currents are almost inexistent in the somatic compartment.

To remedy this problem, we finally added the three missing dendritic currents in our model, which are a P-type calcium current, a SK (small conductance) and a BK (high conductance) calcium-dependent potassium currents, leading to the model

$$C \dot{V} = I_{app} - I_{NaF} - I_{NaP} - I_{CaT} - I_{Kh} - I_{Kdr} - I_{KM} - I_{KA} - I_{CaP} - I_{SK,Ca} - I_{BK,Ca} - I_{leak}. \quad (4.4)$$

A detailed discussion of the specific dynamics of the P-type calcium current I_{CaP} and of the calcium-dependent currents are postponed to Chapter 5.

We stress however that it is physiologically relevant to include those currents in a somatic compartment because experimental studies on disassociated (that is soma isolated) Purkinje cells have shown their importance [Swensen and Bean, 2003].

4.2.2 Results

The model built in the previous subsection is a model that contains every current recognized in the Purkinje neuron to date. It is a complex model because of its many parameters.

4.2.2.1 Comparison of experimental and model simulations

A first illustration is the response of the model when a long-step current is applied. Our model reveals that traces close to experimental traces can be obtained by retaining only two of the ten currents: the delayed rectifier and the fast sodium current. Those are the currents that have the highest maximum conductance value.

We see in Figure 4.11 a pattern that looks like an experimental recording presented in Section 3.2 of Chapter 3 (Figure 3.10). For an easier comparison, we show again this picture in Figure 4.12.

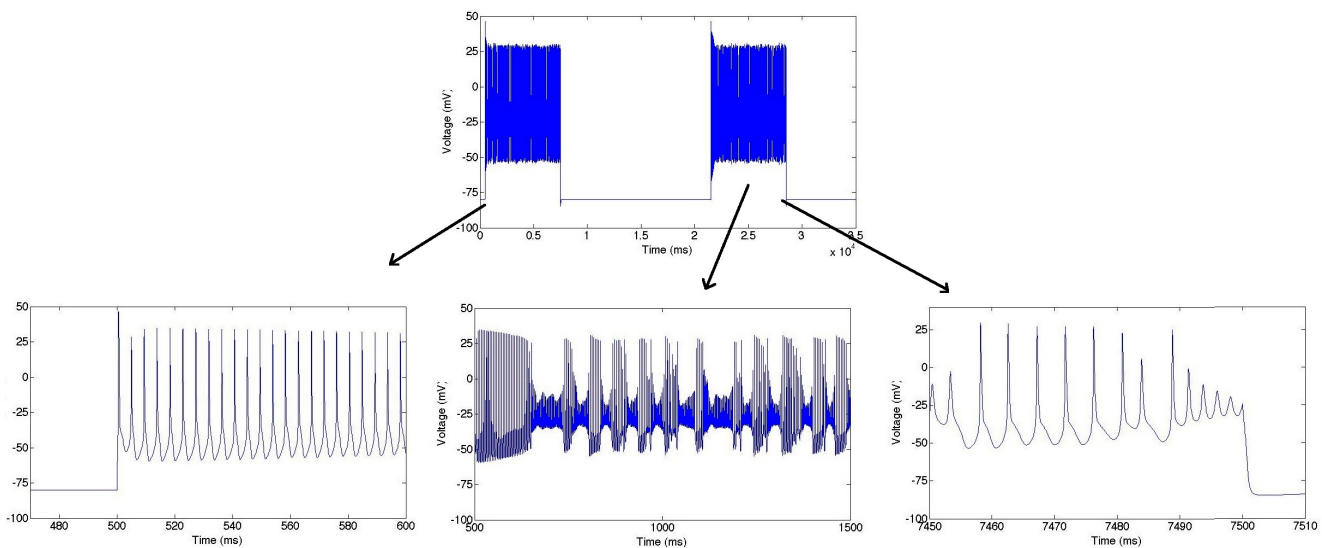


Figure 4.11: Model (4.4) with all maximal conductances set to zero except for I_{NaF} and I_{Kdr} ; $\bar{g}_{Na,F} = 7500 \text{ mS/cm}^2$ and $\bar{g}_{Kdr} = 600 \text{ mS/cm}^2$. Long-step current with an amplitude of 0.8 nA and a duration of 7 s .

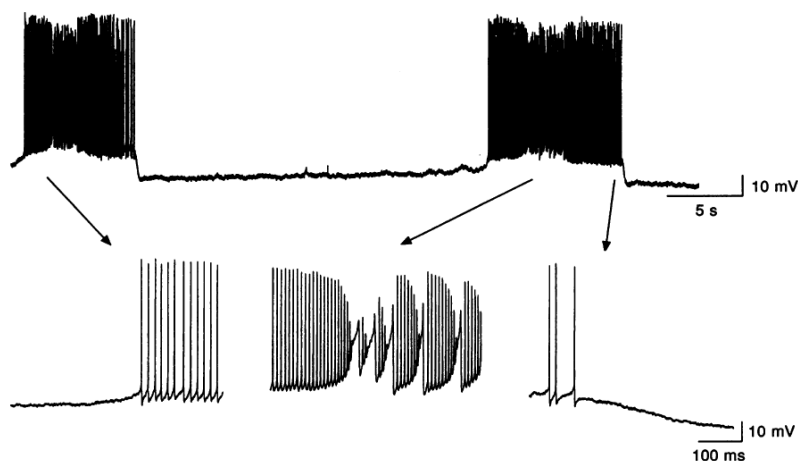


Figure 4.12: Intracellular recording of a guinea pig Purkinje cell [Rapp et al., 1994].

In the top plot of Figure 4.11, it seems that the activity is just made of periodical simple spikes. However, as it can be observed in the central zoom in Figure 4.11, the up-state is made up of very particular spikes. Indeed, the beginning of the temporal trace near 0.5 s looks like simple spikes. Then the maximum potential of the spikes is decreasing whereas the lowest potential is increasing; this activity continues until there is an interruption with very small spikes. After that, we observe again high-level spikes and so on and so forth while the current is non-zero. Moreover, the critical amplitude is about -25 mV. This amplitude represents the middle potential of the small spikes. Furthermore, it is the potential at which the delayed rectifier has its inactivation that switches from the ultraslow scale to the slow scale. Thus it is likely that the change of time scale has a large importance in the particular up-state pattern obtained with this model.

If we observe the experimental traces in Figure 4.12, we conclude that there are some good results already reproduced in these simulations; the beginning of the up-state is similar, there is a plateau potential and an activity that looks like the dendritic spike bursts. Furthermore, Figure 4.13, which comes from Chapter 3, is also close to the middle plot of Figure 4.11. Indeed, there is repetitive fast firing interrupted by low-amplitude spikes, called dendritic spike bursts. These bursts obtained in our model can be more easily observed in Figure 4.14(b).

When the current returns to zero, a latency is observed in the experimental recordings of Figure 4.12. Nevertheless, it is clearly not present with this model. Indeed, this is illustrated in Figure 4.14(c).

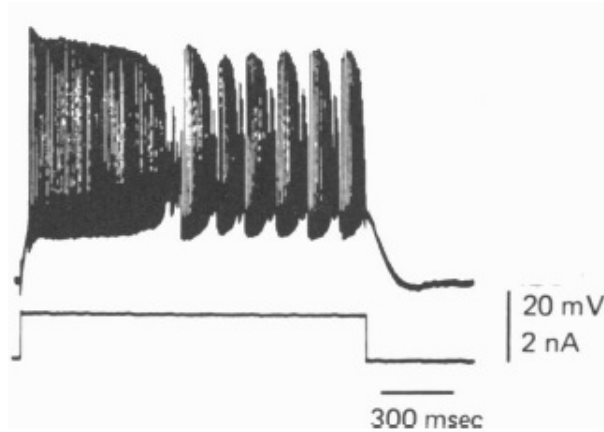
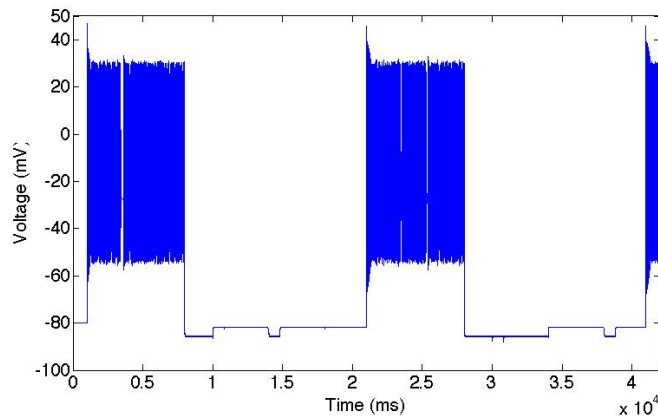
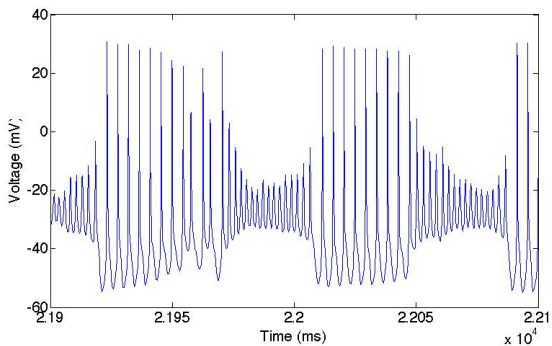


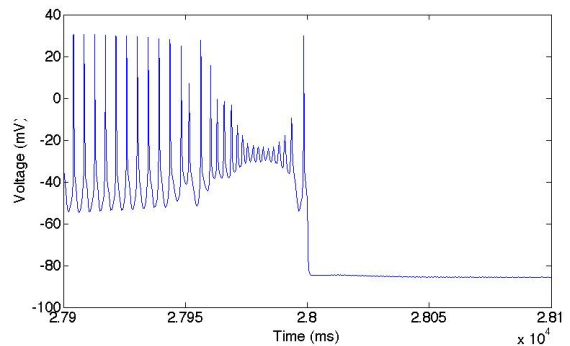
Figure 4.13: Somatic firing resulting of a DC depolarization for a guinea pig Purkinje cell [Llinas and Sugimori, 1980a].



(a) Whole temporal trace.



(b) Zoom-in on Figure 4.14(a) during the current stimulation.



(c) Zoom-in on Figure 4.14(a) at the end of the current stimulation.

Figure 4.14: Details of the temporal traces for another similar simulation than that of Figure 4.11. Model (4.4) with all maximal conductances set to zero except for I_{NaF} and I_{Kdr} ; $\bar{g}_{Na,F} = 7500 \text{ mS/cm}^2$ and $\bar{g}_{Kdr} = 600 \text{ mS/cm}^2$. Long-step current with an amplitude of 0.8 nA and a duration of 7 s . Simulation time of 42 s .

Thus this first example shows clearly that the delayed rectifier and the fast sodium current

are important to reproduce the electrical activity of the cell, because we obtain good results without any other currents. It also illustrates the absence of latency in the absence of regenerative currents.

Now it is interesting to show a behaviour obtained with all the currents of model (4.4). Indeed, another example of pattern well reproduced with this complicated model is the complex spike. In the thesis, we are not especially interested by the climbing fibre activation and the complex spike response; we focus on the bistability. Nevertheless, it was interesting to observe that our model is not limited to the study of the specific up-state exhibited by the Purkinje cell electrophysiology. The complex spike is a response to stimulations on dendrites. However, it can be obtained by a somatic stimulation if a bi-exponential current is applied [Davie et al., 2008]. To mimic this, we used the complete model (4.4) and applied a triangular current rather than an exponential current because there were integration problems with the exponential behaviour. We obtained the trace in Figure 4.15(a) that we can compare, for instance, with that of Figure 4.15(b).

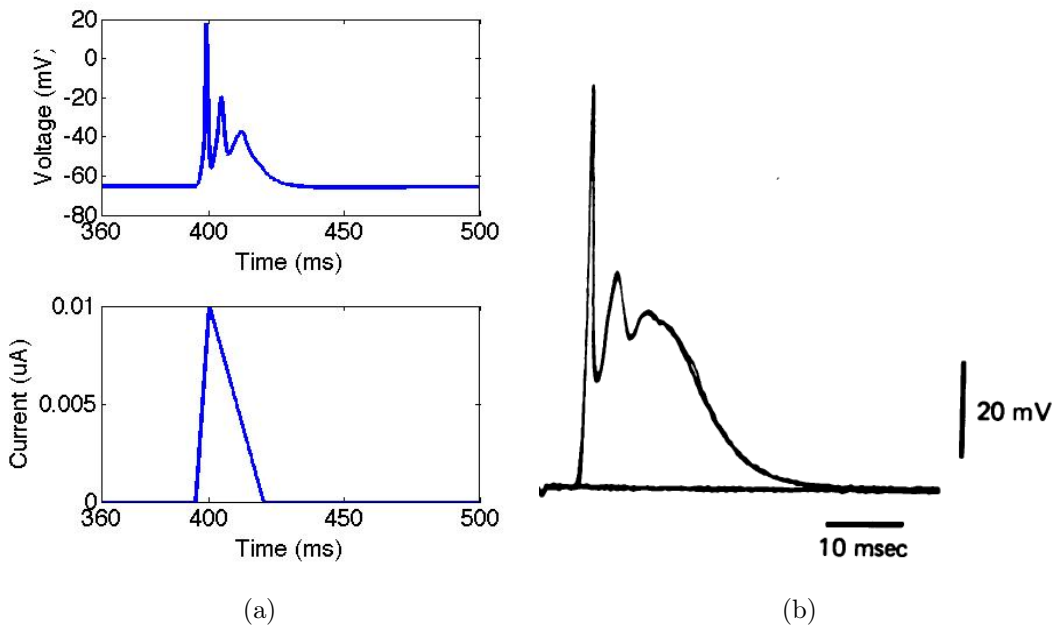
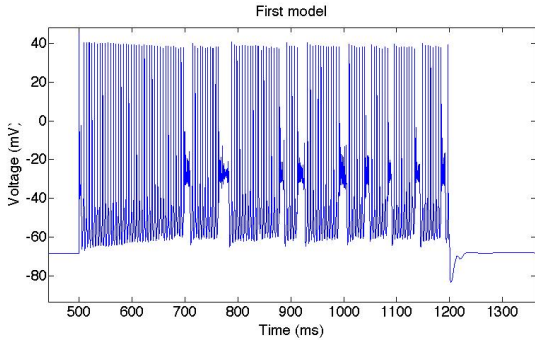


Figure 4.15: Complex spike obtained with model (4.4). (a) Cellular response for a triangular current; $\bar{g}_{Na,F} = 60 \cdot 10^{-3}$ mS and $\bar{g}_{Kdr} = 20 \cdot 10^{-3}$ mS. (b) Climbing fibre activation : complex spike recorded in the soma [Llinas and Sugimori, 1980a].

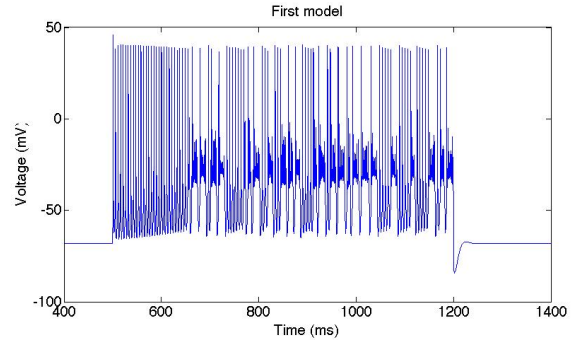
4.2.2.2 Regulation mechanisms

The model (4.4) is not easy to analyse because there are a lot of parameters and we encountered a lot of numerical problems with SIMULINK. Indeed, there are ten types of ionic currents and hence ten maximum conductance values to change; the fragility of the model makes it even difficult to discriminate between parameter changes and changes induced by the numerical integration errors.

The fragility of the model is illustrated even on a simple version without I_{CaP} , $I_{SK,Ca}$ and $I_{BK,Ca}$. A current of 0.5 nA with a duration of 2.1 s was applied, resulting in Figure 4.16(a). Notice that the choice of the solver in SIMULINK has a large importance because it can change the result very much. Indeed, the same simulation with ODE45 instead of ODE15S gives the result in Figure 4.16(b). The simulation results are quite different, and it took us some time before realizing this. As a matter of fact, ODE15S gives accurate simulation results and is thus more convenient for solving differential equations with respect to a neuronal behaviour. Indeed, ODE15S is concerned by stiff problems whereas ODE45 is for nonstiff system.



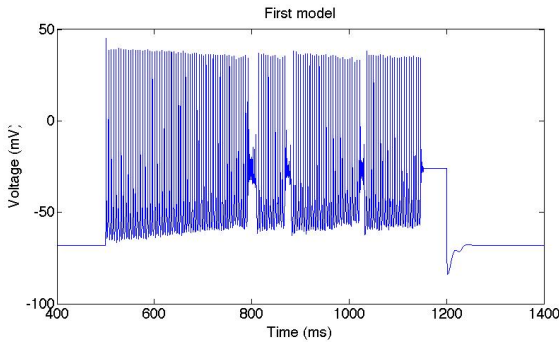
(a) Response with ODE15S.



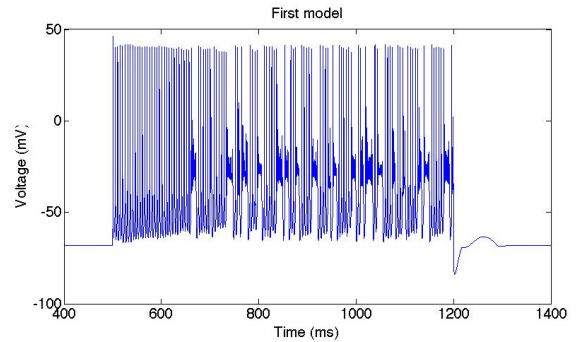
(b) Response with ODE45.

Figure 4.16: Response of the model (4.4) for a 0.5 nA current.

To illustrate that the model mostly depends on two currents, we modified the maximum conductance values of the fast sodium current and the delayed rectifier, separately. We can observe the consequences of these changes in Figure 4.17 and Figure 4.18 respectively. These changes have a pronounced effect on the temporal characteristics of the up-state.



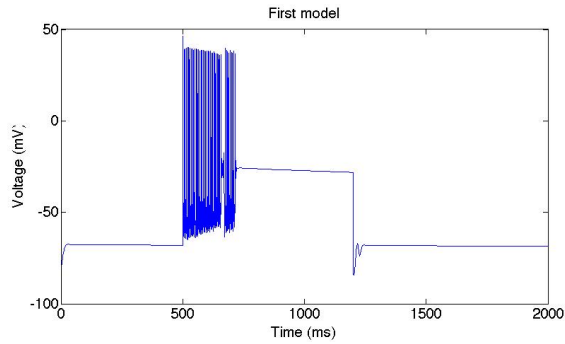
(a) Response with $\bar{g}_{NaF} = 6500 \text{ mS/cm}^2$.



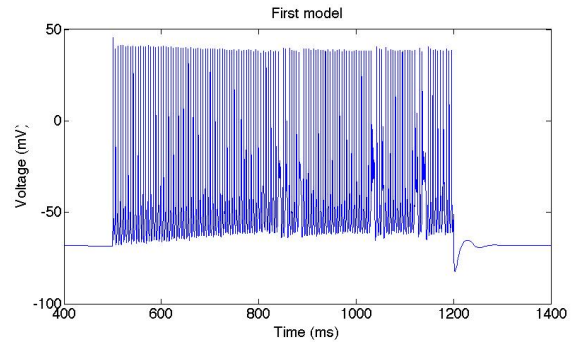
(b) Response with $\bar{g}_{NaF} = 8500 \text{ mS/cm}^2$.

Figure 4.17: Simulation of model (4.4). Modulation of the up-state activity by a variation of \bar{g}_{NaF} .

Indeed, in Figure 4.17(a), the maximum conductance value of the fast sodium current is reduced. The fast spiking activity has longer period and there are less small oscillations. We observe the opposite trend when \bar{g}_{NaF} is increased in Figure 4.17(b).



(a) Response with $\bar{g}_{Kdr} = 500 \text{ mS/cm}^2$.



(b) Response with $\bar{g}_{Kdr} = 750 \text{ mS/cm}^2$.

Figure 4.18: Simulation of model (4.4). Modulation of the up-state activity by a variation of \bar{g}_{Kdr} .

A decrease in \bar{g}_{Kdr} induces a diminution in the up-state spiking activity. When \bar{g}_{Kdr} is increased, the behaviour tends to a simple repetitive firing activity. It is shown in Figure 4.18(b).

This model is interesting because it highlights the central role of two currents in the up-state: the delayed rectifier I_{Kdr} and the fast sodium current I_{NaF} . They play an important role in the electrical activity and it is what we showed in this subsection. Then, in the next chapter, we will only retain these two restorative currents and add the regenerative effect of the calcium current on the cellular activity. It will be much easier to analyse the regulation mechanisms with fewer parameters.

Chapter 5

A reduced physiological model of Purkinje cell

This chapter presents the main contribution of the thesis. We extract from the detailed model studied in Chapter 4 the four currents that are sufficient to capture the Type V excitability of the Purkinje cell: a bistable neuron with a strongly hyperpolarized down-state and a highly excitable up-state.

The proposed model contains four ion channels :

- the two slow restorative currents I_{NaF} and I_{Kdr} that were shown to capture the excitability of the up-state, with the specific kinetics experimentally identified in [De Schutter and Bower, 1994a].
- a slow regenerative calcium current and a calcium-dependent ultraslow potassium current consistent with the experiments in [Swensen and Bean, 2003].

5.1 Modelling of the restorative currents

The model has exactly the same structure as Hodgkin-Huxley model, with adapted kinetics for the fast sodium current and the slow potassium current:

$$\left\{ \begin{array}{l} C \dot{V} = -\bar{g}_{Kdr}(m_{Kdr}^2)h_{Kdr}(V - V_{Kdr}) - \bar{g}_{NaF}(m_{NaF}^3)h_{NaF}(V - V_{NaF}) \\ \quad \quad \quad - \bar{g}_{leak}(V - V_{leak}) + I_{app}, \\ \tau_{m,NaF} \dot{m}_{NaF} = m_{\infty,NaF} - m_{NaF}, \\ \tau_{h,NaF} \dot{h}_{NaF} = h_{\infty,NaF} - h_{NaF}, \\ \tau_{m,Kdr} \dot{m}_{Kdr} = m_{\infty,Kdr} - m_{Kdr}, \\ \tau_{h,Kdr} \dot{h}_{Kdr} = h_{\infty,Kdr} - h_{Kdr}, \end{array} \right. \quad (5.1)$$

where $m_{\infty,NaF}$, $h_{\infty,NaF}$, $m_{\infty,Kdr}$, $h_{\infty,Kdr}$, $\tau_{m,NaF}$, $\tau_{h,NaF}$, $\tau_{m,Kdr}$ and $\tau_{h,Kdr}$ depend on the membrane potential V and their voltage dependence is shown in Figures 4.5(a), 4.5(b), 4.6(a) and 4.6(b). The Nernst potentials are respectively $V_{Kdr} = -85$ mV, $V_{NaF} = 45$ mV and

$$V_{leak} = -80 \text{ mV}.$$

Those equations are sufficient to reproduce the dominant firing pattern observed in the quantitative model; the quiescent state and the specific up-state containing a particular bursting behaviour with amplitude oscillations. The spiking state is generated when a current step is applied and is maintained for the step time interval.

5.2 Modelling the source of bistability

The experiments in [Swensen and Bean, 2003] and the qualitative analysis in Section 4.1 suggest that calcium is an essential source of the bistable behaviour in the Purkinje cell. We will add calcium dynamics to the model (5.1) following the procedure in [Drion et al., 2012].

Hence, the model (5.1) is completed by adding the current

$$I_{Ca} = \bar{g}_{Ca} m_{Ca} (V - V_{Ca}) \quad (5.2)$$

to the main equation. The Nernst potential is 85 mV and the dependence of the steady-state activation and the time constant are plotted in Figure 5.1. The steady-state activation will be changed later to obtain that of the Purkinje P-type calcium channel.

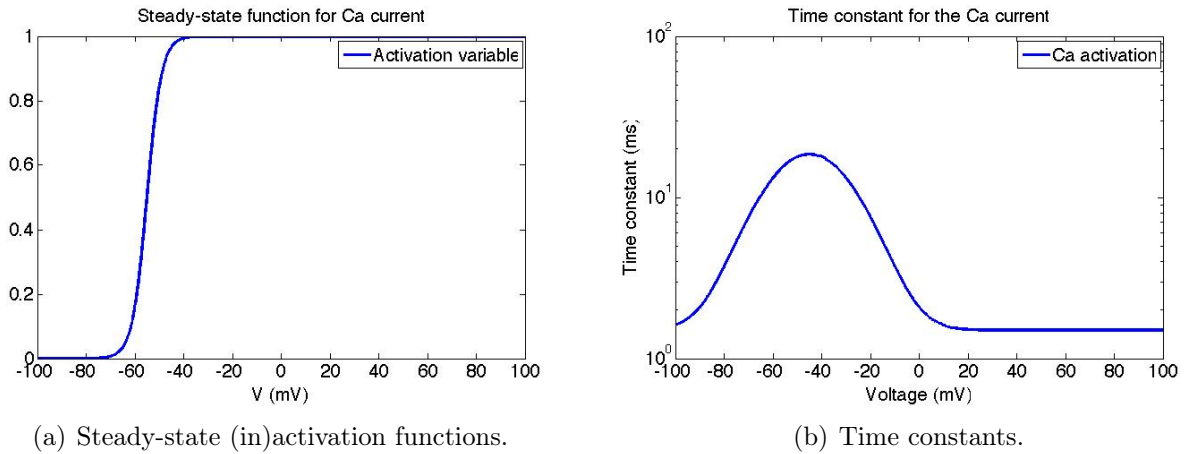
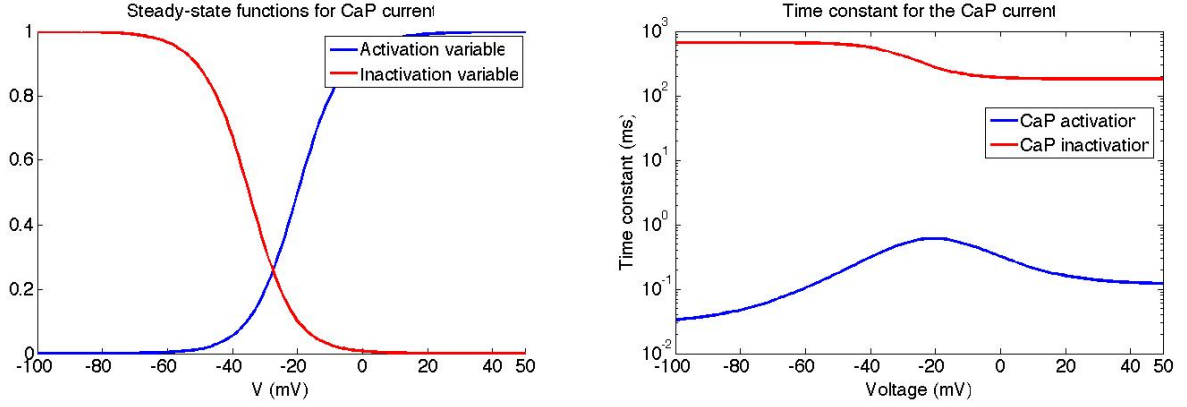


Figure 5.1: Steady-state (in)activation functions and time constants for the calcium current.

The final stage is now the addition of a calcium-dependent potassium current. The calcium-dependent channels are well identified in the Purkinje cell. Notably we know that there are SK (small conductance) Ca^{2+} -dependent K^+ channels in the Purkinje cell membrane. Thus we will test the consequences of the addition of a SK calcium-dependent potassium current on the Purkinje cell behaviour. Following Drion et al. [2011], the calcium dynamics are modelled by

$$\frac{d}{dt}([Ca^{2+}]) = -k_1 \bar{g}_{Ca} m_{Ca} (V - V_{Ca}) - k_c [Ca^{2+}] - k_2 \bar{g}_{Na} (m_{Na}^3) h_{Na} (V - V_{Na}) \quad (5.3)$$



(a) Steady-state (in)activation functions.

(b) Time constants.

Figure 5.2: Steady-state (in)activation functions and time constants for the calcium P-type current.

and the potassium current is represented by the equation

$$I_{K,Ca} = \bar{g}_{K,Ca} \left(\frac{[Ca^{2+}]}{K_D + [Ca^{2+}]} \right)^2 (V - V_{K,Ca}), \quad (5.4)$$

where the Nernst potential is the usual potassium Nernst potential of -85 mV. The parameters k_1 , k_c , k_2 and K_D are regulation parameters like the maximum conductance values \bar{g}_{Na} , \bar{g}_{Kdr} , \bar{g}_{Ca} and $\bar{g}_{K,Ca}$.

Therefore the final proposed model is as follows:

$$\left\{ \begin{array}{l} C \dot{V} = -\bar{g}_{Kdr}(m_{Kdr}^2)h_{Kdr}(V - V_{Kdr}) - \bar{g}_{NaF}(m_{NaF}^3)h_{NaF}(V - V_{NaF}) \\ \quad - \bar{g}_{leak}(V - V_{leak}) + I_{app} \\ \quad - \bar{g}_{Ca}m_{Ca}(V - V_{Ca}) \\ \quad - \bar{g}_{K,Ca} \left(\frac{[Ca^{2+}]}{K_D + [Ca^{2+}]} \right)^2 (V - V_{K,Ca}), \\ \tau_{m,NaF} \dot{m}_{NaF} = m_{\infty,NaF} - m_{NaF}, \\ \tau_{h,NaF} \dot{h}_{NaF} = h_{\infty,NaF} - h_{NaF}, \\ \tau_{m,Kdr} \dot{m}_{Kdr} = m_{\infty,Kdr} - m_{Kdr}, \\ \tau_{h,Kdr} \dot{h}_{Kdr} = h_{\infty,Kdr} - h_{Kdr}, \\ \tau_{m,Ca} \dot{m}_{Ca} = m_{\infty,Ca} - m_{Ca}, \\ \frac{d}{dt}([Ca^{2+}]) = -k_1\bar{g}_{Ca}m_{Ca}(V - V_{Ca}) - k_c[Ca^{2+}] - k_2\bar{g}_{Na}(m_{Na}^3)h_{Na}(V - V_{Na}). \end{array} \right. \quad (5.5)$$

In conclusion, this model contains the four dominant types of ionic currents exhibited by neurons: a sodium current, a potassium current, a calcium current and a calcium-dependent potassium current.

5.3 Results

In this section, we present some simulations of model (5.5) to illustrate the properties of the reduced model.

Firstly, we explore the regulation mechanisms exhibited by this reduced model. It permits to reproduce the bistability of the Purkinje cell and the ionic currents are introduced successively to understand their role. Some comparisons with experimental recordings are included in this study. Moreover, we will be able to illustrate the properties of modulation and robustness exhibited by our novel model. The importance of those properties was emphasized in Chapter 2.

Secondly, we compare by few simulations the qualitative model with this novel model. Although the temporal traces obtained with each model are distinct, we can conclude about the advantages of such models and try to draw a parallelism between them.

5.3.1 Regulation mechanisms

Figure 5.3 illustrates three simultaneous tests; a short pulse of current with high amplitude, a long current step with low amplitude and a hyperpolarizing current are applied successively. From top to bottom, the first plot is the response of the simplest version of our model. It means the version which contains only the potassium current and the sodium current present in the Purkinje neuron. Then the middle graph represents the response of this model when a calcium current has been added to it. Finally, the current I_{app} applied to our models is plotted in the lower part of the Figure.

The first tests concern only the application of different currents with fixed values for \bar{g}_{NaF} , \bar{g}_{Kdr} and \bar{g}_{Ca} . More precisely, we have $\bar{g}_{NaF} = 750 \mu\text{S}$, $\bar{g}_{Kdr} = 60 \mu\text{S}$ and $\bar{g}_{Ca} = 0.02 \mu\text{S}$.

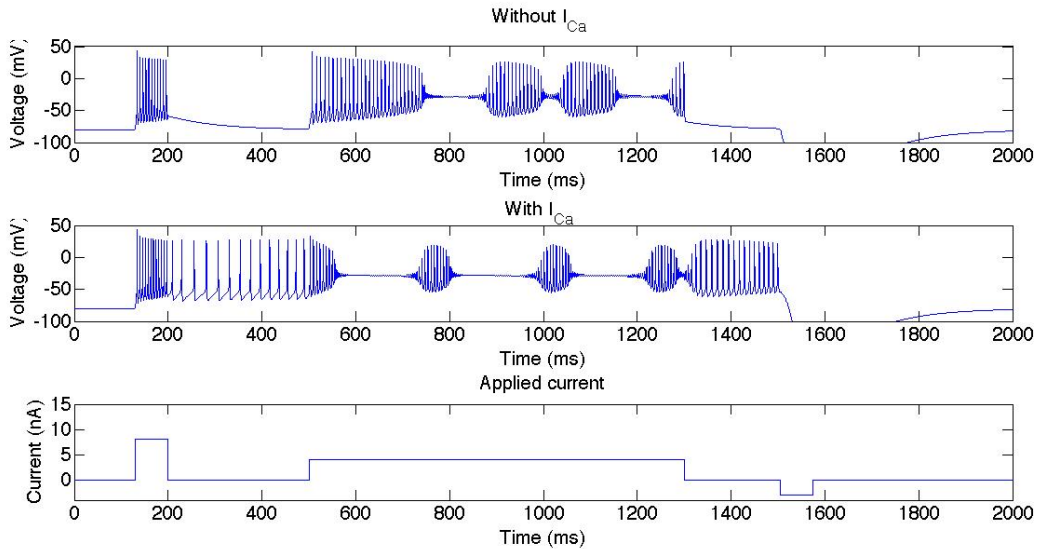


Figure 5.3: Simulation of model (5.5) for different pulses of applied current; a short high pulse, a long small pulse and a short hyperpolarizing pulse. The maximum conductance values are fixed such as $\bar{g}_{NaF} = 750 \mu\text{S}$, $\bar{g}_{Kdr} = 60 \mu\text{S}$ and $\bar{g}_{K,Ca} = 0 \mu\text{S}$ whereas $\bar{g}_{Ca} = 0 \mu\text{S}$ and $\bar{g}_{Ca} = 0.02 \mu\text{S}$ for the first and the second plot respectively.

We first analyse the model behaviour in the absence of calcium current. When a short pulse of current is applied, the cell has a repetitive firing activity with high frequency. The amplitude is slowly decreasing whereas the value of the hyperpolarized potential is increasing. The potential does not return to the rest immediately when the current is cut off. The beginning of the behaviour is similar when a long step of current is applied but the amplitude continues to decrease until there is an interruption which leads to a potential near to -25 mV. Actually this potential is not stable but it is composed of small oscillations which lead to fast spikes again after a time. Thus the up-state activity is made up of spike amplitude oscillations which are Hopf oscillations. Like the case of a short pulse, the firing activity is cut off when the current is returned to zero. Thus an activity is obtained only when a current is applied.

When a calcium current is added, the electrical activity changes a lot. Indeed, a short current is sufficient to switch in the up-state and the cell remains in this state while the current is cut off. Moreover, the application of a constant current during the up-state produces shorter periods of spiking activity and longer periods of small oscillations around -25 mV. We see in Figure 5.3 that a simple repetitive firing activity is found again when the long step current is relaxed but the up-state activity is nevertheless persistent. Hence, thanks to the addition of the calcium current, the model becomes bistable. Furthermore, the cell returns to the down-state when a sufficient hyperpolarizing current is applied. Another observation is interesting: as in the plot above it, without I_{Ca} , the plateau potential is clearly visible. Indeed, the lower potential in the spikes of the up-state is higher than the membrane resting potential.

However, in this Figure, it is difficult to know how the up-state would evolve if the long step of current between 500 ms and 1300 ms was not applied. So, Figure 5.4 shows that a short pulse is sufficient to activate the calcium current and to obtain an oscillatory up-state after a time of repetitive firing activity.

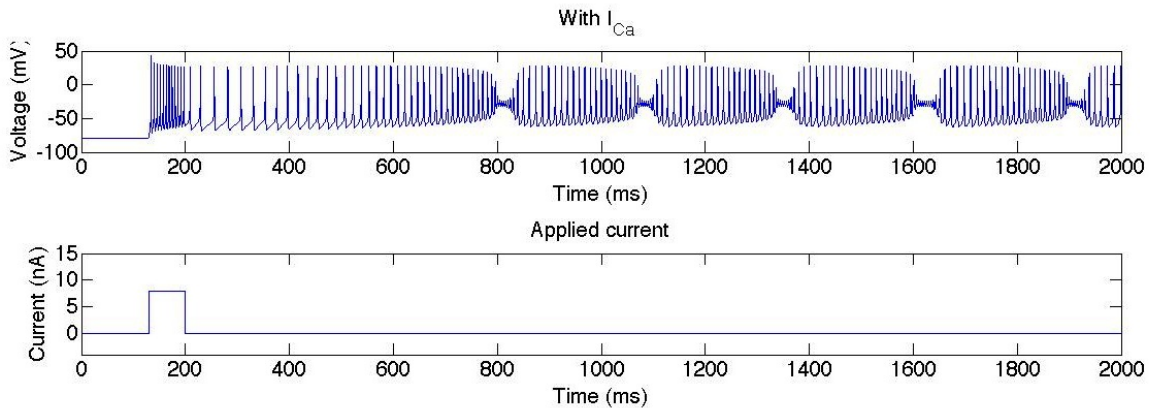


Figure 5.4: Simulation of model (5.5) for a short pulse of applied current. The consequences of the calcium current. The maximum conductance values are fixed such as $\bar{g}_{NaF} = 750 \mu\text{S}$, $\bar{g}_{Kdr} = 60 \mu\text{S}$, $\bar{g}_{K,Ca} = 0 \mu\text{S}$ and $\bar{g}_{Ca} = 0.02 \mu\text{S}$.

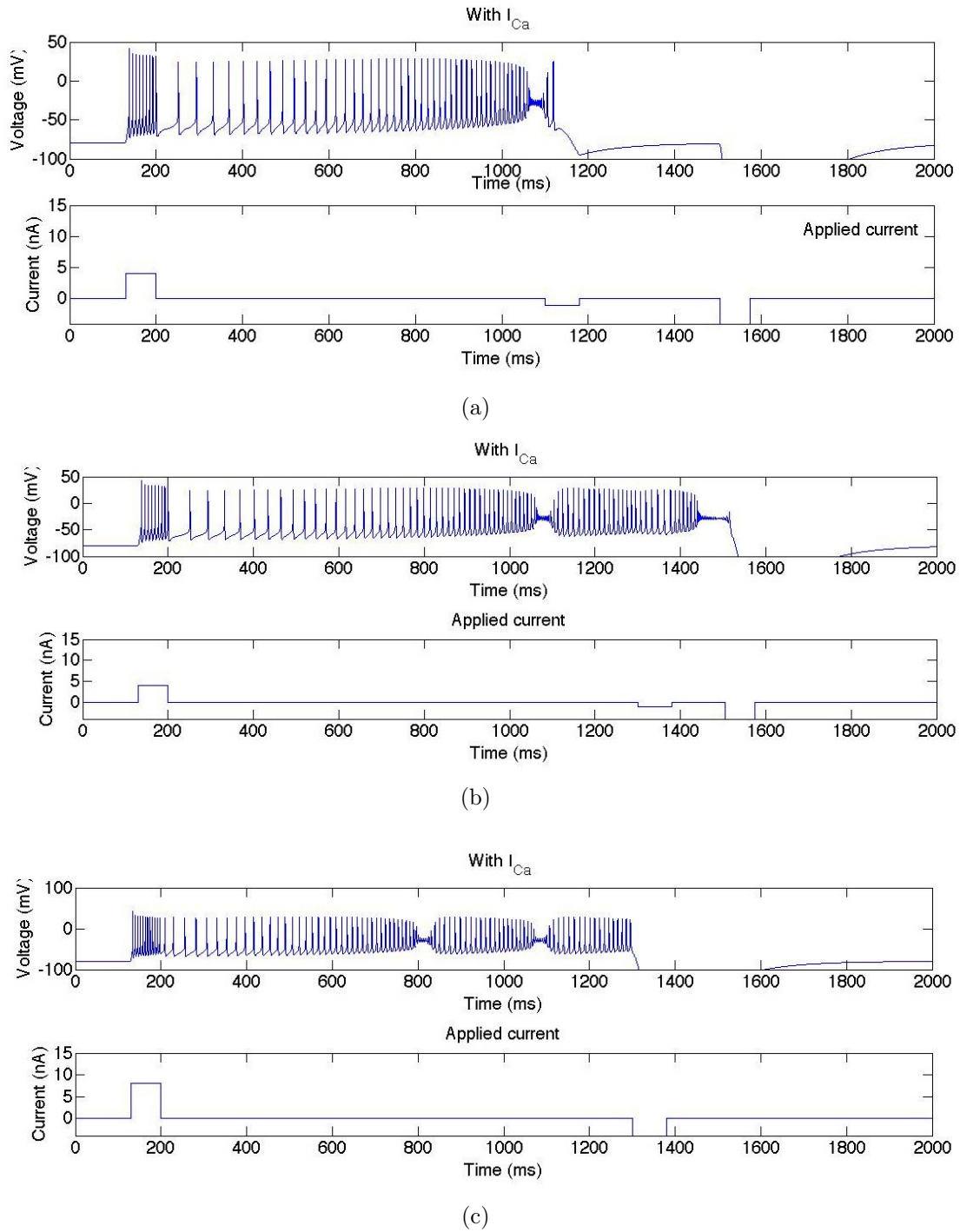


Figure 5.5: Simulation of model (5.5) for different pulses of hyperpolarizing applied current. The maximum conductance values are fixed such as $\bar{g}_{NaF} = 750 \mu\text{S}$, $\bar{g}_{Kdr} = 60 \mu\text{S}$, $\bar{g}_{K,Ca} = 0 \mu\text{S}$ and $\bar{g}_{Ca} = 0.02 \mu\text{S}$.

Another interesting observation concerns the hyperpolarizing current. If the cell is in its up-state, a hyperpolarizing current can induce the switch to the down-state but it is not obvious. Actually, it depends on the time of application and on the amplitude of this current. This feature is exhibited in Figure 5.5. In Figure 5.5(a), the negative current induces the cell to go back to rest whereas the same current has no effect when it is applied a bit later

in Figure 5.5(b). Furthermore, the amplitude of the current is also an important parameter because if we increase the amplitude of this current while applying it at the same time and with the same duration, the cell switches to the down-state. Indeed, this phenomenon can be observed in Figure 5.5(c).

We analyse now another example illustrated in Figure 5.6. There are two different tests here; the response to a short current with small amplitude and the response to a long step with high amplitude. A hyperpolarizing current is applied also, but this effect has already been studied.

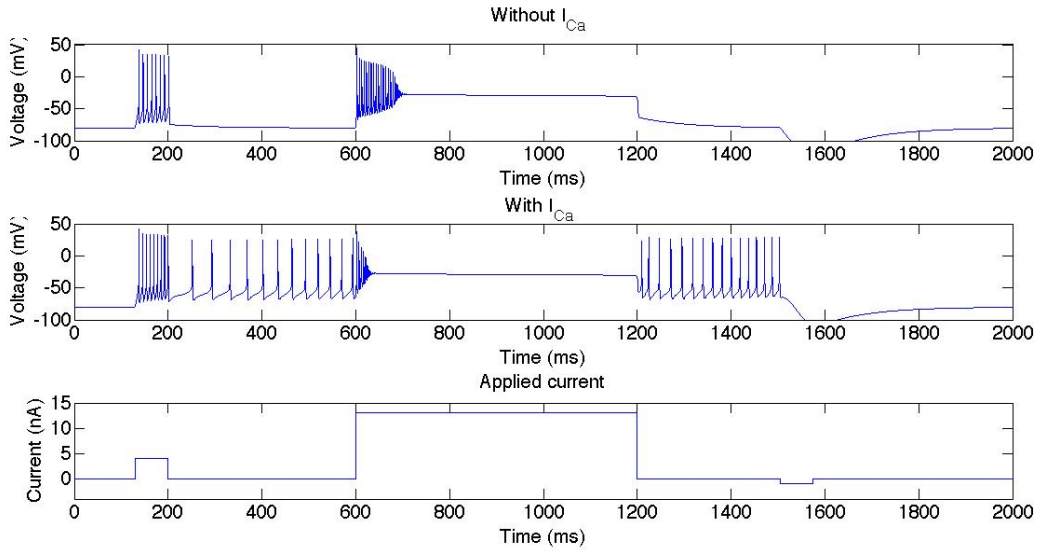


Figure 5.6: Simulation of model (5.5) for different pulses of applied current; a short small pulse, a long high pulse and a short hyperpolarizing pulse. The maximum conductance values are fixed such as $\bar{g}_{NaF} = 750 \mu\text{S}$, $\bar{g}_{Kdr} = 60 \mu\text{S}$ and $\bar{g}_{K,Ca} = 0 \mu\text{S}$ whereas $\bar{g}_{Ca} = 0 \mu\text{S}$ and $\bar{g}_{Ca} = 0.02 \mu\text{S}$ for the first and the second plot respectively.

In the absence of calcium current, a small current pulse produces a repetitive spiking activity as in Figure 5.3. However, the frequency of the firing is less important. Thus an increase in the amplitude of the pulse creates an increase in the frequency of the spiking activity. For the model with calcium current, the observation is quite similar. Indeed, the frequency during the pulse is decreased. Another remark can be made; there is a latency that appears between the end of the pulse and the periodical spikes.

Furthermore, a very high amplitude and long current induces the cell to stabilize itself in the up-state. This observation can also be made when a calcium current is added. Indeed, the neuronal state is a stable node in the up-state when the current is high. In the first case, the neuron returns to the rest state when the current is relaxed whereas the state is a repetitive firing activity with the addition of a calcium current. It means that there should be a stable limit cycle in the phase portrait of this system.

The consequences of the addition of a calcium current were clearly explored and shown by some examples. The next task was to add a calcium-dependent current. After that we can try to obtain some features that look like experimental recordings. Thus these tasks are performed with the model (5.5).

The first tests are the same than in Figure 5.3 and 5.6 with the aim of observing some consequences of the addition of a calcium-dependent current. The parameters are fixed as previously such that $\bar{g}_{NaF} = 750 \mu\text{S}$, $\bar{g}_{Kdr} = 60 \mu\text{S}$ and $\bar{g}_{Ca} = 0.02 \mu\text{S}$ whereas the new parameters are $\bar{g}_{SK, Ca} = 0.0144 \mu\text{S}$, $k_1 = 0.1375 \cdot 10^{-3}$, $k_c = 0$, $k_2 = 0.018 \cdot 10^{-4}$ and $K_D = 0.4 \cdot 10^{-3} \text{ nM}$. We can observe in Figure 5.7 the patterns obtained when a short high pulse or a small long step are applied whereas it is the contrary in Figure 5.9. In both figures, a small pulse of hyperpolarizing current is also applied.

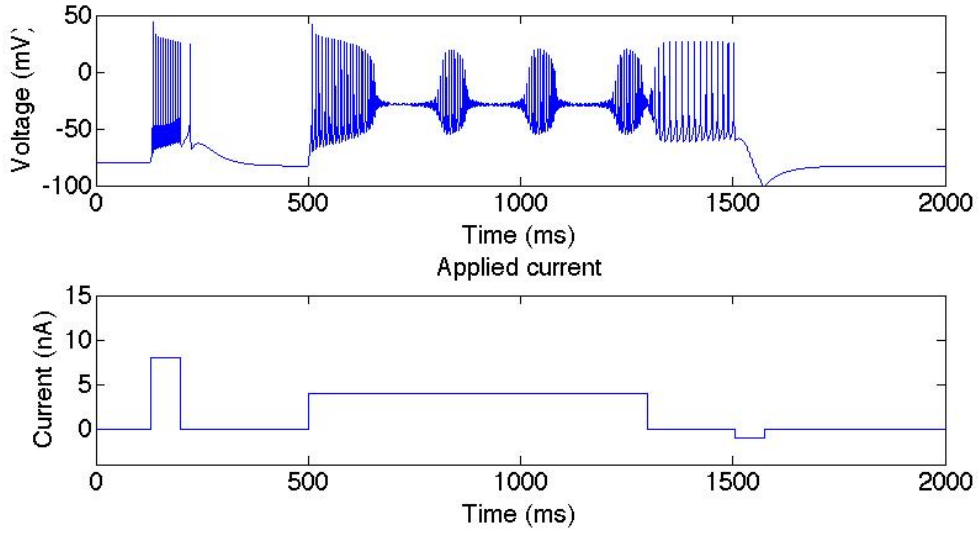


Figure 5.7: Simulation of model (5.5). Addition of a SK channel such as $\bar{g}_{SK, Ca} = 0.0144 \mu\text{S}$, $k_1 = 0.1375 \cdot 10^{-3}$, $k_c = 0$, $k_2 = 0.018 \cdot 10^{-4}$ and $K_D = 0.4 \cdot 10^{-3} \text{ nM}$. Same simultaneous tests than Figure 5.3 with $\bar{g}_{NaF} = 750 \mu\text{S}$, $\bar{g}_{Kdr} = 60 \mu\text{S}$ and $\bar{g}_{Ca} = 0.02 \mu\text{S}$.

By comparison with the results in Figure 5.3, we observe new interesting patterns in Figure 5.7. Indeed, the application of a short step of current does not anymore generate the switch towards the up-state; there are periodical spikes for the current duration and when the current returns to zero, a spike appears and it is followed by a small rebound and a latency before the returning to the rest. Nevertheless when the duration of the step is long enough, we observe similar electrical features than those observed before with the calcium current. When the current is relaxed, a repetitive firing activity continues. In Figure 5.7, it is stopped by the hyperpolarizing current which induces the cell to come back at rest. It is more clearly illustrated what happens when the long step current is stopped in Figure 5.8.

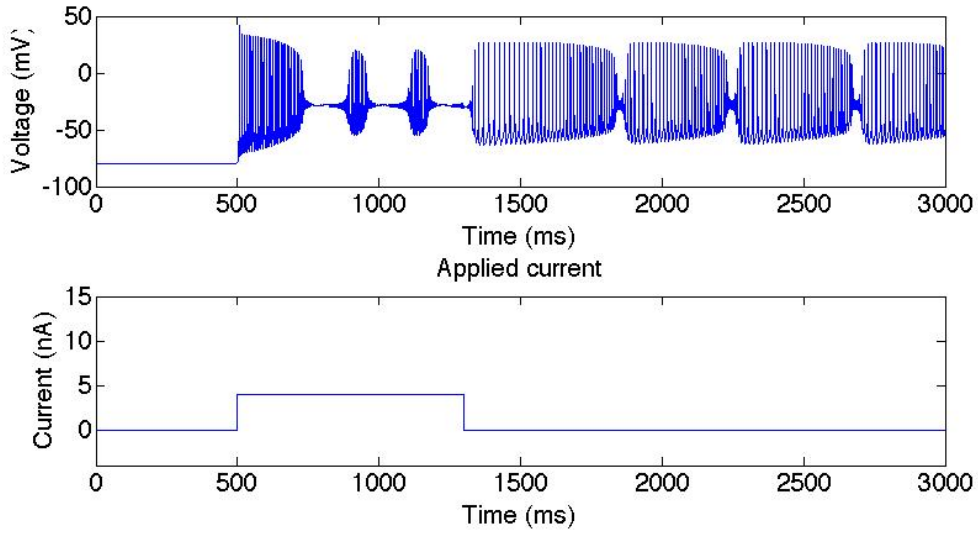


Figure 5.8: Simulation of model (5.5). Addition of a SK channel. The effect of a long duration current.

Indeed, there is a spontaneous activity. The bursts have a longer duration whereas the time of small oscillations is shorter. It is an observation already seen with the calcium current. A current applied during the up-state moves the bursts away from each other. So, there are fewer periods of spiking activity when a current is applied during the up-state.

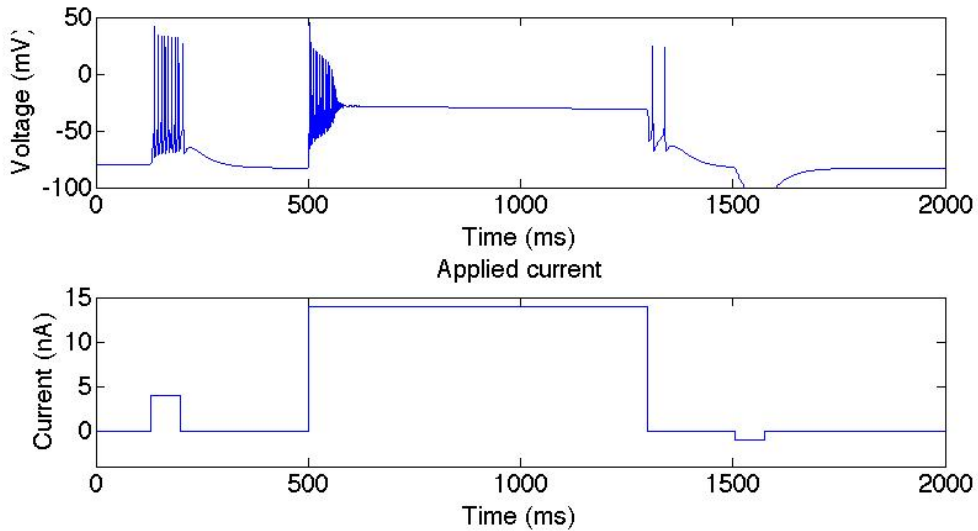


Figure 5.9: Simulation of model (5.5). Addition of a SK channel such as $\bar{g}_{SK,Ca} = 0.0144 \mu\text{S}$, $k_1 = 0.1375 \cdot 10^{-3}$, $k_c = 0$, $k_2 = 0.018 \cdot 10^{-4}$ and $K_D = 0.4 \cdot 10^{-3} \text{ nM}$. Same simultaneous tests than Figure 5.6 with $\bar{g}_{NaF} = 750 \mu\text{S}$, $\bar{g}_{Kdr} = 60 \mu\text{S}$ and $\bar{g}_{Ca} = 0.02 \mu\text{S}$.

About Figure 5.9, a smaller short pulse is responsible for a smaller latency and no spike is observed just before the rebound. As in the case of the calcium current in Figure 5.6, the

higher current step removes the bursts; the cell is at a stable potential. When the current is relaxed, there are some spikes, a rebound and after a return to the rest. Thus the hyperpolarizing current is unnecessary.

In conclusion, a short step of current induces spikes, an after-depolarization potential and a latency. The latency and the frequency of the spikes increase with the current amplitude.

Nevertheless a very strong pulse induces the switch in the up-state but it has to be stronger than in the calcium case. It is logical because there is a supplementary negative feedback with the SK current and hence a higher amplitude is necessary. It is shown in Figure 5.10.

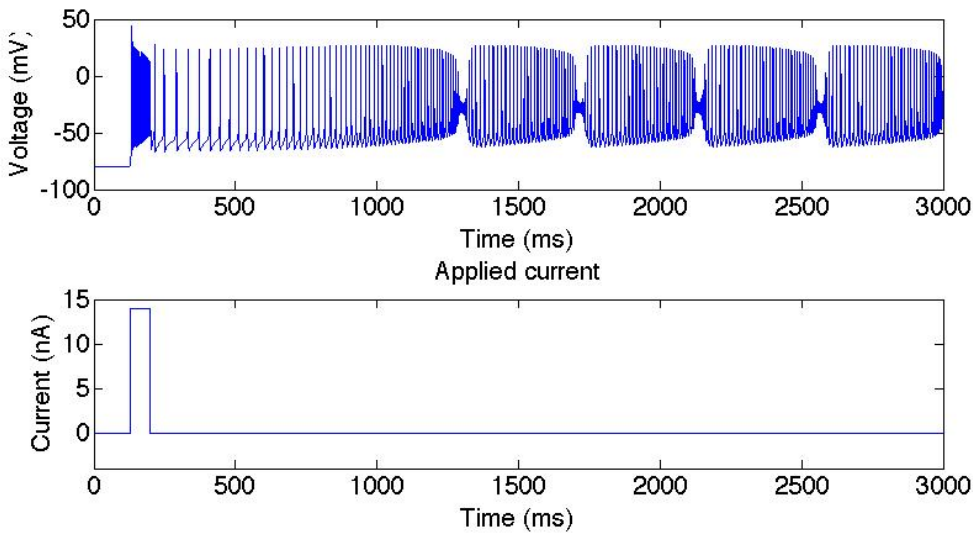


Figure 5.10: Simulation of model (5.5). Addition of a SK channel. Spontaneous cellular activity after a short strong pulse.

The cellular regulation mechanisms described above can be exploited to produce pictures close to experimental recordings. We will change some parameters and observe the consequences.

For instance, the range $\bar{g}_{SK, Ca} = 6 \times [0.0015; 0.0025] \mu\text{S}$ approximately gives behaviours similar than the experimental recordings in Figure 3.8 in Chapter 3 which is reproduced again in Figure 5.11 for a better readability. Indeed, the activity of the cell for $\bar{g}_{SK, Ca}$ in this range when it is stimulated by an increasing short current pulse of 70 ms is shown in Figure 5.12. This is an example of the robustness of our model. Nevertheless, the latency is less present in the model stimulation than in the experimental recordings. This could be solved by adding the persistent sodium current which is well known to exist in the Purkinje neuron. The other characteristics are well reproduced; indeed, we have a latency at the beginning of the excitability and it decreases when the current is increasing. Moreover, there is a latency at the end and an after-depolarization potential. When the current is sufficiently high, the spiking continues with a low frequency.

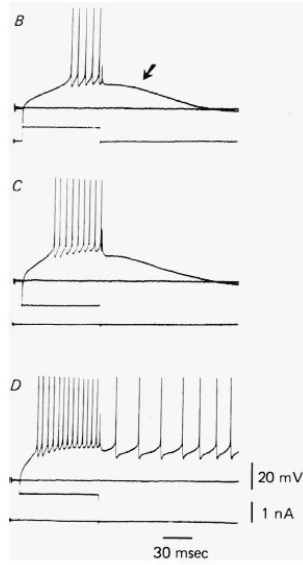


Figure 5.11: Somatic firing resulting of a DC depolarization for a guinea pig Purkinje cell : In B-D a short current pulse is injected [Llinas and Sugimori, 1980a].

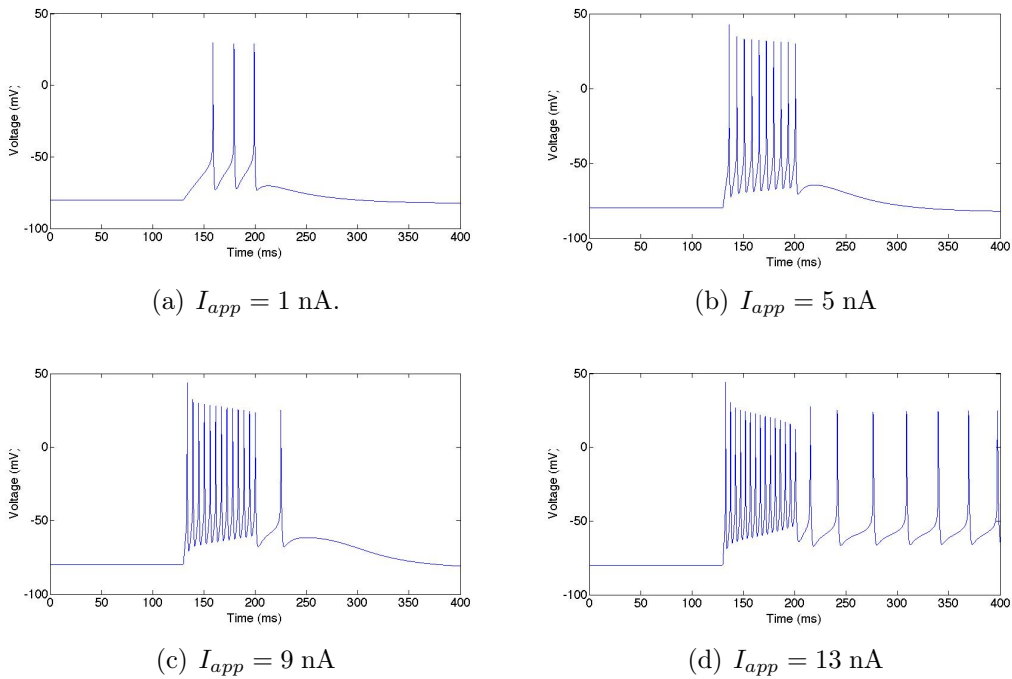


Figure 5.12: Simulation of model (5.5). Results for $\bar{g}_{SK,Ca} = 6 \times 0.002 \mu\text{S}$.

Until now, we exhibited the importance of the calcium current and the calcium-dependent current in the bistability.

Indeed, we saw how the addition of a calcium current can permit to obtain a spontaneous bistability. A depolarizing current induces the switch to the up-state whereas a hyperpolarizing current produces the switch from the up-state to the down-state. It was a result shown

experimentally by Loewenstein et al. [2005]. Go back to Figure 3.12 in Subsection 3.2.1 of Chapter 3 for a reminder. Furthermore, the addition of a SK channel changes a bit the activity but always permits the bistability; it enables the reproduction of more distinct activities.

Thanks to the clear role of each current, we can explore very different combinations of maximum conductance values to produce different patterns. The characteristic of modulation of our model is illustrated in Figure 5.13.

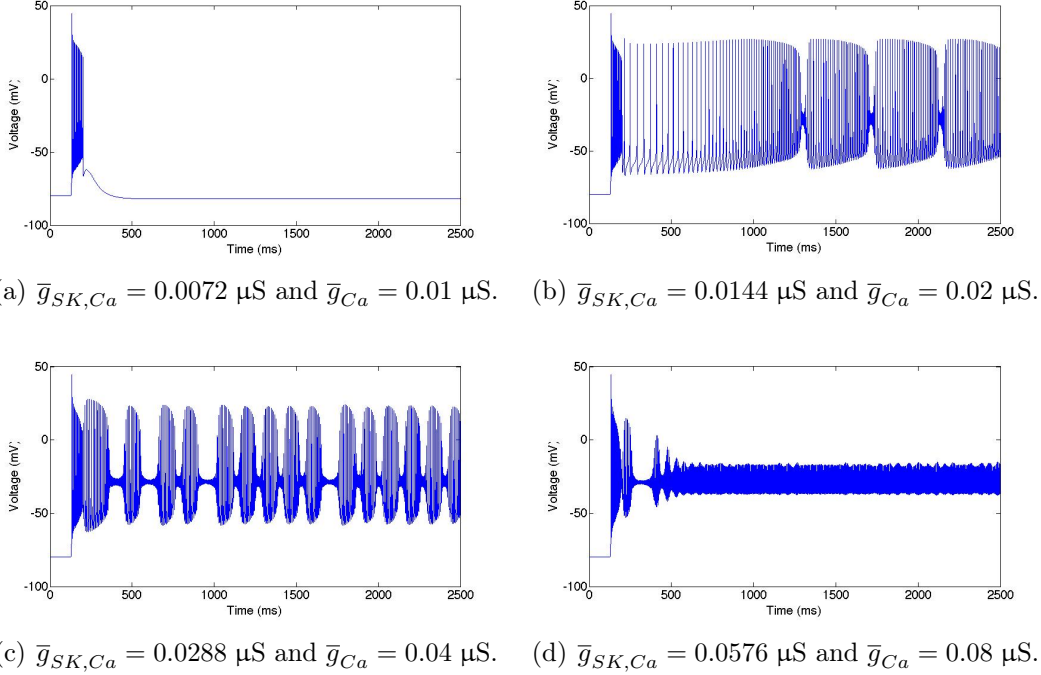
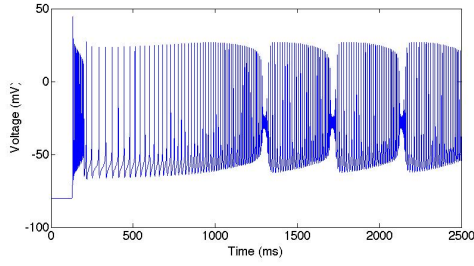


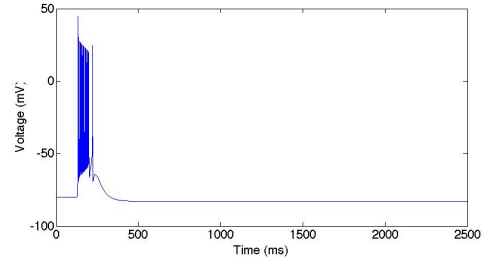
Figure 5.13: Simulation of model (5.5); the modulation principle. Results for $I_{app} = 14 \text{ nA}$ from $t = 130 \text{ ms}$ to $t = 200 \text{ ms}$.

After having shown some examples of neuronal modulation, it would be interesting to prove that our model produces robust results. For this, the parameters that will be varied have to conserve the same equivalent feedback gain of our system. It means that, for example, an increase in \bar{g}_{Kdr} will induce an increase in the slow negative feedback gain. An increase in the slow positive feedback gain will offset this change of \bar{g}_{Kdr} ; thus we will increase \bar{g}_{Ca} . However, $I_{SK, Ca}$ will change because of its calcium dependency, thus we need to modify $\bar{g}_{SK, Ca}$.

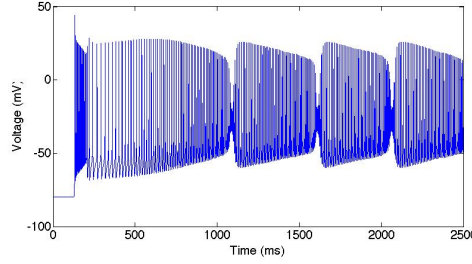
The Figure 5.14 is a very good illustration of this mechanism. This example shows that there are robust patterns reproduced by our model. The graph in Figure 5.14(b) is very different than the plot in Figure 5.14(a) while \bar{g}_{Kdr} was increased only by $20 \mu\text{S}$. Thus we modified the other maximum conductances to compensate the modification.



(a) $\bar{g}_{K_{dr}} = 60 \mu\text{S}$, $\bar{g}_{Ca} = 0.02 \mu\text{S}$ and $\bar{g}_{SK,Ca} = 0.0144 \mu\text{S}$.



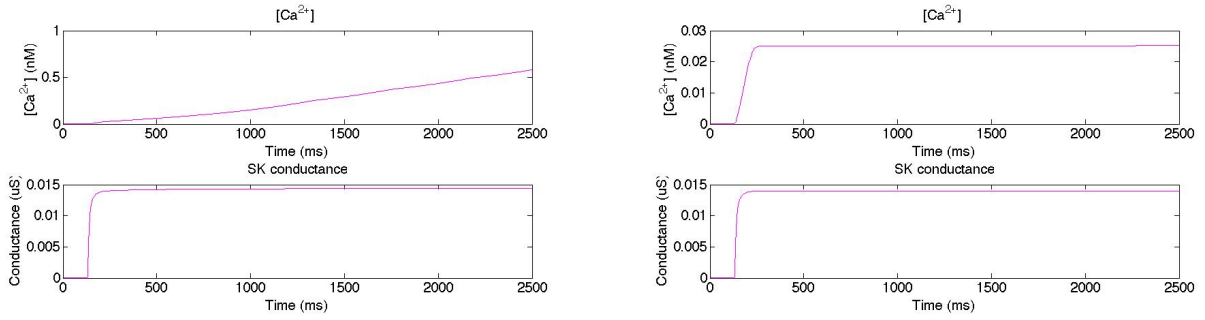
(b) $\bar{g}_{K_{dr}} = 80 \mu\text{S}$, $\bar{g}_{Ca} = 0.02 \mu\text{S}$ and $\bar{g}_{SK,Ca} = 0.0144 \mu\text{S}$.



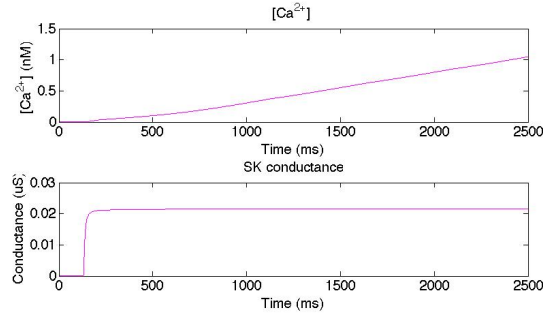
(c) $\bar{g}_{K_{dr}} = 80 \mu\text{S}$, $\bar{g}_{Ca} = 0.0310 \mu\text{S}$ and $\bar{g}_{SK,Ca} = 0.0216 \mu\text{S}$.

Figure 5.14: Simulation of model (5.5); the robustness principle. Results for $I_{app} = 14 \text{ nA}$ from $t = 130 \text{ ms}$ to $t = 200 \text{ ms}$ and $\bar{g}_{Na} = 750 \mu\text{S}$.

Furthermore, the increase in \bar{g}_{Ca} induces a modification in the equivalent conductance $\bar{g}_{SK,Ca} \left(\frac{[Ca^{2+}]}{K_D + [Ca^{2+}]} \right)$ which could be observed in Figure 5.15. As K_D has a low value compared with $[Ca^{2+}]$, the equivalent conductance rapidly converges to $\bar{g}_{SK,Ca}$. Indeed, the time function $[Ca^{2+}]$ in Figure 5.15(a) and in Figure 5.15(b) are very different, nevertheless the equivalent conductances $\bar{g}_{SK,Ca}$ tend to the same value. Moreover, the concentration values are too low; it is not realistic calcium concentrations. Usually, the calcium internal concentration has a magnitude approximately ten times as big. For this, we should change the parameters k_1 , k_c and k_2 . To obtain a conductance that depends more in calcium concentration, we should modify K_D because it has a too small value currently. Indeed, K_D is fixed at $0.4 \cdot 10^{-3} \text{ nM}$ and, hence, $\frac{[Ca^{2+}]}{K_D + [Ca^{2+}]} \simeq 1$. We should continue researching about the calcium concentration and the calcium-dependent channels in the Purkinje cell for obtaining more realistic results about this but this will not be performed in this thesis. However, we can try to modify K_D or the other parameters to satisfy our curiosity and conclude about some other regulation mechanisms contained in this model.



(a) $\bar{g}_{Kdr} = 60 \mu\text{S}$, $\bar{g}_{Ca} = 0.02 \mu\text{S}$ and $\bar{g}_{SK,Ca} = 0.0144 \mu\text{S}$. (b) $\bar{g}_{Kdr} = 80 \mu\text{S}$, $\bar{g}_{Ca} = 0.02 \mu\text{S}$ and $\bar{g}_{SK,Ca} = 0.0144 \mu\text{S}$.



(c) $\bar{g}_{Kdr} = 80 \mu\text{S}$, $\bar{g}_{Ca} = 0.0310 \mu\text{S}$ and $\bar{g}_{SK,Ca} = 0.0216 \mu\text{S}$.

Figure 5.15: Simulation of model (5.5); analysis of $g_{SK,Ca}$. Results for $I_{app} = 14 \text{ nA}$ from $t = 130 \text{ ms}$ to $t = 200 \text{ ms}$ and $\bar{g}_{Na} = 750 \mu\text{S}$.

For instance, if we increased K_D from $0.4 \cdot 10^{-3} \text{ nM}$ to 0.4 nM which is a value nearer to the calcium concentration than the previous value, we would obtain a conductance that would follow more or less the calcium concentration. Indeed, this test is illustrated in Figure 5.16 which is obtained for the same parameters and currents than the Figure 5.14(a); the unique modification is about K_D .

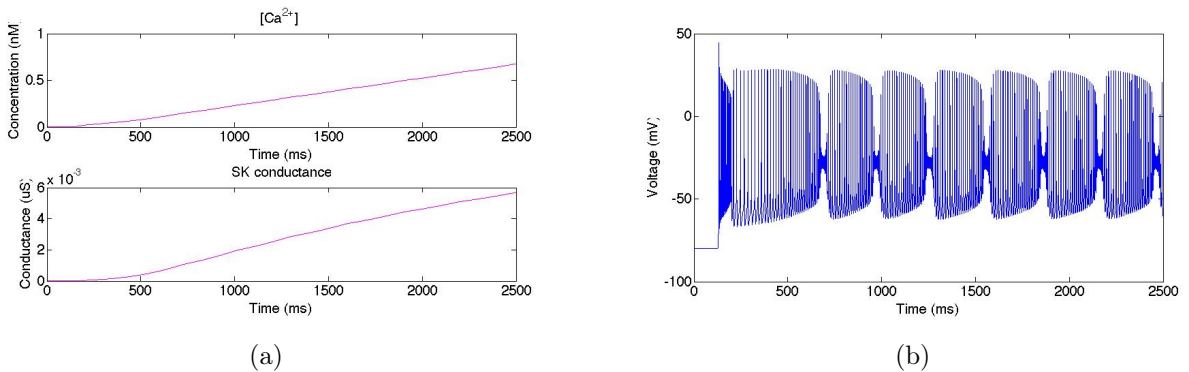
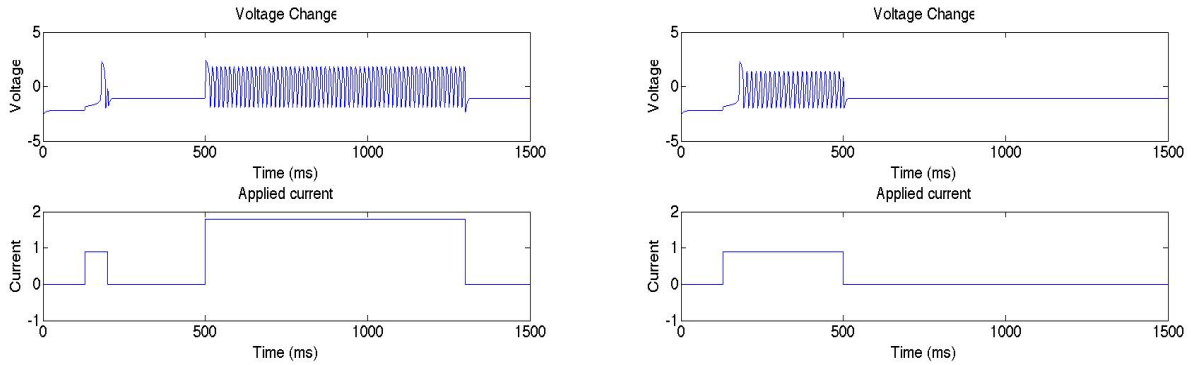


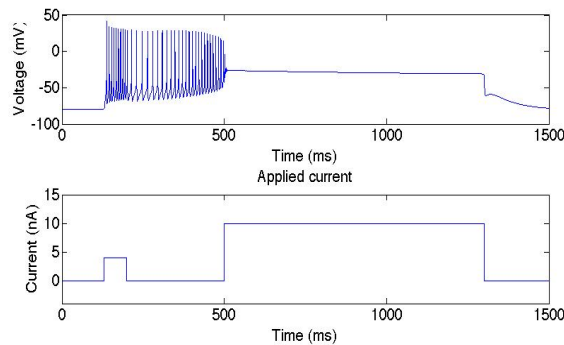
Figure 5.16: Simulation of model (5.5); $K_D = 0.4 \text{ nM}$. $I_{app} = 14 \text{ nA}$ from $t = 130 \text{ ms}$ to $t = 200 \text{ ms}$, $\bar{g}_{Na} = 750 \mu\text{S}$, $\bar{g}_{Kdr} = 60 \mu\text{S}$, $\bar{g}_{Ca} = 0.02 \mu\text{S}$ and $\bar{g}_{SK,Ca} = 0.0144 \mu\text{S}$.

5.3.2 Comparison with the qualitative model

We can also try to compare results of the qualitative model and some obtained with this model in Figure 5.17. We observe that the Figure 5.17(c) gives an electrical activity nearer this of Figure 5.17(b) than Figure 5.17(a) while the applied current are more distinct.



(a) Simulation of model (4.1); short low pulse and long high pulse of applied current. (b) Simulation of model (4.1); long low pulse of applied current.



(c) Simulation of model (5.5); $\bar{g}_{Ca} = 0.05 \mu\text{S}$.

Figure 5.17: Result with the qualitative model and the model (5.5).

Actually the mirrored FitzHugh-Nagumo model [Franci et al., 2012] is just useful to identify the main patterns contained in the excitability of the cell. Hence it is difficult to compare with a more complex model containing some currents recognized to be present in the neuron.

5.4 Advantages of the proposed model

A main advantage of model (5.5) is that it captures the specific excitability properties of the Purkinje cell while sharing the regulating feedback structure of many other neurons: one sodium current for the fast positive feedback, one potassium rectifier current for the slow negative feedback, one calcium current for the slow positive feedback and one calcium-dependent potassium current for the ultraslow negative feedback. Neurons sharing this feedback structure include most neurons that can switch from a low state to a high state: thalamocortical

neurons [McCormick and Huguenard, 1992], STN (Subthalamic nucleus) neurons [Beurrier et al., 1999], and other examples discussed in [Franci et al., 2013].

Extracting this core feedback structure is fundamental to understand robustness and modulation questions. Model (5.5) opens the way to apply such analysis tools to the Purkinje cell.

5.5 Limitations of the proposed model

We briefly discussed two limitations of the proposed model that could not be completely resolved in the framework of this thesis.

5.5.1 Physiological reduction

5.5.1.1 Motivation

The reduced model proposed in this chapter is “semi-quantitative”, it has the form of a conductance based model and each variable has a clear physiological interpretation but the low-dimensional model is not derived as a formal mathematical reduction of the detailed model studied in Chapter 4. We briefly describe below an unsuccessful attempt to reduce in a more systematic way the model of De Schutter and Bower [1994a].

5.5.1.2 Attempt at a formal reduction

A burst is made up of three different time scales: a fast scale for the depolarization of each spike, a slow scale for the hyperpolarization which defines the intra-burst period, and an ultraslow scale for the inter-burst period. The idea was thus to define a three-dimensional model, with a single variable for each time-scale, aggregating the contribution of all currents in that particular scale.

The first step of the procedure was to classify each current in one of the three scales in function of the value of the time constant at low voltages (less than -25 mV). For instance, the three sets of time scale can be approximately $[0; 1]$ ms, $[1; 100]$ ms and $[100; +\infty)$ ms corresponding to the fast scale, the slow scale and the ultraslow scale respectively.

We proceeded to the reduction of the quantitative model from De Schutter and Bower [1994a]. For instance, the sodium activations were in the fast scale and the fast sodium current activation represented the fast variable; the sodium inactivation, the calcium activation and the potassium delayed rectifier activation were classified in the slow scale whereas the ultraslow scale was represented by the potassium inactivation. For this test, each time constant was fixed to a constant value.

The fast variables were set to the steady-state. We chose, for example, the potassium activation for the slow variable. Then the second stage was to express each variable as a function of the variable representing its scale. This requires for instance to express the calcium

activation as a function of the potassium activation.

Hence, remind briefly the explanations about the reduction introduced in Chapter 2. For the variables classified in the same scale, we can assume that their time constants are equal. For example, two variables m_1 and m_2 belonging to the same scale present the time constants τ_1 and τ_2 respectively; thus we assume $\tau_1 = \tau_2 = \tau$ where τ is chosen to be approximately the mean of τ_1 and τ_2 . We want to express m_1 as a function of m_2 such that $m_1 = F(m_2)$ with

$$\tau \dot{m}_i = m_{\infty,i}(V) - m_i \text{ where } i = 1, 2. \quad (5.6)$$

Thus, the function F has to satisfy the equation

$$F(x) = (m_{\infty,1} \circ m_{\infty,2}^{-1})(x) \quad (5.7)$$

as it was shown in Chapter 2.

To obtain easy invertible functions, each steady-state (in)activation function was expressed with the formalism

$$m_{\infty}(V) = \frac{1}{1 + \exp \frac{V-V_0}{A}} \quad (5.8)$$

such that

$$m_{\infty}^{-1}(m_1) = V_0 + A \ln\left(\frac{1}{m_1} - 1\right). \quad (5.9)$$

This procedure is good for some simple neuronal models, such as the Hodgkin-Huxley model in Chapter 2. But this procedure gave unsatisfactory results for the Purkinje cell because there is not a clear division among time scales of the different currents of the Purkinje cell. It is important in particular to keep the voltage dependency of the time constants in our case.

We have to consider the fact that each variable can change of time scale depending on the membrane potential. Thus we tried a different method. In this method we choose also one variable for each scale but the other variables will depend on the three scales at the same time and the weight of each scale will change as a function of the potential. Note that the three main variables can not be chosen in an arbitrary way. Indeed, we have to pay attention to the sign of the feedback. More precisely, we can summarize what are the needs of the feedback system of a burster: a fast positive feedback, to enable the neuron to fire, a slow positive or negative feedback for the periodic spiking activity and an ultraslow negative feedback for the adaptation.

Mathematically, if a variable m belongs to two different time scales along the membrane potential values, like the potassium inactivation, we use the approximation

$$m = \alpha F(x_s) + (1 - \alpha) G(x_{us}) \quad (5.10)$$

with $\tau_{x_s} \leq \tau_m \leq \tau_{x_{us}}$. α depends on the membrane potential because it could be expressed by

$$\alpha = \frac{\tau_m - \tau_{x_s}}{\tau_{x_{us}} - \tau_{x_s}}, \quad (5.11)$$

where τ_{x_s} , $\tau_{x_{us}}$ and τ_m are functions of the membrane potential. This is a possible choice for α but it is not optimal and could be changed. α is chosen to minimize the error between the two transfer functions $\frac{1}{\tau_m s + 1}$ and $\frac{\alpha}{\tau_{x_s} s + 1} + \frac{1-\alpha}{\tau_{x_{us}} s + 1}$.

Although this technique goes well for some neurons, the result was not good for the Purkinje cell. The scales are really mixed and it is hard to aggregate the variables without removing important electrical behaviours.

We proceeded to the reduction of the model (5.5) built in Section 5.2 to work on a less complex model. The model (5.5) exhibits the time constants represented in Figure 5.18.

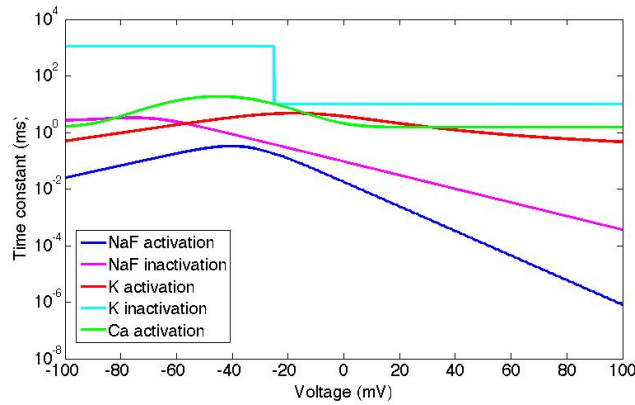
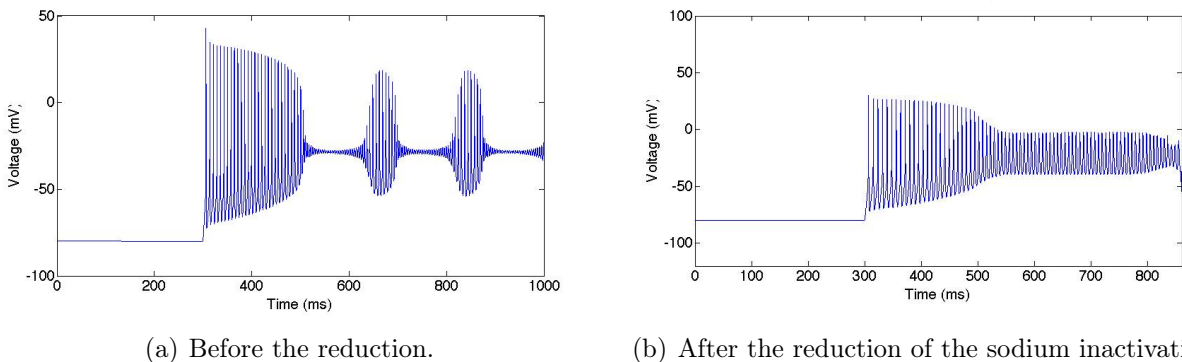


Figure 5.18: Time constants of the model (5.5).

Figure 5.19 illustrates that the reduction of a single current of model (5.5) suffices to change significantly the temporal behaviour.



(a) Before the reduction.

(b) After the reduction of the sodium inactivation.

Figure 5.19: Comparison of the reduced model with the non-reduced model. $I_{app} = 5$ nA from $t = 300$ ms. Reduction such as we chose the sodium activation for the fast scale, the potassium activation for the slow scale and the potassium inactivation for the ultraslow scale.

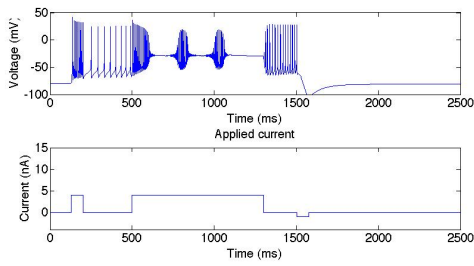
5.5.2 P-type calcium current

The calcium current considered in this chapter has no inactivation variable and activates at low potential. This feature is typical of a T-type calcium current but very different from a P-type current. The P-type current has both an activation variable and an inactivation variable and this is a current activated at high potential around -25 mV. See Figures 5.1 and 5.2 for the precise shape of the steady-state (in)activation variables and the time constants.

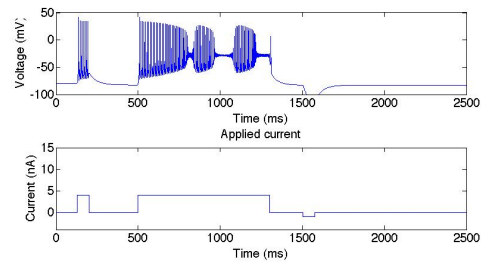
Because many papers put more emphasis on the presence of a P-type current than on a T-type current in Purkinje cells, we explored the effect of replacing the current of model (5.5) with a P-type current.

We realized a first test which is represented in Figure 5.20. The Figure 5.20(a) does not contain any new information compared with the previous results. After changing the dynamic of the calcium current, we observe in Figure 5.20(b) that the spontaneous activity seems removed. Indeed, when the applied current is stopped, the cell returns to the rest. The bistability between the particular up-state and the down-state is still observed transiently, not permanently.

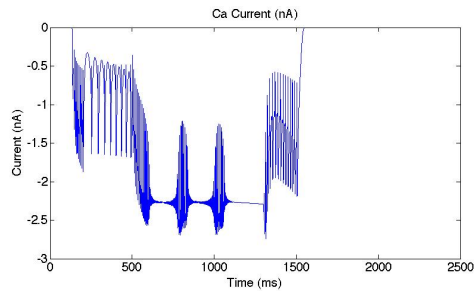
We can also compare the Figure 5.20(c) and the Figure 5.20(d) which represent the calcium current before and after the modification respectively. We see in Figure 5.20(c) that once the calcium current is activated, it remains activated until a hyperpolarizing current is applied. It is very different for the P-type current. The steady-state conductance is non-zero only in a potential range of $[-50; 0]$ mV; thus, it is likely that the bistability is removed because of the inactivation. However, the inactivation is ultraslow and the initial value is at 1, thus it should have a period in which the spontaneous activity would be possible but it is not what we observe. A plausible explanation is that the range of activation is too high whereas the half-activation was -55 mV for the previous calcium current. Nevertheless, we need to realize some other tests to conclude and some of them are illustrated in Figure 5.21.



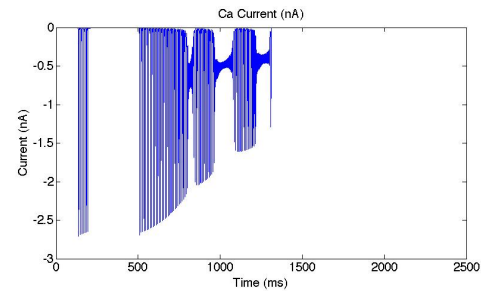
(a) Electrical pattern before the modification; for a T-type calcium current.



(b) Electrical pattern after the modification; for a P-type calcium current.

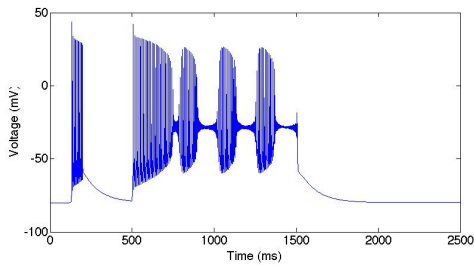


(c) Calcium current before the modification: T-type Ca current.

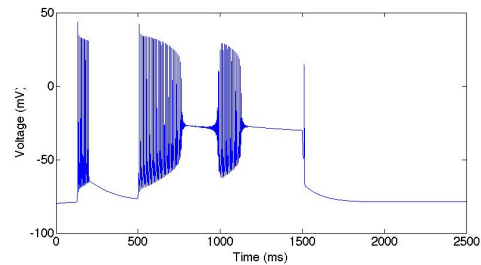


(d) Calcium current after the modification: P-type Ca current.

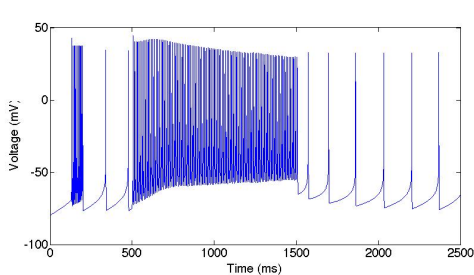
Figure 5.20: Substitution of the T-type calcium current by a P-type calcium current.



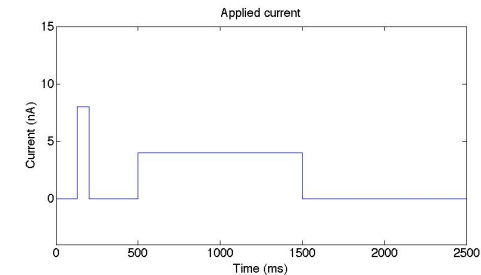
(a) Electrical pattern for $\bar{g}_{Ca} = 0.01 \mu\text{S}$.



(b) Electrical pattern for $\bar{g}_{Ca} = 0.2 \mu\text{S}$.



(c) Electrical pattern for $\bar{g}_{Ca} = 1 \mu\text{S}$.



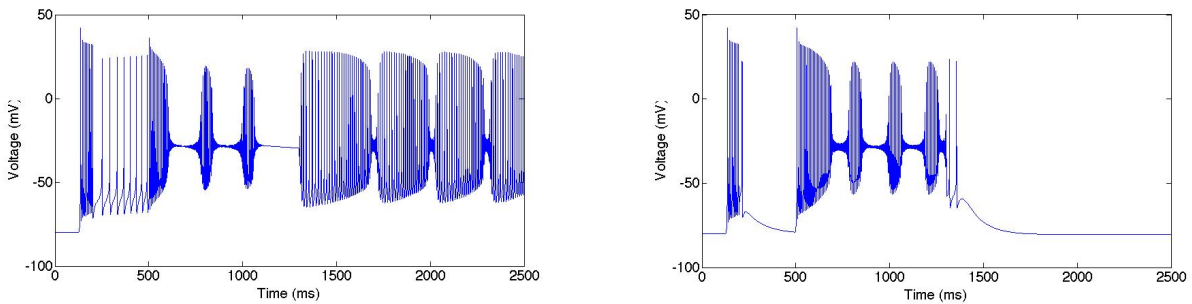
(d) Applied current.

Figure 5.21: Example of modulation for \bar{g}_{Ca} for P-type current.

In Figure 5.21, we tried three different values of maximum conductance \bar{g}_{Ca} . The Figure 5.21(a) and the Figure 5.21(b) illustrate quite similar behaviour whereas the Figure 5.21(c) is

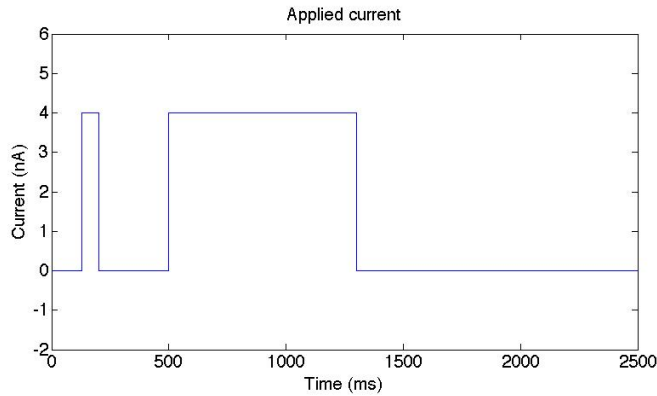
very far from the patterns observed before. When the maximum conductance value is sufficiently high, there is a spontaneous repetitive spiking activity that remains when the applied current is stopped. This electrical feature is also a long way from the Purkinje cell activity which contains a plateau potential, oscillations and latency at the beginning of the up-state. So, it is not a right track to increase again \bar{g}_{Ca} .

A supplementary test can help us to conclude about the removal of the spontaneous up-state activity. Indeed, we considered again the previous version of our model, which means the version with the arbitrary calcium current. In this version, we changed the half-activation potential of the calcium current from -55 mV to -25 mV. Thus we can observe the result which is plotted in Figure 5.22.



(a) $V_{\frac{1}{2}} = -55$ mV and $\bar{g}_{Ca} = 0.02$ μ S.

(b) $V_{\frac{1}{2}} = -25$ mV and $\bar{g}_{Ca} = 0.02$ μ S.



(c) Applied current.

Figure 5.22: Simulation of model (5.5). Modification of the half-activation potential for the calcium current.

A brief conclusion can already be stated. To maintain a spontaneous activity, we need a current activated at low potential, non-inactivating or slowly inactivating. Two such currents are identified in the Purkinje cell: the persistent sodium current and the T-type calcium current. The first is activated at low potential and is non-inactivating whereas the second is slowly inactivating. The T-type calcium current is slowly regenerative and it is necessary to have a slow regenerative current for bistability. Moreover, the calcium current qualifies to interact with a calcium-dependent potassium current which plays an important role in the

switch too.

The conclusion of our analysis is that it is the T-type calcium current that is critical for the excitability of the Purkinje cell. The specific role of the P-type calcium current was not identified in our study.

Chapter 6

Conclusions and perspectives

The main contribution of the thesis is to propose a new model of the electrophysiology of the Purkinje cell. The proposed model (Chapter 5) is less detailed than the quantitative model of [De Schutter and Bower, 1994a] studied in Chapter 4 but retains the main ionic currents in the form of a one-compartment conductance based-model. The model contains the four ionic currents shared by most neurons that exhibit bistability between an excitable “up-state” and a resting hyperpolarized “down-state”: a fast sodium current, a slow potassium current, a slow calcium current, and an ultraslow calcium-dependent potassium current. It was found that it is mostly the particular kinetics of the slow potassium current that differentiates the excitability properties of the Purkinje cell from other bistable neurons. The model was shown to be a good compromise between purely qualitative models that lose the link to the physiology and detailed quantitative models that are efficient at faithfully reproducing a particular experimental behaviour of the neuron but too complex to address important questions such as the modulation and robustness of the neuronal behaviour in different regimes.

The four chapters of the thesis summarize the main steps that were followed to derive the proposed model.

Chapter 2 detailed the modelling of the electrical activity of a neuron using the non-linear circuit principles introduced by Hodgkin and Huxley and the planar reduction of Hodgkin Huxley model amenable to phase portrait analysis. It was also shown how the addition of a calcium current in this model modifies the classical phase portrait of neuronal excitability and is fundamental to bistable neuronal behaviours.

Chapter 3 detailed the particular physiology of the Purkinje cell. We reviewed the role of Purkinje cells in the cerebellum, the experimental evidence of its bistability, and the type of excitability experimentally observed in the depolarized state of the neuron. Finally, we reviewed the list of ionic currents that have been identified in the neuron.

Chapter 4 presented two existing models of interest for the Purkinje cell: a qualitative model and a quantitative model. The qualitative model is not specific to Purkinje cell but was useful to show that the mere addition of a calcium current to the currents of Hodgkin-Huxley model is sufficient to obtain the different firing patterns observed in the Purkinje cell. The quantitative model was derived from an existing detailed model from the literature [De Schutter and Bower, 1994a]. This compartmental model did not reproduce bistability

and focused on the reproduction of the specific up-state excitability. Moreover, it was too complicated and contained too many details. This model was useful to identify the particular kinetics of the different currents and to evaluate the importance of spatial phenomena in the excitability of the neuron. It was found that most of the simulations could be reproduced by aggregating the somatic and dendritic currents in a single compartment. We could also illustrate the fragility of a detailed quantitative model, reflected for instance in the choice of the numerical integrator chosen for the simulations. This model with only one compartment was not still very easy to parameterize.

Chapter 5 presented the novel model extracted from the detailed model following the paper [De Schutter and Bower, 1994a]. This novel model is midway between the empirical model and the conductance-based model of the previous chapter permitting to study the neuromodulation of the Purkinje cell, as it was achieved for the STG neuron [Drion et al., 2013]. This new model is a conductance-based model and reproduces the bistability of a Purkinje neuron thanks to the introduction of a slow regenerative calcium current. This calcium current has an activation kinetics similar to a T-type calcium current. The P-type current, which is present in the cell too, would seem not to be responsible for bistability. Furthermore the particular up-state excitability is obtained by specific sodium and potassium current interactions. Generally, too many models are focused on either the up-state excitability or the bistability but not both. It is an issue that is solved by a model such as the model built in Chapter 5.

6.1 Perspectives

The novel model proposed in Chapter 5 raises several questions that could not be completed in the thesis but would be worth exploring further.

6.1.1 Physiological modelling

One disappointment encountered in the thesis was our unsuccessful attempt to obtain the novel model of Chapter 5 as a systematic mathematical reduction of the detailed model from the literature studied in Chapter 4.

It would also be of interest to acquire more knowledge about the physiology of the Purkinje cell for a better justification of the novel model. The paper [De Schutter and Bower, 1994a] is not very recent and new knowledge has been accumulated about the ionic currents of the Purkinje cell and in particular the role of calcium currents.

Finally, we suggested in Chapter 5 that the P-type calcium current was not responsible for bistability of Purkinje neurons. The P-type current could play a role in the up-state excitability and it is a subject that could be interesting to deal with too.

6.1.2 Spatial phenomena

The physiology of the Purkinje cell and its particular anatomy suggest that the channel expression of different channels is markedly different in the soma and in the dendrites. It would be interesting to investigate the functional role of this heterogeneity. One direction would be to study a two-compartment version of the model proposed in Chapter 5, one for the soma and one for the dendrites. First attempts in that direction were unsuccessful but it could be another valuable research direction.

In particular, we considered one compartment with the dendritic currents and another compartment with the Hodgkin-Huxley formalism for the somatic currents. This last one contains two ionic currents responsible mostly for the unusual up-state excitability: the sodium current and the potassium delayed rectifier current.

Briefly, it is as if the compartment for the bistability was the dendrites while the other one was the soma for the up-state excitability. The dendrites should cause the switching of the somatic membrane potential because of the calcium and the potassium calcium-dependent channels in the dendrites.

Hence, this idea gave the following model:

$$\left\{ \begin{array}{l} C_s \dot{V}_s = -\bar{g}_{Kdr}(m_{Kdr}^2)h_{Kdr}(V_s - V_{Kdr}) - \bar{g}_{NaF}(m_{NaF}^3)h_{NaF}(V_s - V_{NaF}) \\ \quad - \bar{g}_{leak}(V_s - V_{leak}) + I_{app} + G_i(V_d - V_s), \\ C_d \dot{V}_d = -\bar{g}_{Ca}m_{Ca}(V_d - V_{Ca}) - \bar{g}_{K,Ca} \left(\frac{[Ca^{2+}]}{K_D + [Ca^{2+}]} \right)^2 (V_d - V_{K,Ca}) \\ \quad + G_i(V_s - V_d). \end{array} \right. \quad (6.1)$$

However, we did not achieve the regulation of this model, despite the relevant idea hidden by it. It seems interesting to separate the bistability and the up-state excitability by two compartments. This is a possible research direction.

Bibliography

- The Brain from Top to Bottom., January 2002. URL http://thebrain.mcgill.ca/flash/i/i_06/i_06_cr/i_06_cr_mou/i_06_cr_mou.html.
- Human Anatomy and Physiology, April 2011. URL http://andreeasanatomy.blogspot.be/2011/04/you-need-to-step-up-on-step-to-reach_23.html.
- N. H. Barmack and V. Yakhnitsa. Functions of interneurons in mouse cerebellum. *The Journal of Neuroscience*, 28(5):1140–1152, 2008.
- M. F. Bear, B. W. Connors, and M. A. Paradiso. *Neuroscience*. Wolters Kluwer Health, 2007.
- C. Beurrier, P. Congar, B. Bioulac, and C. Hammond. Subthalamic nucleus neurons switch from single-spike activity to burst-firing mode. *J Neurosci*, 19(2):599–609, Jan 1999.
- A. D. Coop and G. N. Reeke. Simulating the temporal evolution of neuronal discharge. *Neurocomputing*, 32:91–96, 2000.
- J. T. Davie, B. A. Clark, and M. Häusser. The origin of the complex spike in cerebellar Purkinje cells. *The Journal of Neuroscience*, 28(30):7599–7609, 2008.
- E. De Schutter and J. M. Bower. An active membrane model of the cerebellar purkinje cell. i. simulation of current clamps in slice. *Journal of neurophysiology*, 71(1):375–400, 1994a.
- E. De Schutter and J. M. Bower. An active membrane model of the cerebellar purkinje cell. ii. simulation of synaptic responses. *Journal of Neurophysiology*, 71(1):401–419, 1994b.
- G. Drion, L. Massotte, R. Sepulchre, and V. Seutin. How modeling can reconcile apparently discrepant experimental results: the case of pacemaking in dopaminergic neurons. *PLoS Comput Biol*, 7(5):e1002050, May 2011. doi: 10.1371/journal.pcbi.1002050.
- G. Drion, A. Franci, V. Seutin, and R. Sepulchre. A novel phase portrait for neuronal excitability. *PLoS ONE*, 7(8):e41806, 08 2012. doi: 10.1371/journal.pone.0041806. URL <http://dx.doi.org/10.1371/journal.pone.0041806>.
- G. Drion, A. Franci, V. Seutin, and R. Sepulchre. Modulation and robustness of endogenous neuronal spiking. *Submitted to PloS Comp Bio. Preprint: <http://arxiv.org/abs/1311.2200>*, 2013.
- J. Eccles, R. Llinas, and K. Sasaki. The inhibitory interneurons within the cerebellar cortex. *Experimental Brain Research*, 1(1):1–16, 1966.

- J. R. Edgerton and P. H. Reinhart. Distinct contributions of small and large conductance Ca^{2+} -activated K^+ channels to rat Purkinje neuron function. *The Journal of physiology*, 548(1):53–69, 2003.
- J. D. Engbers, D. Anderson, G. W. Zamponi, and R. W. Turner. Signal processing by T-type calcium channel interactions in the cerebellum. *Frontiers in cellular neuroscience*, 7, 2013.
- R. Feil, J. Hartmann, C. Luo, W. Wolfgruber, K. Schilling, S. Feil, J. J. Barski, M. Meyer, A. Konnerth, C. I. De Zeeuw, et al. Impairment of LTD and cerebellar learning by Purkinje cell-specific ablation of cGMP-dependent protein kinase I. *The Journal of cell biology*, 163(2):295–302, 2003.
- A. Franci, G. Drion, and R. Sepulchre. An organizing center in a planar model of neuronal excitability. *SIAM J Appl Dyn Syst*, 11(4):1698–1722, 2012. doi: 10.1137/120875016. URL <http://epubs.siam.org/doi/abs/10.1137/120875016>.
- A. Franci, G. Drion, V. Seutin, and R. Sepulchre. A balance equation determines a switch in neuronal excitability. *PLoS Comput Biol*, 9(5):e1003040, 2013. doi: 10.1371/journal.pcbi.1003040. URL <http://dx.doi.org/10.1371%2Fjournal.pcbi.1003040>.
- P. Gilbert and W. Thach. Purkinje cell activity during motor learning. *Brain research*, 128(2):309–328, 1977.
- T. Hirano and S. Hagiwara. Kinetics and distribution of voltage-gated Ca, Na and K channels on the somata of rat cerebellar Purkinje cells. *Pflügers Archiv*, 413(5):463–469, 1989.
- A. Hodgkin and A. Huxley. A quantitative description of membrane current and its application to conduction and excitation in nerve. *J. Physiol*, 117:500–544, 1952.
- E. M. Izhikevich. *Dynamical systems in neuroscience: the geometry of excitability and bursting*. MIT Press, Cambridge, Mass., 2007.
- R. Llinas and M. Sugimori. Electrophysiological properties of in vitro Purkinje cell somata in mammalian cerebellar slices. *The Journal of Physiology*, 305(1):171–195, 1980a.
- R. Llinas and M. Sugimori. Electrophysiological properties of in vitro Purkinje cell dendrites in mammalian cerebellar slices. *The Journal of Physiology*, 305(1):197–213, 1980b.
- Y. Loewenstein, S. Mahon, P. Chadderton, K. Kitamura, H. Sompolinsky, Y. Yarom, and M. Häusser. Bistability of cerebellar Purkinje cells modulated by sensory stimulation. *Nature neuroscience*, 8(2):202–211, 2005.
- D. A. McCormick and J. R. Huguenard. A model of the electrophysiological properties of thalamocortical relay neurons. *J Neurophysiol*, 68(4):1384–400, Oct 1992.
- A. Pellionisz and R. Llinás. A computer model of cerebellar Purkinje cells. *Neuroscience*, 2(1):37–48, 1977.
- M. Rapp, I. Segev, and Y. Yarom. Physiology, morphology and detailed passive models of guinea-pig cerebellar Purkinje cells. *The Journal of physiology*, 474(1):101–118, 1994.

- M. Sausbier, H. Hu, C. Arntz, S. Feil, S. Kamm, H. Adelsberger, U. Sausbier, C. Sailer, R. Feil, F. Hofmann, et al. Cerebellar ataxia and Purkinje cell dysfunction caused by Ca^{2+} -activated K^+ channel deficiency. *Proceedings of the National Academy of Sciences of the United States of America*, 101(25):9474–9478, 2004.
- J. D. Schmahmann. Disorders of the cerebellum: ataxia, dysmetria of thought, and the cerebellar cognitive affective syndrome. *The Journal of Neuropsychiatry and Clinical Neurosciences*, 16(3):367–378, 2004.
- D. Shelton. Membrane resistivity estimated for the Purkinje neuron by means of a passive computer model. *Neuroscience*, 14(1):111–131, 1985.
- A. M. Swensen and B. P. Bean. Ionic mechanisms of burst firing in dissociated Purkinje neurons. *The Journal of neuroscience*, 23(29):9650–9663, 2003.
- J. T. Walter, K. Alvina, M. D. Womack, C. Chevez, and K. Khodakhah. Decreases in the precision of Purkinje cell pacemaking cause cerebellar dysfunction and ataxia. *Nature neuroscience*, 9(3):389–397, 2006.
- D. Z. Wetmore, D.-A. Jirenhed, A. Rasmussen, F. Johansson, M. J. Schnitzer, and G. Hesslow. Bidirectional Plasticity of Purkinje Cells Matches Temporal Features of Learning. *The Journal of Neuroscience*, 34(5):1731–1737, 2014.
- Wikipedia. Action potential — Wikipedia, The Free Encyclopedia, 2014a. URL http://en.wikipedia.org/w/index.php?title=Action_potential&oldid=601839114. [Online; accessed 3-April-2014].
- Wikipedia. Cerebellum — Wikipedia, The Free Encyclopedia, 2014b. URL <http://en.wikipedia.org/w/index.php?title=Cerebellum&oldid=598422415>. [Online; accessed 21-March-2014].
- S. R. Williams, S. R. Christensen, G. J. Stuart, and M. Häusser. Membrane potential bistability is controlled by the hyperpolarization-activated current I_H in rat cerebellar Purkinje neurons in vitro. *The Journal of physiology*, 539(2):469–483, 2002.
- O. Zhuchenko, J. Bailey, P. Bonnen, T. Ashizawa, D. W. Stockton, C. Amos, W. B. Dobyns, S. Subramony, H. Y. Zoghbi, and C. C. Lee. Autosomal dominant cerebellar ataxia (SCA6) associated with small polyglutamine expansions in the $\alpha 1A$ -voltage-dependent calcium channel. *Nature genetics*, 15(1):62–69, 1997.